DESIGN AND ANALYSIS OF VISIBLE LIGHT COMMUNICATION AND POSITIONING SYSTEMS

ZHENG HUANHUAN

(*B.Eng, Zhejiang University*)

A THESIS SUBMITTED
FOR THE DEGREE OF DOCTOR OF PHILOSOPHY
DEPARTMENT OF ELECTRICAL AND COMPUTER ENGINEERING
NATIONAL UNIVERSITY OF SINGAPORE

2017

Supervisors:

Associate Professor Mohan Gurusamy, Main Supervisor

Associate Professor Changyuan Yu, Co-Supervisor

Examiners:

Associate Professor Yongxin Guo

Associate Professor Danner, Aaron James

Professor Lian-Kuan Chen, Chinese University of Hong Kong

Dedications:

To my family

who loves me always.

Declaration

I hereby declare that this thesis is my original work and it has been written by me in its entirety. I have duly acknowledged all the sources of information which have been used in the thesis. This thesis has also not been submitted for any degree in any university previously.

Zheng Huanhuan

ZHENG Huanhuan

19 January 2017

Acknowledgment

I feel very fortunate to have had the opportunity to work with and learn from many remarkable people during my Ph.D candidature at the National University of Singapore (NUS). This thesis would not have been possible without their kind help and support.

First and foremost, I would like to express my deepest gratitude and most sincere appreciation to my supervisors Prof. Changyuan Yu, Prof. Mohan Gurusamy and Prof. Hoon Kim for their invaluable guidance, helpful supervision and kind encouragement throughout my PhD study. They not only enlighten me by sharing their knowledge, wisdom and experience, but also offer me a valuable research platform. Prof. Yu guided the road of research for me, from idea generation to logic in expression. He not only inspires me to realize my full potential, but also gives me hope and support when I feel helpless and emotional. Prof. Mohan and Prof. Kim, who

constantly give me their support and trust, are not only erudite scholars with prudential attitude, but also very responsible and considerate mentors.

I am grateful to Dr. Zhaowen Xu and Prof. Jian Chen, with whom I gain fruitful knowledge through extensive discussions in both research and personal life. After discussion with them, the difficulty changes from a stone to a piece of feather.

I wish to thank my research partners at NUS and I2R for providing a friendly working environment and exchanging insightful discussions.

Besides, my appreciate also go to my thesis committee for their effort and time devoted to review my thesis.

Last but not least, I am indebted to my parents and other family members for their love, support and sacrifices. My special thanks be to my husband who has been consistently encouraging and taking care of me. It is their love and support that have always confronted and motivated me.

Contents

Summary

Visible Light Communication (VLC) is a green technology that uses light emitting diodes (LEDs) to provide the functions of illumination, communication, and positioning. This high-speed low-cost wireless technique is an alternative candidate for achieving effective and efficient communication or positioning that can cope with the increasing demand for wireless services. The main objective of this thesis is to investigate and develop novel transmission and detection techniques to improve the performance of both indoor communication and positioning systems based on visible light.

Since multiple LED lamps are typically used for illumination in large indoor spaces, light uniformity is important for both luminance and data communication to avoid a combination of dark and bright patches as well as to achieve a uniform signal-to-noise ratio (SNR) throughout the coverage area. Mobility is also important, which defines the communication

coverage of the wireless system. As the channel characteristics are dependent on the room size and the material properties of reflecting surfaces and the indoor objects, the same mobile terminal, may experience an obvious performance variation at different locations. In order to achieve a communication quality that is almost identical, an inverse design based on convex optimization for the LED arrangement is proposed, which can meet the requirements of illuminance and data communication. In order to save the cabling cost, the use of a suboptimal system is also discussed, which shows a trade-off between the system performance and complexity. When compared with the optimal design, the suboptimal arrangement saves 17.8% power consumption and keeps the SNR fluctuation within 3 dB.

By modulating the signal on the visible light, the LED cannot only be used for illumination and data communication, but can also be applied in the positioning system. A novel indoor positioning system (IPS) based on VLC is proposed and demonstrated within a 100 cm $\times$ 118.5 cm $\times$ 128.7 cm space. In this system, four LED lamps are assigned four different center frequencies. When the receiver moves in this space, signals from the four LED transmitters are collected and then distinguished by applying Hamming filters to the received

signal. The received signal strength (RSS), as an asynchronous ranging technique, is used to translate the received power to the estimated distances between the LED transmitters and the photodiode (PD) receiver. The average positioning distance error is 1.72 cm using a two-dimensional (2D) positioning algorithm. However, at the corners of the test-bed, the positioning errors are relatively larger than the central places. Thus, an error correcting algorithm (ECA) is applied to the corners in order to improve the positioning accuracy. The average positioning error of the four corners decreases from 3.67 cm to 1.55 cm. Then, a three-dimensional (3D) positioning algorithm is developed, and the average positioning error of 1.90 cm in space is achieved. Four altitude levels are chosen, and on each receiver plane with different heights, four points are picked on each plane to test the positioning error. A random track in space is also carried out. All these experimental results show that average positioning errors in 3D space are all within 3 cm.

Apart from using different frequencies to distinguish signals from different transmitters, which is called frequency division multiple access (FDMA), code division multiple access (CDMA) can also be applied in visible light positioning (VLP) systems. Synchronization is also necessary among LEDs while putting

the code division multiplexing technique into use. However, in a commercial system, the synchronization is very difficult to achieve since LED lamps may only be used as transmitters and cannot receive the synchronization signals. We propose a delay compensation code division multiplexing technique for the first time. At the receiver side, the identities (IDs) of the nearby LED transmitters can be decoded and the signal strength from different lamps can be measured. Based on the IDs arrangement that we have known, a roughly positioning can be arranged. Then, a trilateration is used to accurately determine the position of the receiver. The simulation is carried out in a typical room with these dimensions: 4 m $\times$ 4 m $\times$ 3 m. The cases of reusing codes are discussed and compared. The best performance is achieved when seven Cyclic Orthogonal Walsh-Hadamard Codes (COWHC) are used. The mean positioning error is only 0.96 cm. The code arrangements for the larger rooms or those with irregular shapes are also discussed. When nine codes are applied, the average positioning error can be as small as 1.23 cm.

List of Tables

List of Figures

List of Acronyms

AOA	Angles of Arrival
BD	Block Diagonalization
BFSA	Basic-Framed Slotted ALOHA
CCM	Code Cycle Modulation
CDMA	Code Division Multiple Access
COWHC	Cyclic Orthogonal Walsh-Hadamard Codes
DC	Direct Current
DD	Direct Detection
DTMF	Dual Tone Multi-Frequency
ECA	Error Correcting Algorithm
EMI	Electromagnetic Interference
FDMA	Frequency Division Multiple Access
FFT	Fast Fourier Transform
FIR	Finite Impulse Response
FOV	Field of View
GPS	Global Positioning System

HPA	Half Power Angle
ID	Identity
IM	Intensity Modulation
IM/DD	Intensity Modulation and Direct Detection
IOT	Internet of Things
IPS	Indoor Positioning System
IR	Infrared
ISI	Inter-symbol Interference
ISO	International Organization for Standardization
ITS	Intelligent Transport System
LAN	Local Area Network
LEDs	Light Emitting Diodes
LOS	Line of Sight
MAI	Multiple Access Interference
MIMO	Multiple Input and Multiple Output
MUI	Multi-User Interference
NR	Newtown-Raphson
NRZ	non Return-to-Zero
non-LOS	non-Light of Sight
OCDMA	Optical Code Division Multiple Access
OFDM	Orthogonal Frequency Division Multiplexing
OOK	On-Off Keying

OOC	Optical Orthogonal Codes
PD	Photodiode
PDOA	Phase Difference of Arrival
PLC	Power Line Communication
PWM	Pulse Width Modulation
RF	Radio Frequency
RFID	Radio Frequency Identification
RGB	Red Green Blue
RMS	Root Mean Square
ROCs	Random Optical Codes
RONJA	Reasonable Optical Near Joint Access
RSS	Received Signal Strength
SINR	Signal to Interference-pluse-Noise Ratio
SNR	Signal-to-Noise Ratio
TDM	Time Division Multiplexing
TDMA	Time Division Multiple Access
TDOA	Time Difference of Arrival
TOA	Time of Arrival
UIR	Uniformity Illuminance Ratio
UWB	Ultra-Wide Band
VLC	Visible Light Communication
VLP	Visible Light Positioning

WDM	Wavelength Division Multiplexing
WLAN	Wireless Local Area Network
2D	Two Dimensional
3D	Three Dimensional

List of Notations

$\|\cdot\|$	the Euclidean norm of a vector
$(\cdot)^T$	the transpose of a vector or a matrix
$(\cdot)^*$	the conjugate only of a scalar or a vector or a matrix
$(\cdot)^H$	the Hermitian transpose of a vector or a matrix
$\lfloor\cdot\rfloor$	downward intergral function
$\lceil\cdot\rceil$	upward intergral function

Chapter 1

Introduction

1.1 Background and Motivations

The concept of visible light communication (VLC) is used to describe the wireless communication system that transmits information by modulating light that is visible to the human eye [1]. As a matter of fact, the light primarily serves as a source of illumination rather than communication, which may not be the chief purpose. With the growth of visible light emitting diodes (LEDs) for illumination, interest in studying VLC has grown rapidly. When a room is already illuminated by LEDs, why not exploit it for data communication too? The sharing of resources not only saves electric power but also reduces the required hardware cost.

In the last few years, we have witnessed development in the VLC technology in both academics and industry [2]. The main driver of this technology is the increasing popularity of LEDs, which is due to their long life time, high data security, energy efficiency, and environment friendliness.

In truth, using visible light as one of the wireless communication media is nothing new [3]. In the past, communication across great distances was

already developed through beacon fires, mirror reflections, and light houses. The first known electronic wireless communication that used sunlight as its light source was developed successfully by Alexander Graham Bell, who invented a photophone in 1880 [4]. By using sunlight beams, this new invention enabled transmissions of modulated voice data over the distance of 200 m. The drawback of this invention is also obvious, as it relied on sunlight, which is available intermittently in a day. From then on, several incremental improvements were carried out based on Bell's design, such as the use of a tungsten lamp with an infrared (IR) filter, high pressure vapor, and mercury [5]. Following this, fluorescent lights with low data rates were also demonstrated for communication [6]. Compared with other types of illuminating systems, the solid-state light source revolutionized indoor illumination for its longer lifespan, lower power consumption, and higher lighting efficiency, resulting in the re-emergence of visible light as an effective and efficient communication medium. In the 1990s, high brightness LEDs were introduced for their general function of illumination. In the following years, LED's luminous efficacy improved rapidly and the lifetime was as high as 100,000 hours [7–9]. Thanks to the fast development of solid-state lighting, Nakagawa Lab in Keio University presented the concept of VLC for the first time in 2003, which was followed by its growing development in both academia and industry at a global scale. The historical development of VLC systems with a timeline starting from the year 2004 is given in Table 1.1.

In 1999, Pang et al. [10] conceived the concept of VLC, which involved modulating signals on fast-switching LEDs. As described by them, VLC systems with LED traffic lights implemented can provide open space wireless broadcasting service for audio messages. In 2001, a free technology project named RONJA (Reasonable Optical Near Joint Access) was developed in

Kulhavy of Twibright Labs in order to set up reliable optical data links over a range of 1.4 km in free space using visible light. As a result of this, the communication speed could reach 10 mbps [11]. By switching phosphorescent white LEDs on and off rapidly, a data rate of up to 40 mbps can be achieved easily. Using the same on-off keying (OOK) scheme, RGB white LEDs achieve a higher data rate of over 100 mbps. In the early 2000s, a 400 mbps data transmission was reported by Tanaka *et al.* based on numerical analysis and computer simulations, making use of white LED for both lighting and data communication [12,13]. Over the past few years, high data rates in terms of gigabits per second became possible for the VLC systems that applied the right modulation, employed line coding schemes, and used equalizers at transmitters and receivers [14–17].

Table 1.1: Timeline Elucidating the Historical Development of VLC.

Time	**Historical Development**
2004	Demonstrated LED light systems with high-speed transmission in data-held and vehicle-borne computing devices (Japan) [2].
2005	Transmitted information to mobile phones with a data rate of 10 kbps for the VLC land trial; facilitated the ability of a throughput to reach several mbps using LED and fluorescent light (Japan).
2006	Combined white light LED with power line communication (PLC) to provide broadcast access for indoor applications [18].
2007	Witnessed the proposal of two standards by the Visible Light [19] Communications Consortium: Visible Light Communication System Standard and
	Continued on next page

Table 1.1 – continued from previous page

Time	Historical Development
	Visible Light identity (ID) System Standard.
2008	Employed IR and VLC technologies to home networks (OMEGA); demonstrated a VLC system using five LEDs with a data rate >100 mbps over a few meters using a direct line of sight (LOS) [2] (OMEGA).
2009	Defined the visible light spectrum allowed for use.
2010	Developed VLC technology for setting up communications among a wide range of electronic products (USA).
2010	Demonstrated a positioning system using visible light (Japan); transmitted VLC signals at 500 mbps over 5 m (Germany) [20].
2011	Demonstrated OFDM-based VLC at 124 mbps real time, using commercial off-the-shelf phosphorescent white LED (UK) [2].
2011	Demonstrated high-definition video transmission from a standard LED lamp, which was shown at TED Global [21].
2012	VLC-based indoor positioning system (IPS) became an attractive topic [22–24].
2014	Launched a commercial bidirectional RGB LED VLC system (both up and down link data rate could reach 300 mbit/s with a range of 25 feet) [25].
2015	Realized location-based services in supermarkets using VLC (France).

On the other hand, VLC technology is derived and standardized with the help of many initiatives. OMEGA (Home Gigabit Access) is a project in Europe, which is run by researchers coming from universities, research

institutions, and technology companies. It aims to develop a home or office access network that could deliver services with a high bandwidth and meet a transmission speed of 1 gbps by using a combination of power cables, radio signals, and light. With the help of the IEEE 802.15.7 task group 7, which was found in 2009, PHY and MAC standards for VLC have been completed [26]. Additionally, the Li-Fi Consortium, which was initiated in 2011, spares no effort in introducing optical wireless technology and guides this new technique to the market. Some other important research institutes that are actively developing and commercializing VLC technology include the University of Oxford, Keio University, the University of Edinburgh, the Smart Lighting Engineering Research Center in Boston University, and the UC-Light Center in the University of California.

1.1.1 Comparison with Other Communication Technologies

Although radio frequency (RF) communication is the most popular technology today, it still has some prominent drawbacks. VLC is compared with RF communication on the basis of five main points [27]:

Capacity: Radio spectrum is highly congested, as it is highly developed. It becomes increasingly difficult to find capacity for radio communication to support wireless data transmissions for media applications. The radio waves are expensive, and only a limited range is available. Visible light band could theoretically offer 400 THz bandwidth (375-780 nm), which is much larger than that of the RF spectrum. Moreover, the entire huge bandwidth can be reused next door without interference.

Efficiency: Radio waves consume more energy when compared with VLC, which is highly energy efficient since illumination and data conveyance

can be done at the same time.

Cost: Transmitter and receiver devices used in VLC systems are cheap in comparison to expensive RF units.

Safety: Radio waves create Electromagnetic interference (EMI), which seriously affects instruments in airplanes and equipment in hospitals, and are potentially dangerous during hazardous operations, such as nuclear generation, coal mining, and oil or gas drilling. However, VLC conveys signals using light, which is intrinsically safe. Hence, this technology could be widely used in many areas.

Security: Radio waves penetrate through barriers such as walls. Hence, they can be intercepted easily. However, visible light cannot generally penetrate solid materials and is confined within the walls of a room, which creates a secure environment for data communication.

Human Health: The transmission power of RF cannot be too high since after increasing the RF power over a certain level, serious health risks for humans will exist. VLC is an attractive candidate in consumer service systems.

Another popular candidate that is discussed for data transmission is IR communication. Some difference points between VLC and IR communication are summarized as below [28]:

Data rate: IR communication operates with a rate of 20 Mb/s while VLC can go up to 100 Mb/s [29]. IR is slower for the following reasons: (1) IR communication suffers more from the multi-path effect, which limits its data rate. (2) Because IR is invisible, the transmitted power is limited to protect human eyes, which also limits the transmission speed.

Distance: In comparison with VLC systems with more than several 10 meters of communication distance, the IR signals can only reach a distance

of $\sim$ 3 m for effective communication.

Noise source: The noise sources will be different due to the wavelength of the light source. For IR communication, noise mainly comes from ambient light containing IR light, while in the case of VLC, sunlight and other sources of illumination can be noise sources.

Services: IR technology has only a communication function while VLC can be used for illumination, data communication, and positioning.

1.1.2 Current and Potential Visible Light Applications

In recent times, emerging indoor and outdoor applications can benefit from VLC, including indoor localization, power line communication, broadband access, vehicle communication, etc. [3].

Home and Office: As many people carry more than one wireless device at any time, such as smart phones, smart watches, tablets, smart glasses, or wearable computers, the data rate required by each device is growing rapidly. In urban surroundings, human beings spend most of their time indoors, where the practicality of VLC technology is self-evident. In these cases, VLC becomes a strong alternative for indoor wireless access that is in high demand, because it is easy to add extra capacity to the office or residential premises with LED infrastructure. In Fig. 1.1, an example of a local area network (LAN) is deployed where a laptop, a smart phone, a smart glass, and a wearable computer are interconnected using VLC [30].

Transport Systems: In order to reduce the number of road casualties and improve traffic efficiency, the intelligent transport system (ITS) becomes a popular topic. Since LEDs are widely and recently used in head or taillights in vehicles, signage, traffic signals, and street lamps, the deployment of an ITS based on VLC is promising. As shown in Fig. 1.2, by using the headlights

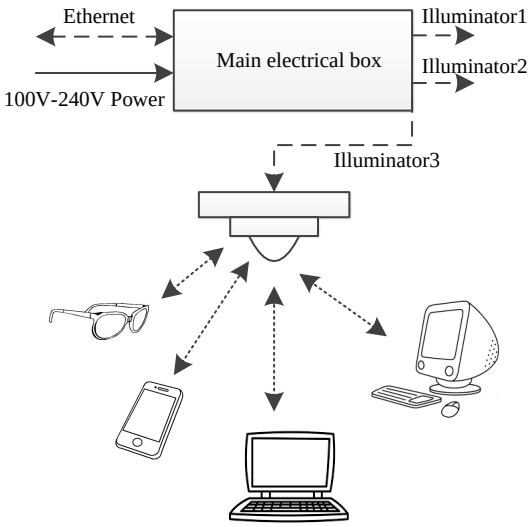

Figure 1.1: VLC used in home and office networks.

and rear lights of cars as transmitters and mounting cameras and detectors as receivers, inter-vehicular communication can be enabled to share information among drivers about routes, speed, traffic, and destinations in order to avoid traffic jams or accidents [31]. Some infrastructures such as billboards and advertising boards can broadcast valuable information to passing vehicles. Besides, street lamps and traffic lights can also be used to display and transmit modulated information to vehicles. Aircraft navigation lights can be used to convey identification. Another promising application can be created by using the lighting installed on aircrafts to broadcast music and videos and to exchange data with wired based stations in the aircraft cabin, which could offer passengers a better experience [32].

Hospitals, Industries, and Dangerous Environments: VLC systems have many advantages in EMI-sensitive environments such as kindergartens, mines, hospitals, and petrochemical plants [33, 34]. The medical community is always looking for ways to improve hospital efficiency and reduce infections in hospitals. One way to achieve these goals is to

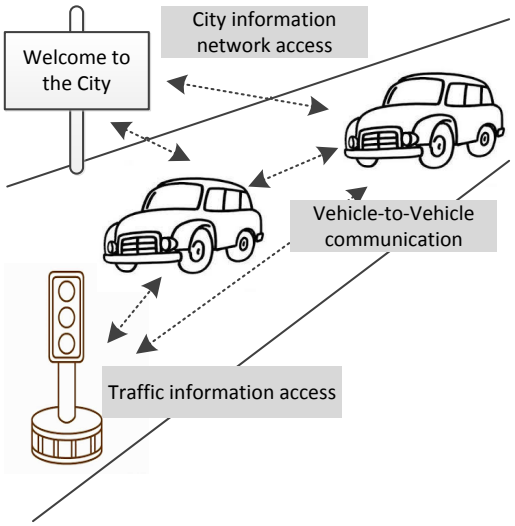

Figure 1.2: VLC used in transport systems.

upgrade communication infrastructure by using wireless technology, which makes it possible for doctors to access patients' data and monitor their well-being remotely using tablets. However, while using RF techniques, information security cannot be guaranteed and interference from nearby devices may congest the communication. Thus, a switch to VLC technology is self-evident, which could offer a mode of communication that is immune to RF interference and jamming. On the other hand, communication and positioning based on visible light are intrinsically safe in places with flammable materials, such as coal mines and oil wells. For example, the workface of a coal mining pit is surrounded by three metal faces and supported by hydraulic machines, and the working condition is changing in the mining process. Furthermore, the skin effect on RF electromagnetic waves leads to a significant degradation of wireless signals. These conditions make it difficult to use conventional RF communication systems in the workface. However, VLC systems are free from these problems and, therefore

can be applied in such a workface [35].

Underwater Communication: In view of underwater communication, RF transmission is extremely hard to implement. Acoustic communication requires expensive equipment and provides a limited data rate. VLC is, therefore, an excellent alternative for this purpose. Several systems have been proposed and demonstrated in remotely operated vehicles, diver communication applications, and wireless sensor networks [36, 37].

Public Areas: Public areas such as theaters, shopping malls, and museums can be equipped with accurate localization and navigation systems based on visible light, which is also called visible light positioning (VLP). Such positioning systems guide members of the audience to their seats in theaters, offer a particular video or audio introduction of items on display in a museum, or help shoppers find new arrivals or discounted goods in a supermarket [38]. In addition, it can be used to broadcast useful information in case of civil contingencies [39]. The presence of VLC could please customers when they arrive in a new public area.

Defense and Security: The VLC technology provides natural advantages such as secure and covert communication without the effects of RF interference. Apart from its high data rate communication, it offers ranging information that is used for localization in many places as well. Thus, it is called indoor global positioning system (GPS). These inherent characteristics make systems using visible light suitable for disaster recovery construction.

Aviation: Radio waves are forbidden in aircrafts while LED-based lights can be safely used in aircraft cabins. VLC can be widely and potentially used to provide both illumination and media services to passengers. Furthermore, such an application will reduce aircraft construction cost and weight.

Device Connectivity: In the near future, billions of sensors and instruments will have wireless connectivity, as triggered by the revolutionary concept of the internet of things (IOT). VLC as a cost-efficient, simple, and immediate technology to connect devices with high speed data does not encroach on the crowed electromagnetic spectrum.

1.2 Main Contributions

In VLC systems, as channel characteristics depend on the room size and the material properties of reflective surfaces, the same VLC mobile terminal may experience different performance styles in different locations. One of the key problems of indoor VLC systems is achieving uniform communication performance at different locations without affecting the primary illumination function. We propose an inverse design based on convex optimization for the LED arrangement, which can meet the requirements of illuminance and data communication. We show that sufficient brightness and uniform signal-to-noise ratio (SNR) can be achieved within the indoor coverage by using the proposed optimal LED arrangement, thus enabling terminal mobility for indoor VLC. The SNR fluctuation can only be 0.7 dB. In order to save cabling cost, a suboptimal system is also discussed, which reduces the power consumption with an acceptable performance degradation. When compared with the optimal design, the suboptimal arrangement saves 17.8 % of the energy and keeps the SNR fluctuation within 3 dB. (Chapter 3)

A novel IPS based on VLC is proposed and demonstrated with the dimensions 100 cm $\times$ 118.5 cm $\times$ 128.7 cm. As we know, in a commercial system, the synchronization is very difficult to realize since LED lamps may only be used as transmitters and cannot receive the synchronization signal.

Thus, an asynchronous ranging technique is promising. In our VLP system, different center frequencies are assigned to LED lamps at the transmitter side and Hamming filters are applied at the receiver side to distinguish the signals of different transmitters. Based on the RSS, this ranging technique without the synchronization requirement is proposed. An error correcting algorithm (ECA) is used to improve the positioning accuracy at the corners of the test-bed. Both two dimensional (2D) and three dimensional (3D) algorithms are investigated, and experimental results with high accuracy are presented. (Chapter 4)

The frequency division multiple access (FDMA) could be built in the VLP systems. Apart from this, code division multiple access (CDMA) as a multiple access technology could be a promising mechanism in the future of VLP systems. In CDMA communications, the Walsh-Hadamard codes are widely used to define individual communication channels. However, if the codes are phase shifted, which happens when the LED transmitters do not turn on simultaneously, the orthogonality property will be lost. In our thesis, a delay compensation CDMA technique with no synchronization requirement on the transmitters is proposed for the first time. At the receiver side, the IDs of the relative LED transmitters can be decoded and the signal strengths from different lamps can also be achieved. Based on this, a trilateration is used to accurately determine the position of the receiver (Chapter 5).

1.3 Organization of the Thesis

The rest of the thesis is organized as follows:

Chapter 1 briefly introduces the background and motivations of the VLC and VLP systems and summarizes the main contributions of the work in this

thesis.

Chapter 2 presents a review of both VLC and VLP. With regard to the VLC, the different types of white LEDs, channel characteristics for indoor VLC, and system performance criteria are introduced, while with regard to the VLP, identity positioning, multiple access technology, trilateration techniques, and evaluation criteria of positioning systems are mentioned.

Chapter 3 proposes the concept of inverse design for LED arrangement in the VLC systems. The optimization principle and procedures are also discussed. For the optimal arrangement based on the inverse design, the SNR fluctuation can be minimized to only 0.7 dB and the illuminance requirement is also achieved. Meanwhile, a suboptimal arrangement is also investigated in order to save cabling cost. There is a trade-off between the system performance and complexity. The suboptimal arrangement saves 17.8 % energy while keeping the SNR fluctuation within 3 dB when compared with the optimal design.

Chapter 4 demonstrates a novel IPS using FDMA with the dimensions of 100 cm $\times$ 118.5 cm $\times$ 128.7 cm. The experiment configuration for this VLP system and the procedure of designing the finite impulse response (FIR) filter are revealed. Further, a 2D positioning algorithm is applied, and the experimental results show that the mean positioning errors are within 3 cm in most locations of the test-bed. However, at the four corners, the positioning error is not as small as expected. Thus, an ECA is applied to the four corners, which helps to decrease the positioning error from 4.53 to 1.70 cm. The 3D positioning algorithm is also developed. The points at four different altitude levels are measured, and a random track is also recorded. While applying our 3D positioning algorithm, we found that the average positioning errors in 3D space are all within 3 cm.

Chapter 5 proposes a delay compensation CDMA technique, which could be used in the IPS with no requirement for transmitter synchronization. In this mechanism, a set of clclic orthogonal walsh-hadamard codes (COWHC) is used to encode the ID of the LED lamps at the transmitter side, while an asynchronous CDMA mechanism is applied at the receiver side to decode signals. Different code reuse strategies are compared. In a typical room with the dimensions 4 m $\times$ 4 m $\times$ 3 m, when seven codes are used, the mean positioning error is only 0.96 cm. Then, the code arrangements for the larger rooms or rooms with irregular shapes are discussed. While reusing nine codes, the average positioning error is as small as 1.23 cm.

Finally, concluding remarks are presented in Chapter 6 and possible extensions of the work in this thesis are recommended.

Chapter 2

Literature Review

2.1 Introduction of VLC Systems

Typical VLC systems based on LEDs are implemented with a LOS configuration using an intensity modulation and direct detection (IM/DD) scheme [3]. This kind of a system can be built by using the current state of off-the-shelf illumination components and photo detectors. A higher bandwidth can be achieved due to lower path loss and dispersion over a short distance [40]. At the transmitter side, controlling the forward current flowing through the LED will change the radiant intensity. Thus, the transmitted signal is modulated into the real-time optical power of the LED. This is the process of intensity modulation (IM). High modulation frequencies are required to avoid flicker, which is not good for human health. At the receiver side, by using direct detection (DD), the transmitted signal could be recovered. Usually, a PD is used to convert the incident optical power into a proportional current. DD is the only possible signal recovery process due to the instantaneous change of signal power. In this thesis, when setting up the VLC system, IM/DD scheme is applied.

2.1.1 Two Technologies for Generating White LEDs

Let's discuss the transmitter part first. There are mainly two types of visible LEDs. One type is single-color LEDs, such as red (R), green (G), or blue (B) LEDs. Typically, red, green, or blue LEDs emit a narrow spectral band, depending on the material system. Red LEDs emits around the wavelength ~ 625 nm, green LEDs ~ 525 nm, and blue LEDs ~ 470 nm. The other type is white LEDs, which draw much attention as the illumination devices.

At present, there are two technologies to generate white light using LEDs. One technology is the mixing of red, green, and blue (RGB) light from individual LEDs, with white light or any other color generated depending on the proportions. Typically, a single package consisting of three emitters and combining optics is often used in applications where variable color emission is required. The advantage of such a device is that color can be controlled to correct for different light intensities of different chips, and three color channels are independent, which can offer wavelength division multiplexing (WDM) for VLC systems. However, in this method, three separate LEDs are used resulting in increased cost of LED luminaire [41].

The other technology creates phosphorescent white LEDs, which are the most predominant type of white LEDs used nowadays. This kind of white light is generated by using a blue LED that has a yellow phosphor coating on the packaging. When electric current flows to the LED chip, blue light is emitted and part of it is absorbed by the phosphor to generate a second color - yellow light. The combination of blue and yellow lights results in a mixture creating white light. White lights with different color temperatures are produced by modifying the thickness of the phosphor layer [41]. Although the phosphor white LED has the advantage of low cost, the direct modulation frequency is limited to a few MHz due to the fact that the response time of

the phosphor is much lower than mixed LED chip [42]. Thus, the direct modulation speed is limited to a few MHz [29]. The power spectrum of such an LED [10] is shown in Fig. 2.1.

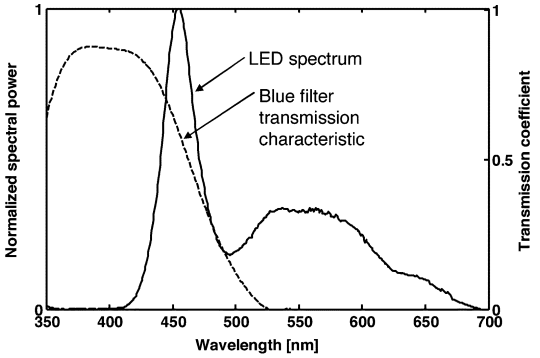

Figure 2.1: Power spectrum of an LED.

From its radiation spectrum, the luminous flux Φ [lm] can be obtained:

$$\Phi = 683\frac{lm}{W}\int_{380nm}^{720nm} p(\lambda)V(\lambda)d\lambda \tag{2.1}$$

where $p(\lambda)$ [W/m] and V(λ) denote the source power spectral distribution and the eye sensitivity function, respectively. The luminous flux presents optical power perceived by the human eye from the source.

2.1.2 Illuminance Calculation

The illuminance $E[lx]$ is defined as luminous flux per unit area, which expresses the brightness of the illuminated surface

$$E = \frac{\partial\Phi}{\partial A} = \frac{I(\theta)}{r^2}. \tag{2.2}$$

Here, the source luminous intensity $I(\theta)$ [cd], in the direction θ, reflects the radiation pattern. The distance to the illuminated surface is represented as r.

When a source is assumed with Lambert radiation and the angle of incidence is accounted for Ψ, the horizontal illuminance is

$$E_h = I_0 \cos^m(\theta) \cos\Psi / r^2, \tag{2.3}$$

where $I_0 = I(\theta = 0) = (m+1)\Phi/(2\pi)$ is the maximal luminous intensity. m is the Lambert index which is defined by the source radiation semi-angle as $m = -1/\log_2(\cos\theta_{max})$.

Modulation bandwidth and optical source power are two relevant parameters for data transmission. Fig. 2.2 shows the measured modulation bandwidth of LED [43]. By suppressing the slow phosphorescent portion of the optical spectrum ($\sim$ 500-700 nm), modulation bandwidth can be enhanced to $\sim$ 20 MHz.

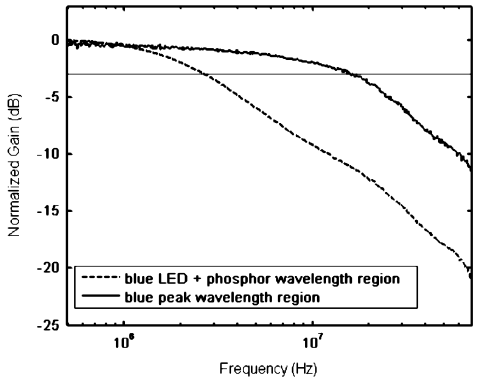

Figure 2.2: Measured modulation bandwidth of an LED.

The source optical power, P [W] (radiant flux) has no relationship to the eye sensitivity, which is given as

$$P = \int p(\lambda) d\lambda. \tag{2.4}$$

By measuring $p(\lambda)$ and knowing $V(\lambda)$, both P and Φ can be evaluated and a conversion factor α can be calculated. Estimation was that the blue peak

contains about 50 % of the source power, leading finally to the expression for optical power available in the blue peak region (for a source with luminous flux Φ)

$$P_r[mW] = \alpha/2[mW/lm]\Phi[lm]. \tag{2.5}$$

2.1.3 Channel Characteristics for Indoor VLC

At the receiver side, the received power is given by the channel direct current (DC) gain on the directed path $H_d(0)$, reflected path $H_{ref}(0)$, and initial transmitted optical power of an LED P_t as:

$$P_r = \sum_i \{P_t H(0)_i + P_t \int_{wall} \mathrm{d}H_{ref}(0)_i\} \tag{2.6}$$

where i is the ith LED, P_t is the transmitted power of each LED, and P_r is the received power. Fig. 2.3 represents the model for the received power from both the LOS and reflected beams.

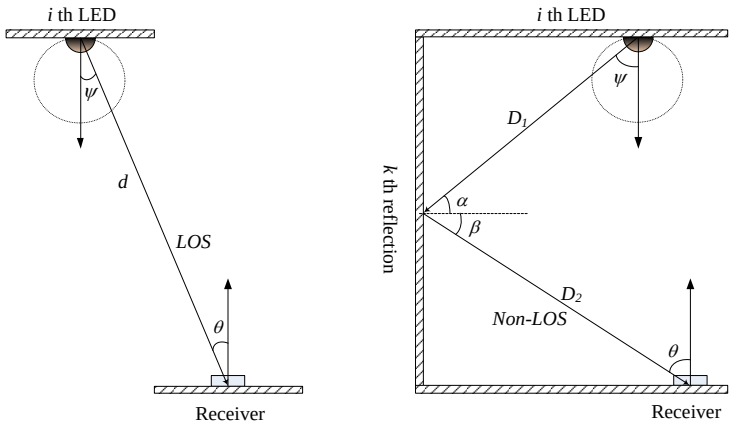

Figure 2.3: LOS and non-LOS paths of the lighting and received communications power model.

$H_d(0)$ and $H_{ref}(0)$ are given by [12]:

$$H_d(0) = \begin{cases} \frac{(m+1)A}{2\pi D_d^2}\cos^m(\psi)T_s(\theta)g(\theta)\cos(\theta), \\ 0 \leq \theta \leq \Theta_c, \\ 0, \\ \theta > \Theta_c, \end{cases} \tag{2.7}$$

where D_d is the distance between the source and the receiver, A is the physical area of the photodetector, θ is the angle of incidence, ψ is the angle of irradiance, $T_s(\theta)$ is the gain of an optical filter, and $g(\theta)$ is the gain of an optical concentrator. Further, Θ_c denotes the width of the field of vision at the receiver.

The optical concentrator gain $g(\theta)$ can be given as

$$g(\theta) = \begin{cases} \frac{n^2}{\sin^2\theta_c}, 0 \leq \theta \leq \Theta_c, \\ 0, \theta > \Theta_c, \end{cases} \tag{2.8}$$

where n denotes the refractive index. Similarly, the DC gain after the first bounce or reflection is given as

$$dH_{ref}(0) = \begin{cases} \frac{(m+1)A}{2\pi^2 D_1^2 D_2^2}\rho \mathrm{d}A_{wall} cos^m(\psi)cos(\alpha)cos(\beta)T_s(\theta)g(\theta)cos(\theta)\cos(\theta), \\ 0 \leq \theta \leq \Theta_c, \\ 0, \theta > \Theta_c, \end{cases} \tag{2.9}$$

where D_1 is the distance between an LED chip and a reflective point, D_2 is the distance between a reflective point and a receiver, ρ is the reflectance factor, $\mathrm{d}A_{wall}$ is a reflective area of the small region, ψ is the angle of irradiance to a reflective point, α is the angle of irradiance to a reflective

point, β is the angle of irradiance to the receiver, and θ is the angle of incidence.

2.1.4 SNR Calculation

Since the expression of received power is given in the channel modeling, SNR as one of the most important criterion when estimating the system performance will be discussed in this subsection. The electrical SNR can be expressed in terms of the photodetector responsively γ, received optical power, and noise variance as

$$SNR = \frac{(\gamma P_r)^2}{\sigma_{shot}^2 + \sigma_{thermal}^2}, \tag{2.10}$$

where P_r is given by

$$P_r = \sum_{i=1}^{N_T} H_i(0) P_i, \tag{2.11}$$

where N_T is the number of transmitters, $H_i(0)$ and P_i are the channel DC gain and instantaneous emitted power for the i-th LED bulb, respectively.

Following Komine and Nakagawas' research [44], the shot noise variance is given by

$$\sigma_{shot}^2 = 2q\gamma(P_r)B + 2qI_{bg}I_2B \tag{2.12}$$

where q is the electronic charge, B is the equivalent noise bandwidth, which is equal to the modulation bandwidth here, I_{bg} is the background current whosetraditional values are 5100 μA given direct exposure to sunlight and 740 μA assuming indirect exposure to sunlight [45], and the noise bandwidth factor, $I_2 = 0.562$.

On the other hand, the thermal noise variance is given by

$$\sigma_{thermal}^2 = \frac{8\pi k T_K}{G}\eta A I_2 B^2 + \frac{16\pi^2 k T_K \Gamma}{g_m}\eta^2 A^2 I_3 B^3, \tag{2.13}$$

where the two terms represent feedback resistor noise and FET channel noise. Here, k is Boltzmann's constant, T_K is absolute temperature, G is the open loop voltage gain, η is the fixed capacitance of photodetector per unit area, Γ is the FET channel noise factor, g_m is the FET transconductance, and $I_3 = 0.0868$.

In the simulation, the following values are used [27]: $T_K = 295K$, $G = 10$, $g_m = 30mS$, $\Gamma = 1.5$, and $\eta = 112pF/cm^2$.

2.1.5 Inter-symbol Interference Calculation

Since the existence of the reflected path as described in the channel modeling, ISI may occur and limit the transmission speed. Thus, in this subsection, we describe how to calculate the ISI. The amount of ISI depends the chosen transmission scenario, such as room properties, distribution of emitter chips at the ceiling and chip properties itself.

Mathematically, the impulse response of the optical wireless channel is calculated by integrating the power of all the components arriving at the receiver after a multi-path propagation. The received signal in the case of non-light of sight (non-LOS) links consists of various components arriving from different paths.

Hence, there is broadening in the pulse. The root mean square (RMS) delay spread D_{rms} is a parameter that is commonly used to quantify the time dispersive properties of multi-path channels and is defined as the square root of the second central moment of the magnitude squared of the channel impulse response, which can be calculated using the following expression [46]:

$$D_{rms} = [\frac{\int (t-\mu)^2 h^2(t) \mathrm{d}t}{\int h^2(t) \mathrm{d}t}]^{1/2}, \tag{2.14}$$

where the mean delay spread μ is given by

$$\mu = \frac{\int t h^2(t) \mathrm{d}t}{\int h^2(t) \mathrm{d}t}, \tag{2.15}$$

and the $h(t)$ is the impulse response of an LOS link and the first diffused reflection.

2.2 Introduction of VLP Systems

Apart from the two functions we have introduced in Section 2.1, which are named illumination and communication, visible light has the third function which is named positioning. As we know, indoor positioning is a key technology that can benefit many industries and customers. With the dramatically increased population of mobile devices, the demand of accurate indoor positioning will also increase. The applications of indoor positioning include location management of products inside large warehouses, location-based services and advertisements for consumers in shopping malls, and indoor navigation services for visitors in museums or theaters.

GPS is a well developed technology that performs well in outdoor applications. However, it is difficult to use it in indoor applications because of its poor coverage of satellite signals. The main reason behind this is the multi-path effects of the RF signals. GPS signals from satellites are easily reflected off by surfaces around the receiver, such as trees, roofs, cars, walls, or human bodies. The multi-path signals will arrive at the receiver side as delayed components, resulting in positioning errors. For an indoor environment, the GPS signal is downgraded to an unacceptable level that causes inaccurate positioning. Besides, artificial sources will potentially infer the GPS signals, further bringing down the performance. Due to the poor performance of the GPS system, an IPS is still in its infancy at the present.

The development of a reliable and accurate system is urgent. Different systems are proposed as candidates so far by using radio wave, acoustic, or optical technologies.

LEDs are replacing today's incandescent and fluorescent bulbs used for lighting due to their higher power efficiency, longer lifetime, and higher tolerance to environmental hazards. What is more, they can be easily modulated. These features enable researchers to explore the possibility of using it to address the indoor positioning problem. Recently, VLC using LEDs was considered as one of the most promising solutions for an IPS, also referred to as indoor localization. It can be used in indoor environments making use of installed lighting equipment as shown in Figure 2.4. The navigation map in Figure 2.5 indicates the route of arriving at the destination. The many features that it brings are listed below:

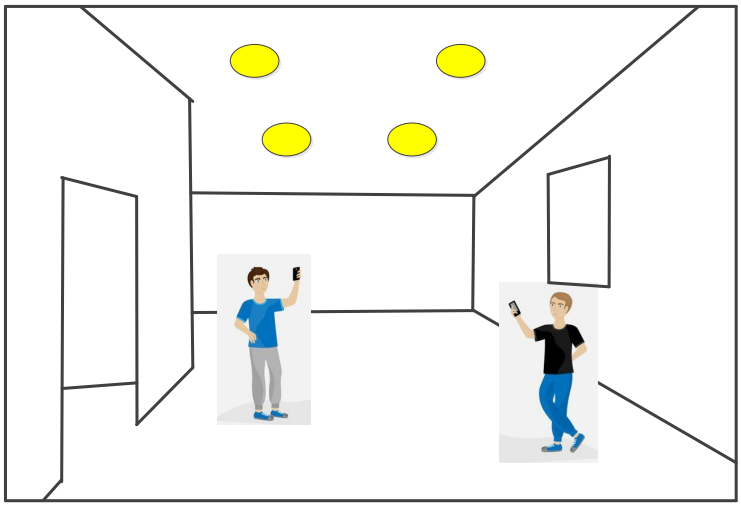

Figure 2.4: VLP systems in indoor environments.

Better Positioning Accuracy: Many attractive indoor positioning solutions are proposed based on radio wave techniques, including cellular devices, Bluetooth, ultra-wide band (UWB), wireless local area network

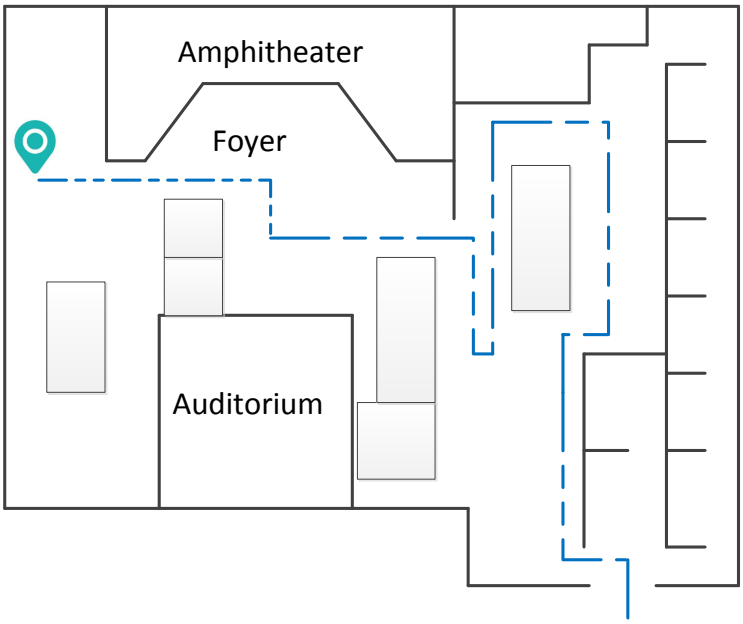

Figure 2.5: The interface on the mobile device.

(WLAN), radio frequency identification (RFID), etc. These methods achieve positioning accuracy from tens of centimeters to several meters, as illustrated in Table 2.1 [47]. VLC-based systems are expected to deliver better positioning accuracy when compared to systems based on radio wave because they suffer less from multi-path effects and interference from other wireless equipment.

Generation of No RF Interference: Apart from the relatively lower accuracy that radio wave approaches can provide, the RF EMI brought in is always a concern for many indoor environments. On one hand, the EM radiation generated by these techniques will occupy the limited mobile band that is already congested, further degrading the performance of other wireless devices. On the other hand, since RF interference can disable certain kinds of medical devices with results ranging from inconvenience to accidental injuries, RF radiation is restricted or even prohibited in some particular

Table 2.1: Positioning accuracy of radio-wave techniques

Positioning method (technology)	**Accuracy(m)**
Sapphire Dart (UWB)	0.3
Ekahau (WLAN)	1
TOPAZ (Bluetooth+IR)	2
LANDMARC (RFID)	2

areas in hospitals, such as intensive care unit, as well as in many other places that are concerned about interference.

Reusing Current Lighting Infrastructure: Although accuracy up to several centimeters can be offered using positioning techniques based on ultrasound and other acoustic waves, the current lighting infrastructure can be reused. However, a dense and calibrated grid of transmitters is required, which may dramatically increase the system cost. In contrast, positioning systems based on VLC reuse current existing light infrastructure that needs no extra installation cost. Meanwhile, little or even no renovation is needed to provide the localization service. Therefore, VLP systems can be called an economical solution.

2.2.1 Identity Positioning

Since the light beams from each LED lamp can only fall within a range of several meters, a large number of LED lamps is required in a VLP system. In order to distinguish the signals from different transmitters, each LED is assigned a unique ID number. The light sent from the LEDs is received by a dedicated receiver. A rough position of the receiver could be known based on the ID retrieved from the received signal. Such a positioning system is called a VLP ID transmission system. An example is given in Figure 2.6. When

ID1, ID5, and ID6 are the three IDs retrieved, the position of the receiver is roughly determined inside the shadow area.

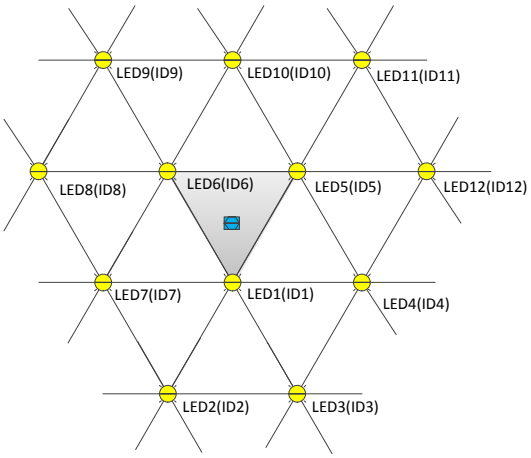

Figure 2.6: ID allocation to large numbers of LEDs in a large area.

2.2.2 Multiple Access Technology

In order to achieve more accurate positioning, signals from different transmitters are required to be distinguished at receiver side. Thus, multiple access technology should be applied.

We will introduce two kinds of multiple access technologies in the following discussion.

Frequency Multiple Access Technology

FDMA is a multi-carrier multiple access scheme where different users are assigned individual frequency bands. Unlike other solutions such as time division multiple access (TDMA) and time difference of arrival (TDOA) that need a backbone network, systems that adopt FDMA can send their information asynchronously to the receiver. In [48], an asynchronous system

based on FDMA is built where every LED gets a different carrier frequency and sends data using QPSK. Despite the fact that sufficient accuracy can be achieved for indoor positioning, this system requires an analog front-end where carrier frequencies are chosen above 1 MHz, which is close to the LED bandwidth. An FDMA solution utilizing OOK in a practical setup is proposed in [49]. However, its positioning error is not sufficient, which is as large as a few meters. In [50], by using the properties of square waves in the frequency domain, a VLP system using FDMA is presented. At the transmitter side, neighboring LEDs use multiples of the ground frequency that is assigned to the first LED, while at the receiver side, a Fast Fourier Transform (FFT) is carried out to retrieve the RSS for every LED. The positioning error is around 10 cm. However, the computing cost of this system is high.

Code Multiple Access Technology

CDMA is a channel access method used by various radio communication technologies, which allows several users to share a band of frequencies. In order to reduce the interference between the users, each transmitter is assigned an orthogonal code such that the data can be encoded by turning the LED on and off in the time domain [51]. Synchronous CDMA exploits orthogonality properties in the mathematical aspect. Vectors are used to represent the data strings. For example, vector (1,0,1,1) represents the binary string 1011. Vectors can be multiplied by taking their dot product, which sums the products of their respective components. Since orthogonal codes have a cross correlation equal to zero, they do not interfere with each other. The Walsh-Hadamard code is one of the widely used orthogonal codes.

In addition to applying CDMA in optical fiber networks [52, 53], the

principle of optically orthogonal codes is also studied for optical wireless communication. As shown in [51], synchronous CDMA can be implemented using the optical orthogonal codes (OOC) and OOK modulation with LED transmitters. One disadvantage of this technique is that the achievable data rate of devices is limited since the long OOC codes are needed to ensure optimality. The second shortcoming is that when there is a large number of devices sharing the channel access, the OOC codes are difficult to generate [54]. In [55], the code cycle modulation (CCM) is proposed to address the limited data rate issue, where different cyclic shifts of the sequence assigned to devices are used to transmit an M-ary information. Any cyclic shift of an OOC code with length L is considered a symbol, leading to the increase of the spectral efficiency by a factor of $log_2 L$. The second issue of OOC codes stimulates the design of random optical codes (ROCs), which are easy to generate and are able to support a large number of users. However, after studying the performance of the random codes, the researchers found the limits of their spectral efficiency, which was demonstrated in [56]. In [57], the authors proposed a centralized power allocation algorithm that maximizes the minimum signal to interference-plus-noise ratio (SINR) of all devices. However, this algorithm requires all LED transmitters to maintain communication with each other, which will result in a large computational complexity in the indoor environment with large numbers of transmitters and receivers.

2.2.3 Trilateration Technique

Based on the multiple access technologies we have introduced, we can distinguish different signals from different transmitters. The next step is making use of these received signals to realize the function of positioning.

Positioning algorithms that use the geometric properties of triangles for localization are generally named triangulation. There are two branches of triangulation: lateration and angulation. In the lateration method, by measuring the distance between the target location and multiple reference points, the target location can be estimated. For a general VLP system proposed, light sources are assumed as the reference points and an optical receiver as the target. Although it is impossible to measure the distances directly in most cases, they can be calculated mathematically from other measurements such as RSS, time of arrival (TOA), or TDOA. On the other hand, in the angulation method, angles of arrival (AOA) need to be measured, which are relative to the reference points. Then, the target estimation is carried out by finding intersection points of circles with radii from reference points.

Two kinds of measurements named TOA and RSS are mainly used in circular alteration methods. Because light travels at a constant speed in air, the distance between the light sources and the receiver is proportional to the travel time of the optical signals. In TOA-based systems, TOA measurements are required with respect to three light sources to locate the receiver. For 2D positioning, the estimated point is the intersection of three circles, while in a 3D scenario, it is the intersection of three spheres. The widely used GPS system is a good example of a TOA-based system. In the GPS system, the time information is contained in the navigation messages sent from satellites in the form of a ranging code as well as the orbit information for all satellites. Circular lateration, also referred to as trilateration, is performed to determine the receiver's position after receiving the navigation messages from more than three satellites successfully. However, perfect synchronization is required among all the clocks used at the transmitter and receiver sides. For indoor

applications, the positioning accuracy should be in the order of centimeters, which means that the clocks in TOA systems have to be synchronized at the level of a few nanoseconds or even at a higher accuracy. As can be imagined, the cost and complexity of such systems are impractical. Thus, the TOA-based VLP technology is very limited.

Based on the measured received signal strength (RSS), RSS-based systems calculate the propagation loss that the emitted signal experiences. Then, a range estimation is made based on a proper path loss model because in most indoor environments, LOS channels are available. RSS becomes a confidence candidate to deliver a good performance. The target can be estimated with a positioning error of ~ 0.5 mm, according to the simulated performance in [58]. By taking the rotation and moving speed of the receiver into consideration, [59] shows that an overall accuracy of around 2.5 cm can be obtained when the typical moving speed of the receiver is assumed. In [45], precision of 5.9 cm with 95% confidence can be achieved considering the possible installation errors of the LED lamps as well as the orientation angle of the receiver.

Next, we will introduce the mathematical expression for circular lateration in 2D space. The expression for 3D is similar. Let (X_i, Y_i) represent the position coordinates of the i-th transmitter, also referred to as the reference point, on a 2D plane and (x, y) denote the position coordinates of the receiver. If the measured distance between the i-th transmitter and receiver is R_i, then every circle as shown in Figure 2.7 is a set of possible locations of the receiver determined by a single range measurement, which is as follows:

$$(X_i - x)^2 + (Y_i - y)^2 = R_i^2, \tag{2.16}$$

where $i = 1, 2, \cdots, n$ and n is the number of transmitters involved in the range measurements. If we don't consider noise interference, the circles given by Eq. 2.16 should intersect at one point theoretically. However, range measurements are not noise free in a realistic environment. Multiple solutions appear in the system described by Eq. 2.16 because of the noisy range measurements. In this scenario, as discussed in [60, 61], the least squares solution provides a standard approach to an approximate solution of the positioning system.

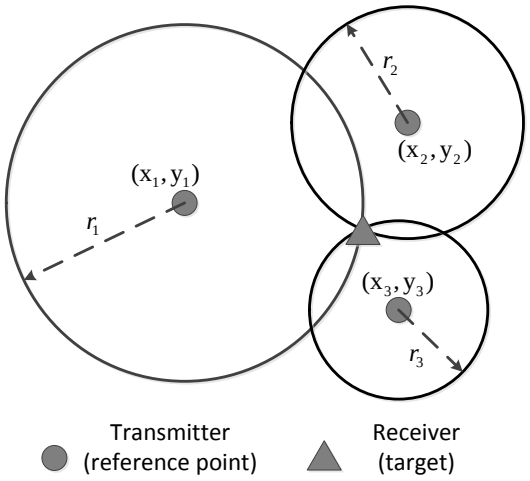

Figure 2.7: The schematic diagram of the circular alteration.

$$\begin{aligned} R_i^2 - R_1^2 &= (x - X_i)^2 + (y - Y_i)^2 - (x - X_1)^2 - (y - Y_1)^2 \\ &= X_i^2 + Y_i^2 - X_1^2 - Y_1^2 - 2x(X_i - X_1) - 2y(Y_i - Y_1), \end{aligned} \tag{2.17}$$

where $i = 1, 2, \cdots, n$. Rewritting equations describing the system in the matrix form [61] as

$$AX = B, \tag{2.18}$$

where

$$X = [x\ y]^T, \tag{2.19}$$

$$A = \begin{bmatrix} X_2 - X_1 & Y_2 - Y_1 & R_{21} \\ \vdots & \vdots & \vdots \\ X_n - X_1 & Y_n - Y_1 & R_{n1} \end{bmatrix}, \tag{2.20}$$

and

$$B = \frac{1}{2} \begin{bmatrix} (X_2^2 + Y_2^2) - (X_1^2 + Y_1^2) - R_{12}^2 \\ \vdots \\ (X_n^2 + Y_n^2) - (X_1^2 + Y_1^2) - R_{n1}^2 \end{bmatrix}. \tag{2.21}$$

The least squares solution to the system is given by

$$X = (A^T A)^{-1} A^T B. \tag{2.22}$$

2.2.4 Evaluation of Positioning Systems

Since we can get the estimated positions using the trilateration technique, then how to evaluate the system's positioning performance? While evaluating the overall performance of a VLP system, there are some evaluation criteria.

Accuracy: Positioning error is defined as the difference between the actual and estimated location coordinates [62]. The error is usually represented by the mean distance error that is the average Euclidean distance between the estimated position (X_e, Y_e) and the real position (x, y) on planar configurations. Lower values of the positioning error mean a higher location accuracy and vice versa. It is an important parameter that determines whether the solution is suitable for a specific application. For example, higher precision is required for positioning that serves a robot when compared to an LBS system in a museum. In most cases, the accuracy is a trade-off between other criteria. Apart from the mean positioning error on the estimated

position, the standard deviation is also of importance, which reflects the variation of the position error. In most cases, the P95 rule is used to give an indication of the precision [63–65]. The positioning accuracy provided by many designs is very high. However, in practical settings, it is not easy to achieve high accuracy. First, this is because the propagation of light does not follow the simplified Lambertian model, which is mostly assumed in the literature. Second, in most cases, the LOS transmission is assumed. Reflection, diffusion, and scattering of light from various objects are not considered in indoor environments. Third, simple models are used to generate thermal and shot noises.

$$error = \sqrt{(x - x_e)^2 + (y - y_e)^2} \tag{2.23}$$

Complexity: The complexity of a positioning system is determined by two components: hardware and software. The hardware complexity refers to all the hardware components and the effort required to integrate them in order to develop a VLP system. Low hardware complexity means smaller design requiring LEDs, less processing, and fewer circuit components and sensors. Photodiode (PD)-based designs, such as TDMA, have more complex transmitters due to their strict timing and synchronization requirements. On the other hand, designs employing FDMA are more complex on the receiver side since several filters are required to distinguish signals from different transmitters. AOA-based designs can decrease the complexity by placing the receiver parallel to the ceiling. In order to reduce the installation cost, expansive large network infrastructure should be avoided.

Low complexity software plays an important role in operation speed and power consumption. Algorithms with low complexity of mathematical computation are always desirable because lower power consumption will help

in extending the life of a mobile device's battery. In most cases, because the receiver is usually a mobile device with limited resources and energy, it is important to keep these limitations in mind. Additionally, when compared to more complex methods, lower computational complexity can also provide a faster response time so that the estimated position is quickly updated. While positioning people, the requirement for an updated rate is not so high. However, while positioning moving objects such as robots that travel faster, a higher update rate is necessary [63, 64].

Among PD designs, simultaneous equation-solving algorithms have the least computational complexity, whereas trilateration, triangulation, and multilateration algorithms require iteration to determine the target position, which increases their computing time.

Robustness: The robustness of a design is defined as an adequate positioning estimate in the absence of minimal system requirements, even when signals are absent. Sometimes, signals may be obstructed due to the presence of physical objects or parameters used for positioning algorithms deliver unrealistic values in some circumstances. All these problems should be avoided as much as possible in the first place. However, when they do occur, the system with strong robustness should be able to recognize them and still deliver relevant information [63, 64].

In PD-based designs, TDMA requires strict timing synchronization between transmitters, which means that if the synchronization property is not held, a huge impact will occur on the performance. In FDMA designs, the quality of bandpass filters and frequency mismatch between crystal oscillators will decrease the positioning quality. AOA-based techniques cannot be used in the absence of a dominant LOS path, whereas TDOA-based techniques are extremely sensitive to phase and timing errors.

Scalability: When a positioning system is implemented in large rooms or rooms with irregular shapes, the functionality for positioning should be valid over the entire area. In most cases, the positioning error becomes larger when the distance between the references and target increases. Additionally, when the density of the reference beacons increases (which means that more beacons exist per square area), the inter-channel interference will increase and thus decrease system accuracy. Apart from the scalability in 2D positioning, the 3D case should also be considered in a system with good scalability [63, 64].

Cost: As indicated before, the cost of a system not only depends on the installation cost, for example, hardware and software components but also on the time needed to build and maintain the system, the space it occupies, and the power and energy it consumes. The potential reuse of the existing lighting infrastructure helps in reducing costs. Now, the most important factor is the energy consumption of the system [63, 64]. Typically, three or four LED lamps are used for the positioning algorithm in a VLP system. If more transmitters are applied, the robustness in non-ideal conditions will increase. However, this scheme is more expensive and complex.

In PD-based designs, TDMA requires synchronization, thus making the transmitter circuit costlier, whereas the receiver design based on FDMA is more complex and therefore expensive.

2.3 Conclusion

This chapter provided a brief introduction for both visible light communication and visible light positioning systems. With regard to the VLC, two ways to generate white LEDs were discussed. The channel

characteristics were modeled. The system performance criteria such as illumination, SNR, and RMS delay spread were clarified in detail. With regard to the VLP, the motivation of introducing identity positioning was discussed. Two widely used multiple access technologies were reviewed in particular. Trilateration techniques were also discussed and compared. Then, the evaluation criteria of positioning systems were listed.

Chapter 3

VLC system with Novel LED Arrangement

3.1 Overview

For VLC systems, as the channel characteristics depend on the room size, and the material properties of reflective surfaces, the same VLC mobile terminal may experience different performance in different locations. One of the key problems for indoor VLC systems is to achieve uniform communication performance at different locations without affecting the primary illumination function. In [66], the luminance performance is compared with different ceiling plans for the LED array layouts. A novel LED lamp arrangement with 12 LEDs evenly distributed on a circle and four LEDs located at the corner is proposed to reduce the uniform SNR fluctuation, which guarantees users can achieve almost identical communications quality in [67]. Two indoor lighting systems using the square and hollow designs are compared, showing that there is a considerable potential to optimize the layout of luminaries within a room, as [68] shows. [69] proposes a modern style lighting design relying on

four LED lights placing at the corner of the room and one LED light being placed at the center of the area to make the light uniformly distribute. [70] analyzes the illumination properties using rectangular and circular LED arrangements with adjustable distance between the lamps and the center of the ceiling. However, in all above works the system performances are based on the fixed LED arrangement. In [71, 72], an evolutionary algorithm based optimization scheme is proposed to realize uniform received power and illumination distribution on the communication floor. However, genetic algorithm sometimes converges to local optimum, thus cannot reach the global optimum. The performance of the algorithm varies with the number of the initial population.

However, in this chapter, we propose an inverse design based on convex optimization for the LED arrangement, which can meet the requirements of illuminance and data communications. As far as I know, our optimal design can offer a smaller SNR distribution compared with other literature. In order to save the cabling cost, a suboptimal system is also discussed, which shows a trade-off between the system performance and complexity. Compared with the optimal design, the suboptimal arrangement saves 17.8 % energy and keeps the SNR fluctuation within 3 dB. This chapter is organized as follows. In section 3.2, the system model is outlined. The optimization procedures are introduced in section 3.3. The performance evaluation is described in section 3.4, followed by the concluding remarks in section 3.5.

3.2 System Model

In VLC systems, a certain level of illumination by the LEDs is required for lighting and SNR for data communications. In this work, there are N LED

locations uniformly distributed on the ceiling. Each LED has a Lambertian radiation pattern. A number of LEDs can be placed at each location. M receivers are also uniformly located on the communication plane, 0.85 m above the ground. Each receiver is orientated vertically upwards.

The received power is given by the channel gain on the directed path $H_d(0)$, reflected path $H_{ref}(0)$ and the transmitted optical power of the LED P_t as

$$Pr_j = \sum_i \{Pt_i H_d(0) + Pt_i \int_{wall} dH_{ref}(0)\}, \tag{3.1}$$

where Pt_i is the transmitted power from ith LED location, Pr_j is the received signal power of jth receiver and $1 \leq i \leq N$, $1 \leq j \leq M$. The simplified expressions for $H_d(0)$ is given by [73]:

$$H_d(0) = \begin{cases} \frac{(m+1)A}{2\pi D_d^2}\cos^m(\psi)\cos(\theta) & 0 \leq \theta \leq \Theta_c \\ 0 & \theta \geq \Theta_c \end{cases}, \tag{3.2}$$

where D_d is the distance between the source and the receiver, A is the physical area of photodetector, θ is the angle of incidence, ψ is the angle of irradiance, and Θ_c denotes the width of the field of vision at the receiver. The Lambert index m depends on the source half power angle (HPA) $\Psi_{1/2}$ as

$$m = -1/\log_2(\cos\Psi_{1/2}). \tag{3.3}$$

Similarly, the DC gain after one bounce or reflection is given as:

$$dH_{ref}(0) = \begin{cases} \frac{(m+1)A}{2\pi D_1^2 D_2^2}\rho \mathrm{d}A_{wall}\cos(\psi)\cos(\alpha)\cos(\beta)\cos(\theta) & 0 \leq \theta \leq \Theta_c \\ 0 & \theta \geq \Theta_c \end{cases}, \tag{3.4}$$

where D_1 is the distance between an LED chip and a reflective point, D_2 is the distance between a reflective point and a receiver, ρ is the reflectance factor, $\mathrm{d}A_{wall}$ is a reflective area of small region, ψ is the angle of irradiance

to a reflective point, α is the angle of incidence to a reflective point, β is the angle of irradiance to the receiver, θ is the angle of incidence. We can see that the relationship between the received power and transmitted power is determined. For practical implementation, the distribution of received power within the indoor coverage can be obtained by channel estimation with the help of pilot symbols. With the knowledge of relationship between the transmit power and received power, our inverse design scheme can be applied. In the following discussion, we present the received power for illumination as $Pr(ill)$ while for communication as $Pr(sig)$.

In indoor VLC systems, the data rate limitation is mainly attributed to the first reflection, hence in this chapter, the impulse response of the LOS link and the first order reflection are taken into account to investigate the performance of the proposed system model [2].

3.3 Optimization Principle

In the first step, the transmitted power for data communications at different LED locations will be calculated in order to achieve an uniform SNR distribution on the receiver plane.

We define the SNR as the total electrical signal power generated by the PD over the noise power in bandwidth B. Thus, SNR $= 2\gamma^2 Pr^2(sig)/(N_0 B)$, where γ denotes receiver responsivity, and N_0 the double-sided noise power spectral density over the bandwidth B. The dominant noise factor is the background shot noise. As the received optical signal power is the sum of powers coming from all LED lights as outlined in Eq. 3.1, it can be also expressed in matrix format: $Pr(sig) = Pt(sig)H$, where H is the $N \times M$ channel gain matrix and $H_{i,j}$ is the channel gain from ith transmitter to jth

receiver. $Pr(sig)$ is a $1 \times M$ vector, in which the jth element means the received signal power at jth receiver. In a similar way, the ith element in the $1 \times N$ vector $Pt(sig)$ is the transmit power value at ith transmitter. Thus, the SNR can be expressed as:

$$\text{SNR} = 2\gamma^2 Pt^2(sig)H^2/(N_0 B). \tag{3.5}$$

The probability of error for non return-to-zero (NRZ) OOK optical data, detected with a PD, can be expressed as a function of the SNR [74]:

$$\text{BER}_{NRZ-OOK} = \frac{1}{2} erfc(\frac{1}{2\sqrt{2}}\sqrt{\text{SNR}}). \tag{3.6}$$

In order to achieve a quasi-error free communication, where BER = 10^{-9}, SNR should be at least 21.6 dB according to Eq. 3.6.

We assume that the average SNR of all receivers is 10log$C$ dB, where C is the average SNR of all receivers. Then we determine the transmit signal power at each LED location inversely. If we choose the average SNR as 21.6 dB, at the some place, the SNR will smaller than 21.6 dB and cannot achieve BER = 10^{-9}. In order to guarantee everywhere in the receiver plane can achieve the quasi-error free communication, we choose the average SNR as 22 dB to make sure that SNR at all the receiver plane is above 21.6 dB. The objective function can be written as:

$$\begin{aligned} &\text{minimize} \quad \|(2\gamma^2 Pt^2(sig)H^2/(N_0 B) - C)\| \\ &\text{subject to} \quad Pt_i(sig) \geq 0. \end{aligned} \tag{3.7}$$

In the above objective problem, the only variable that needs optimizing is $Pt(sig)$. That means after properly choosing the value for Pt, the SNR value of each receiver is fluctuating slightly around 22 dB. The operation $\| \ \|$ means the Euclidean norm. However, it is hard to solve it efficiently since the objective function is not a convex function. Because γ, H, N_0 and B are all

determined variables, we introduce a $N \times M$ matrix $K = \sqrt{(2\gamma^2)/(N_0 B)}H$ as a matter of convenience. After easy algebraic transformation, we can also recast the objective function in a new expression:

$$\begin{aligned} &\text{minimize} \quad \|(Pt(sig)K - \sqrt{C})\| \\ &\text{subject to} \quad Pt_i(sig) \geq 0. \end{aligned} \tag{3.8}$$

As Eq. 3.8 is a convex quadratic function, then we can apply barrier method to solve it efficiently [46]. This problem with inequality constrain can approximate to

$$\text{minimize } f = t \times (Pt(sig)K - \sqrt{C})(Pt(sig)K - \sqrt{C})^* - \sum_i \log Pt_i(sig), \tag{3.9}$$

which is still convex and differentiable. Here, t is a parameter that sets the accuracy of the approximation and $*$ means the conjugate operation.

The Gradient and Hessian of Eq. 3.9 are:

$$\nabla f = 2tPt(sig)KK^* - 2t\sqrt{C}K - 1/Pt(sig), \tag{3.10}$$

$$\nabla^2 f = 2tKK^* + diag(1/Pt^2(sig)). \tag{3.11}$$

As t increases, the approximation becomes more accurate. On the other hand, when the parameter t is large, the Eq. 3.9 is difficult to minimized by Newton's method, since its Hessian varies rapidly near the boundary of the feasible set. It is a tradeoff between the accuracy and stability. This problem can be circumvented by solving a sequence of problems with form (3.9), increasing the parameter t (and therefore the accuracy of the approximation) at each step, and starting each Newton minimization at the solution of the problem for the previous value of t. We refer to each execution of Newton minimization as a centering step or an outer iteration, and to the first centering step as the initial centering step. We term the Newton

iterations or steps executed during the centering step as inner iterations. Then, the Newton step is computed, which means a descent direction. Both of them are determined by the Gradient and Hessian of the convex problem. Next, whether the stop criterion can be satisfied is checked. If not, apply the backtracking line search to choose a suitable step size, which can be used to update the value of $Pt(sig)$. Based on the aforementioned process to solve the convex optimization problem, a set of optimal value for $Pt(sig)$ is found, which matches well with the results solved by CVX (a matlab toolbox). The detail description of applying the above-mentioned method to our convex problem is summarized in Algorithm 1.

Usually, the total transmit power can be written in this way: $Pt = P_0(1+ M_{index}x(t))$, where P_0 is the DC power, M_{index} is the modulation index and $x(t) \in [-1, 1]$ is the transmit signal for the bipolar OOK modulation. Then, we can deduct that $Pt(ill) = P_0$ and $Pt(sig) = M_{index}P_0$. That means

$$M_{index} = Pt(sig)/Pt(ill). \tag{3.12}$$

Based on the determined $Pt(sig)$ value, the value of $Pt(ill)$ for each LED location can be known when M_{index} is determined. Given that for each LED chip the level of optical power is p mW, we can deduce that the number of LED chips n at different locations is $n = Pt/p$. For $Pt = 0$, it means no LED ($n = 0$) will be located at the given point.

In the next step, we will verify whether our LEDs arrangement can provide sufficient brightness for a typical office environment. As mentioned in [42,43], the source optical power can be expressed as $Pt(ill) = \alpha \times \Phi$, where α is a conversion factor, and Φ is the luminous flux. After simple mathematical transformations, the $Pr(ill)$ can be calculated from the received brightness level as:

$$Pr(ill) = EA_R\alpha, \tag{3.13}$$

Algorithm 1 Barrier Method

Require:

Given a strictly feasible point $Pt_i(sig) > 0$, $1 \leq i \leq N$; $t := t^{(0)} > 0$; $\mu > 1$; ▷ $\mu = 15$ tolerance $\epsilon > 0$ ▷ $\epsilon = 1e-8$ $k = 1$; tolerance $NewtonStop > 0$; ▷ $NewtonStop = 1e-6$;

$s = 1$; $\zeta = 0.01$; $\eta = 0.5$;

repeat

  repeat ▷ Centering step

    $dPt^{(k)}(sig) \leftarrow -\nabla f^{(k)}/\nabla^2 f^{(k)}$; ▷ f is Eq. 3.9

    $Pt^{(k+1)}(sig) \leftarrow Pt^{(k)}(sig) + s * dPt^{(k)}(sig)$;

    $\lambda^{(k)} = (\nabla f^{(k)})^2/(\nabla^2 f^{(k)})$;

    while $P_i(sig) < 0$ **do** $s \leftarrow \eta s$

    end while

    $fd^{(k)} = f(Pt^{(k+1)}(sig))$

    while $fd^{(k)} > f^{(k)} + \zeta * s * (\nabla f^{(k)} * dPt^{(k)}(sig))$ **do**

      $s \leftarrow \eta s$;

      $fd^{(k)} \leftarrow f(Pt^{(k+1)}(sig))$;

    end while

    $k \leftarrow k + 1$;

  until $\lambda^{(k)} \leq NewtonStop$;

  Update: $Pt(sig) := Pt^{\star}(sig)$;

  Increase t: $t := \mu t$;

until $\frac{m}{t} \leq \epsilon$

where E expresses the brightness of the illuminated surface. It is defined as luminous flux per unit area: $E = \partial\Phi/\partial A_R$, where A_R is the detector's area. According to the International Organization for Standardization (ISO), an illumination level between 300 and 1500 lx is required for sufficient illumination [73]. Since we have known $Pr(ill)$, we can readily calculate the illumination value E and verify if it is sufficient for an office. What is more, a general recommendation is that on the desk, the illuminance is expected uniform. The ratio of the minimum to the average illuminance is defined as the uniformity illuminance ratio (UIR), which should be larger than 0.7, according to lighting engineers [73].

In the third step, based on our LEDs arrangement, we analyze the distribution of RMS delay spread to see whether the inter-symbol interference (ISI) will occur. The definition of RMS delay spread is described in Eq. 2.14. For each transmitted symbol, we assume that all signals arriving at the receiver with a delay of more than half of the symbol period T_{sym} after the first signal contribute to ISI. Therefore, the received optical signal power is

$$P_{R,sig} = \sum_i P_R(t_i \leq T_{sym}/2), \tag{3.14}$$

$$P_{R,ISI} = \sum_i P_R(t_i > T_{sym}/2). \tag{3.15}$$

Given the bandwidth of the transmitted signal is limited to the LED modulation bandwidth B, the Nyquist symbol period T_{sym} is limited to $1/(2B)$ ns, and ISI will occur if transmitted data symbols experience delays larger than $T_{sym}/2$ ns. In a more realistic case, when raised-cosine pulses with a roll-off factor of e.g., Γ=0.5, ISI will occur when delays are larger than T_{sym} ns. By analyzing the delay spread, we check whether our LEDs arrangement can achieve ISI-free communication.

3.4 System Performance Based on Inverse Design

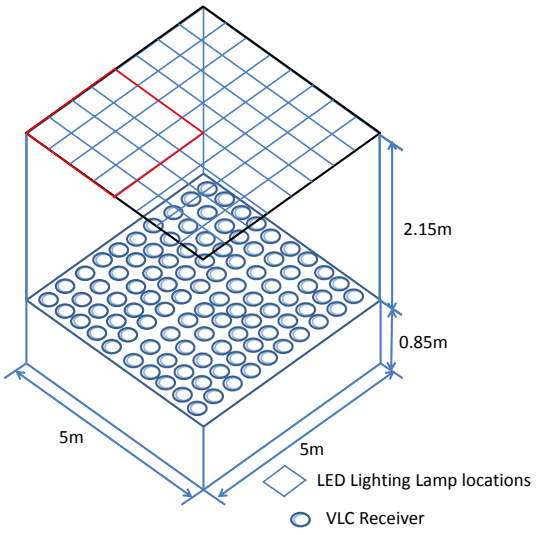

Figure 3.1: A room with 64 LED locations and 100 receivers.

An example system with 64 LED locations (N=64) and 100 receivers (M=100) is discussed in this section, as shown in Fig. 3.1. Our room model with dimensions $5 \times 5 \times 3(m^3)$ is adopted in many papers [43, 73]. The LED chips which are used to place at different locations in this paper are the commercially available white light LED (blue LED pulse phosphorous layer). We choose the same LED chip as [43], in which the level of optical power for each LED chip is 63 mW [75]. The manufacturer provides the figures for radiation angle and possible luminous intensity, power, and the conversion factor of 2.1 mW/lm is obtained for this type of LED. By suppressing the slow phosphorescent portion of the optical spectrum (∼500-700 nm), the modulation bandwidth can be enhanced from 2 to 20 MHz. That means, without any blue filtering, the modulation bandwidth is 2 MHz. In order to attain high modulation bandwidths and thus high data rates, it is possible

Table 3.1: Simulation parameters

Parameters	Value
LED half angle power ($\Psi_{1/2}$)	60 (deg)
Receiver detector area	3 (cm^2)
Half field of view (Θ_c)	80 (deg)
Room dimensions	$5 \times 5 \times 3$ (m^3)
Receiver plane height	0.85 (m)
LED plane height	3 (m)
Wall reflection coefficient (ρ_{wall})	0.7
Responsivity (γ)	0.28 (A/W)
Conversion factor (α)	2.1 (mW/lm)
Modulation bandwidth (B)	20 (MHz)

to enhance the modulation bandwidth (B) to 20 MHz [76]. After blue-light filtering, the induced photocurrent at the receiver becomes four times smaller than usual case, which we assume as $I_{photo} = 0.62$mA, and the noise power spectral density is $N_0 \cong N_{shot} = qI_{photo} \sim 10^{-22}\text{A}^2/\text{Hz}$ [42, 43], where q is the electron charge. The detail calculation of the parameters about the noise has been introduced from Eq. **??** to Eq. 2.13 in Chapter 2. Usually, the maximum modulation depth chosen is 0.25 [77], which is limited by the maximum output power of the generator. The responsivity of Si-based photodiodes is ∼0.28 A/W in the blue region [43]. Other relative system parameters are summarized in Table 3.1.

In the first step, after solving Eq. 3.7, the transmit power needed to allocate at different places can be known. Then, the number of LED chips for each location can be determined. Based on the LEDs arrangement, we can get the SNR and illumination distributions on the receiver plane. Both

the detail view and the full view of the SNR distribution are given in Fig. 3.2. The warm-toned color means the larger value than the cool-toned color. Here, due to the geometric symmetry of room, only one quarter of the receiver plane is demonstrated in detail view. we see that the maximum and minimum values of SNR are 22.4 dB and 21.7 dB, respectively. The SNR fluctuation is only 0.7 dB.

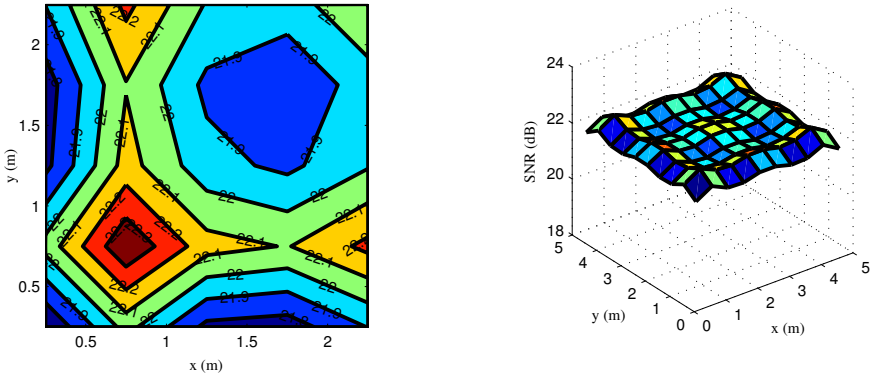

(a) (b)

Figure 3.2: (a) Detail view of the SNR [dB] distribution on the left bottom quarter of the working plane. (b) Full version of the SNR distribution with the optimal LED arrangement.

However, the illuminance level is between 56 lx and 81 lx, which is much lower than the brightness requirement, as shown in Fig. 3.3. Since the general lighting is considered as the primary purpose for an LED source (with data transmission as its secondary function), our design needs to ensure sufficient horizontal brightness at the desktop surface.

As the horizontal brightness has a linear relationship with the received power and the received power can be raised by increasing the transmit power, we can conclude that if we proportionally increase the number of LED chips at different locations, the brightness of the receiver plane will increase while the SNR variance can be kept. If the number of LED chips is increased to 8 times

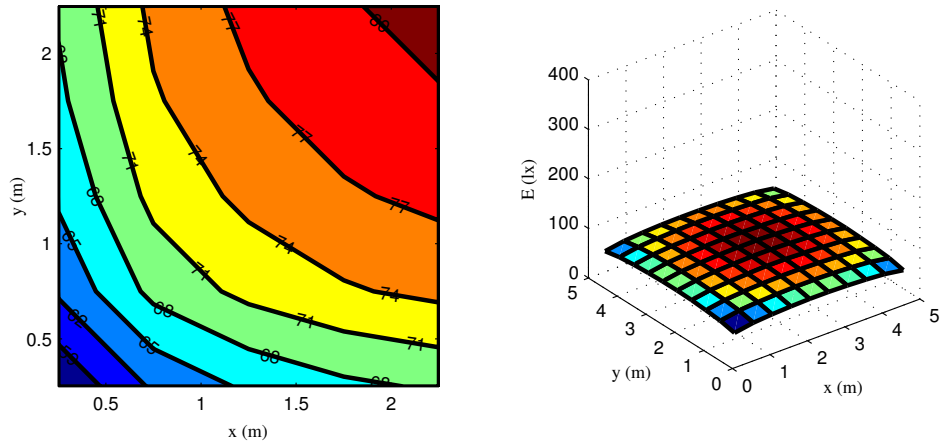

(a) (b)

Figure 3.3: (a) Detail view of horizontal brightness E [lx] on the left bottom quarter of the working plane. (b) Full version of E [lx] with the optimal LED arrangement.

of the original design, the configuration of the LED arrangement is shown in Fig. 3.4 (a). We call this Case 1 design. Due to the geometric symmetry of the room, only one quarter of the 64 LED locations is demonstrated, as shown in the red square in Fig. 3.1. Thus, according to the solution of Eq. 3.8, the average power of each LED chip, and the requirement of brightness, the number of LED chips in each location is determined. Different colors are used to present LED locations with different numbers of LED chips. Purple, red, blue, green, and yellow squares mean LED locations with 93, 50, 37, 20 and 17 LED chips, respectively. This definition can also be applied to Case 2 to Case 4. Under Case 1 design, the brightness requirement can be achieved, as shown in Fig. 3.4 (b). The horizontal brightness varies from 450 lx to 648 lx, which is between 300 lx to 1500 lx. The SNR fluctuates from 39.8 dB to 40.5 dB, with 0.7 dB fluctuation, as revealed in Fig. 3.4 (c). The distribution of the RMS delay spread under this LED arrangement

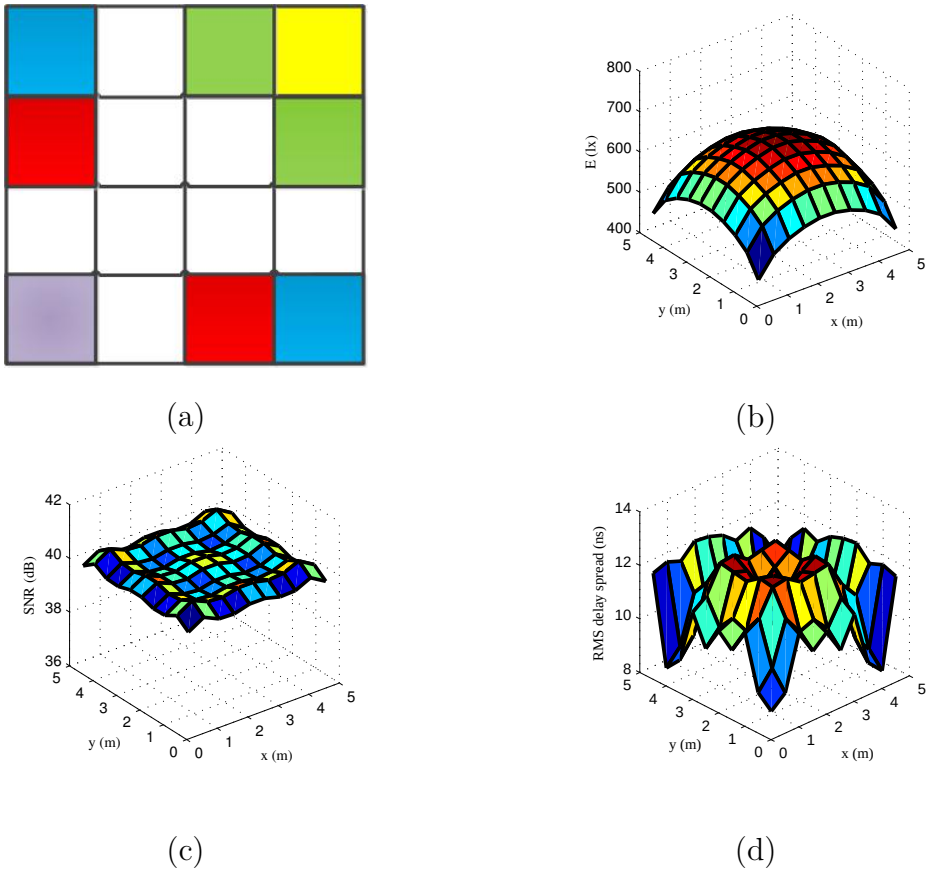

Figure 3.4: Case 1 design (a) LED configurations (Purple, red, blue, green, and yellow squares mean LED locations with 93, 50, 37, 20 and 17 LED chips, respectively), (b) the corresponding horizontal brightness distribution, (c) the corresponding SNR distribution, and (d) the corresponding RMS delay spread.

at the desktop surface is drawn in Fig. 3.4 (d). The RMS delay spread for the system varies from 8.1 ns to 12.6 ns. That means all signal components arrive at the receiver within much less than half of the symbol time (50 ns) and the ISI free communication can be realized.

However, the number of LED chips needed is too high for a small room in our system. In order to save energy, reduce the system complexity and save cabling cost, we will not place LEDs at the locations where contains small

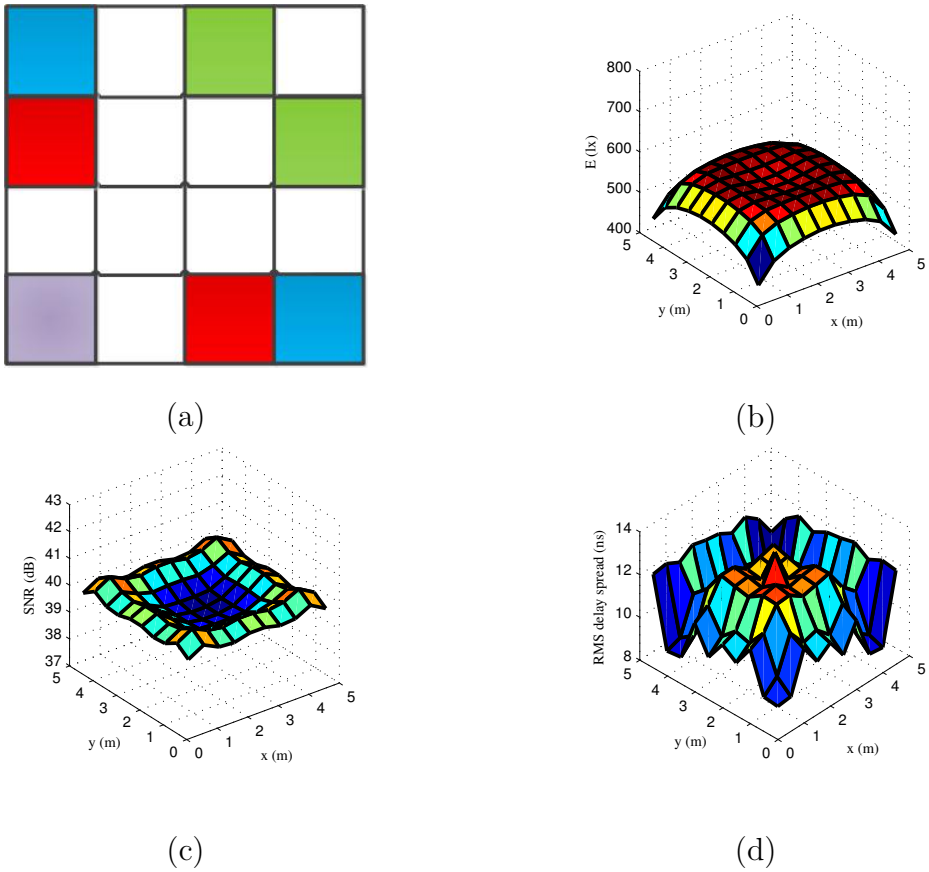

Figure 3.5: Case 2 design (a) LED configurations (Purple, red, blue, and green squares mean LED locations with 93, 50, 37, and 20 LED chips, respectively), (b) the corresponding horizontal brightness distribution, (c) the corresponding SNR distribution, and (d) the corresponding RMS delay spread.

number of LED chips based on the optimization design (Fig. 3.4). Because the yellow square means LED location with only 17 LED chips, in which place the least number of LED chips are contained, the LEDs located here are deleted first in order to save cabling cost. Then, we get Case 2 design, as Fig. 3.5 shows. It is necessary to mention again that when showing LED configurations, we only reveal one quarter of the 64 LED locations as shown in the red square in Fig. 3.1. It is not difficult to get the whole plane's LED

arrangement based on the symmetry of the transmitter plane. By deleting the yellow square, the illumination fluctuation becomes smaller with minimum value 436 lx and maximum value 561 lx. The SNR fluctuation increases from 0.7 dB to 1.1 dB, with the minimum SNR 39.3 dB and maximum 40.4 dB. Then, whether it can offer the ISI-free communication is checked in Fig. 3.5 (d). As is shown, the RMS delay spread of Case 2 fluctuates from 8.4 ns to 13.3 ns. Case 2 achieves quite similar performance with Case 1 because smallest change has been made from Case 1 to Case 2.

In Fig. 3.6 (a), the green squares are deleted which contain the least number LED chips among the rest LED locations. The illumination variance becomes even smaller compared with Case 2, which varies from 375 lx to 470 lx. That means Case 3 can still offer sufficient brightness. The SNR fluctuated between 37.4 dB and 40.2 dB. The fluctuation becomes 2.8 dB. The RMS delay spread varies from 8.8 ns to 13.2 ns, which means ISI free communication can still be guaranteed.

However, if reducing the number of LED locations further, as shown in Fig. 3.7, the illumination requirement cannot hold because it ranges from 242 lx to 361 lx, while the minimum tolerance brightness is 300 lx. The SNR variation increases to 4.0 dB, which varies from 23.4 dB to 27.4 dB while the RMS delay spread varies from 7.9 ns to 13.0 ns.

The numerical system performance is summarized in Table 3.2. From the SNR uniformity point of view, although SNR fluctuation in Case 3 is slightly larger than Case 1 and Case 2, it is still no more than 3 dB, which is not very significant variation as we assumed [78]. Compared with Case 1, Case 3 not only saves 17.8 % energy, but also cabling cost. As for illumination, although the UIRs for all four cases are more than 0.7, only the first three cases meet the illuminance requirement of ISO. However, Case 3

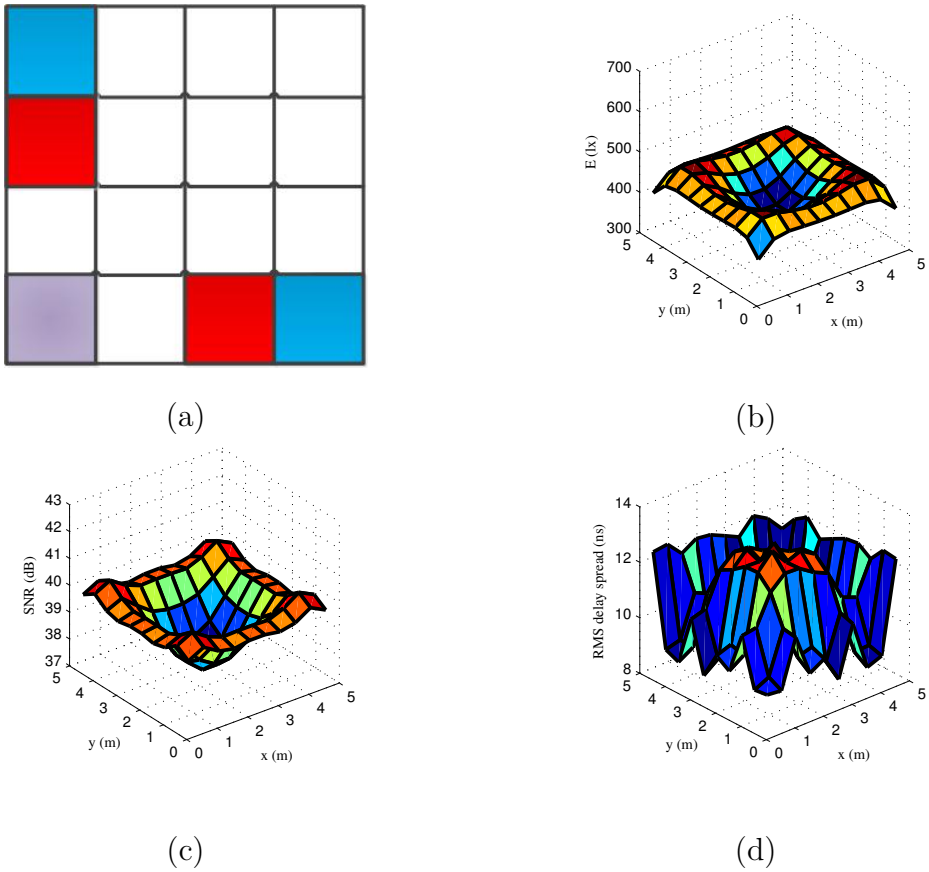

Figure 3.6: Case 3 design (a) LED configurations (Purple, red, and blue squares mean LED locations with 93, 50, and 37 LED chips, respectively), (b) the corresponding horizontal brightness distribution, (c) the corresponding SNR distribution, and (d) the corresponding RMS delay spread.

offers the minimum brightness fluctuation, which is only 95 lx. This steady illuminance performance can be also reflected by the largest UIR value that Case 3 achieved. After balancing the number of LED locations and SNR uniformity, Case 3 is selected as the suboptimal arrangement. As for the RMS delay spread, ISI free communication can be guaranteed for all four cases luckily. Nevertheless, ISI can potentially be encountered in large rooms with high ceilings (e.g., conference halls, churches and auditoriums) where

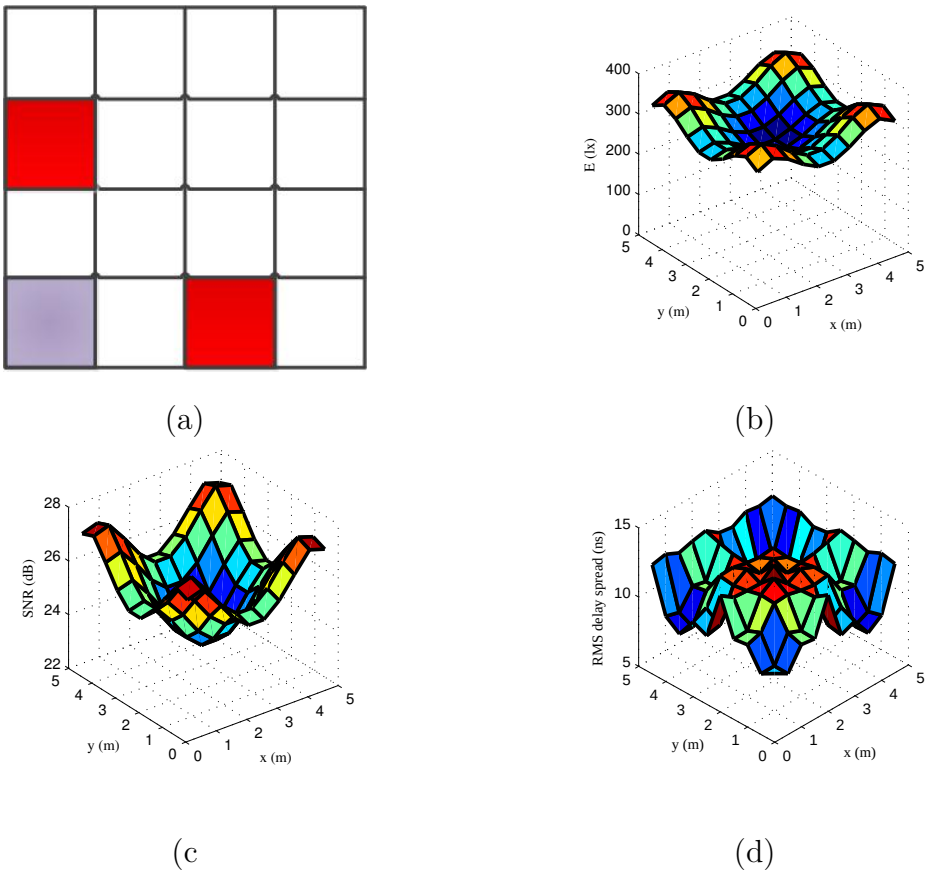

Figure 3.7: Case 4 design (a) LED configurations (Purple and red squares mean LED locations with 93 and 50 LED chips, respectively), (b) the corresponding horizontal brightness distribution, (c) the corresponding SNR distribution, and (d) the corresponding RMS delay spread.

differences in optical paths become significant with respect to the symbol length.

3.5 Conclusion

In this chapter, we proposed to formulate the LED distribution as a convex optimization problem by using the concept of inverse design. Sufficient

Table 3.2: System performance for four cases with various LED arrangements

LED arrangement	SNR			Illuminance			RMS delay spread	
	Min (dB)	Max (dB)	SNR fluctuation (dB)	Min (lx)	Max (lx)	UIR	Min (ns)	Max (ns)
Case1	39.8	40.5	0.7	450	648	0.78	8.1	12.6
Case2	39.3	40.4	1.1	436	561	0.82	8.4	13.3
Case3	37.4	40.2	2.8	375	470	0.86	8.8	13.2
Case4	23.4	27.4	4	242	361	0.80	7.9	13.0

brightness and uniform signal to noise ratio can be achieved using the LED arrangement optimized by the proposed scheme. The suboptimal LED arrangement design was provided, which can reduce the power consumption of the system with acceptable performance degradation.

Chapter 4

Asynchronous VLP system with FDMA

4.1 Overview

For VLP systems, some main ranging techniques include RSS, TDOA, and phase difference of arrival (PDOA) [79, 80]. However, for those systems using TDOA or PDOA, perfect synchronization is required. For the systems applying RSS, when time division multiplexing (TDM) technique is used to differentiate the light from different LEDs [58, 81], synchronization is also required among LEDs. As we know, in a commercial system, the synchronization is very difficult to realize, since the LED lamps are usually used only as transmitters, so they cannot receive synchronization signal. Thus, an asynchronous ranging technique is promising.

Although RSS is widely used in the indoor VLC-based positioning systems and the positioning accuracy of some reported indoor RSS-based VLP systems can reach a few centimeters, however, most of them can only realize the 2D localization [23, 45, 48]. In [81, 82], positioning error of less than 3 cm

have been reported in 3D localization, however, besides the light sensor, an extra accelerometer or gyro-sensor is required for the system, which increases the positioning algorithm complexity. An asynchronous IPS using VLC technology has been demonstrated in [45]. The Basic-framed slotted ALOHA (BFSA) protocol is used to solve the channel multiaccess problem. An accuracy of 5.9 cm can be achieved when locating the target receiver, with over 95 % confidence. However, this work is only based on simulation in a typical LOS communication environment. In practical systems, a multi-path model is preferred since signals can be reflected by multiple surfaces. In our previous work [83], a positioning system is built and the experiment is carried out. The experiment results show that the average distance errors of x and y coordinates are 1.7 cm and 2.1 cm, respectively. However, this result is based on the the experiment done in the central area of the test bed because on the margin area, the positioning accuracy could become much worse. In this work, the experiment can be carried out on the whole test-bed. Not only 2D but also 3D positioning algorithms are developed and demonstrated. What is more, an ECA is also developed to improve the corner performance of system. With the help of RSS measurements from the modulated LEDs, the asynchronous positioning with high accuracy is achieved in the experiments.

This chapter is organized as follows. The system model and relevant notations are described in Section 4.2. Both the 2D and 3D positioning algorithms for indoor PD-based VLP are proposed and the ECA is also introduced in Section 4.3. The experiment results are given in Section 4.4 and the conclusion is drawn in Section 4.5.

4.2 System Configuration for Indoor Positioning

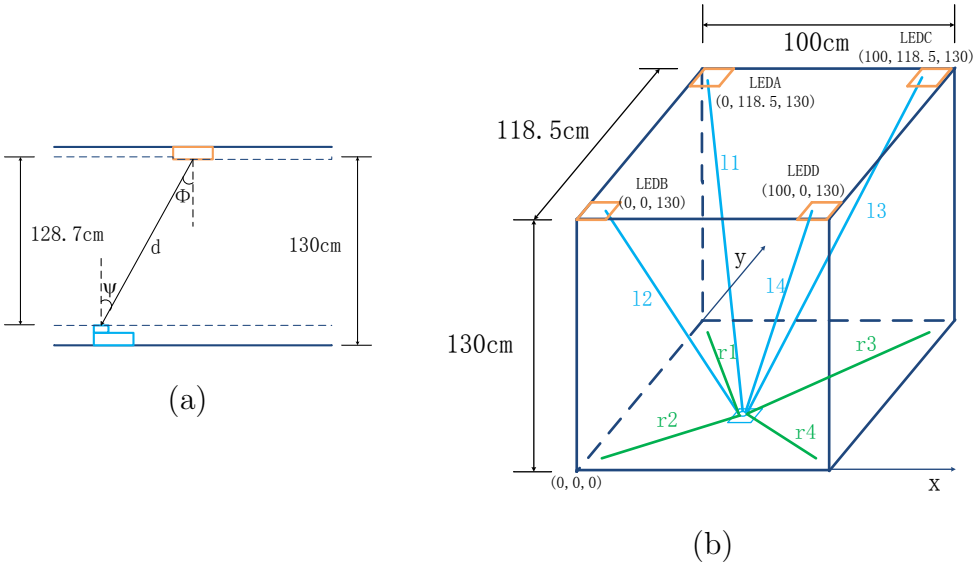

Figure 4.1: (a) Side version of the system. (b) System structure diagram.

Fig. 4.1 describes the proposed system configuration and Fig. 4.2 shows a picture of the test-bed environment we have built. Four LED lamps (LEDA, LEDB, LEDC, LEDD) are located on the ceiling. The receiver is a wide field of view (FOV) PD, which is OSD-15E manufactured by Centronic, as shown in Fig. 4.2. In order to distinguish the light signals from multiple LED lamps, different lamps are modulated by different center frequencies. Experiments are carried out at the space of 118.5 cm × 100 cm × 128.7 cm. When the receiver is placing in this space, signals from different LED lamps could be collected and then distinguished by applying Hamming filters to the received signals. RSS measurements can be translated into estimated distance between LED transmitters and the PD receiver. Then trilateration

algorithm is used to determine the position details of the receiver.

Figure 4.2: Experiment set-up.

Four different carrier frequencies (12.5 kHz, 25 kHz, 50 kHz and 100 kHz) are assigned to four LED lamps, thus four hamming filters are required to separate signals from different lamps. Next are three steps to design the FIR filters.

step 1 According to the performance requirements, such as stopband attenuation and transitional bandwidth, the suitable windowing filter type and the filter order N are determined. Since the stopband attenuation as -53 dB and the transition bandwidth f_{Tr} as 5 kHz are chosen, Hamming filter can meet the design requirements and the designing of Hamming filter is simpler than other window filters, such as Hanning filter, Blackman-Harris filter and Cassell filter.

step 2 Generally, the impulse response for the FIR filter could be presented as: $h(n) = h_d(n)w(n), (n = 0, 1, 2, ..., N-1)$. For Hamming filter, $N = 3.3f_s/f_{Tr}$, where f_s is the sample frequency. $w(n)$ is defined as: $w(n) = 0.54 - 0.46\cos(2n\pi)/(N-1)$. According to the expected frequency response $H_d(e^{j\omega})$, the impulse response $h_d(n)$ can be

determined utilizing inverse Fourier transfer. In this way, the impulse response in our design is $h_d(n) = \frac{\sin((n-N)\times\omega_2)-\sin((n-N)\times\omega_1)}{(n-N)\pi}$, where ω_2 and ω_1 are the upper and lower cut-off angular frequency, respectively.

step 3 The signal after FIR filter can be presented as the convolution of the input signal and the impulse response: $y(n) = \sum_{k=0}^{N-1} h(k)x(n-k)$, where $y(n)$ is the signal after FIR filter while x(n) is the signal before filtering.

LEDs can be generally modeled as Lambertian sources since the large beam divergence [84]. Denote P_t^i as the transmitted power difference between logical zeros and ones for the i-th transmission while P_r^i $(i = 1, 2, 3, 4)$ as the power difference at the receiver side. Without loss of generality, a simplified relationship between the transmitter and receiver power is [83, 85]:

$$P_r^i = \frac{C}{d_i^2}\cos(\phi)\cos(\psi)P_t^i, i = 1, 2, 3, 4, \tag{4.1}$$

where ψ is the angle of incidence, ϕ is the angle of irradiance, d_i is the distance between the i-th LED transmitter and the PD receiver and C is a constant value, as Fig. 4.1 (a) shows. Substituting the geometrical relationship $\cos(\phi) = \frac{h}{d}$ and $\cos(\psi) = \frac{h}{d}$ into Eq. 5.36, the following expression would be achieved:

$$P_r^i = \frac{Ch^2}{d_i^4}P_t^i. \tag{4.2}$$

Assuming P_0^i is the reference received power just under the i-th lamp and the vertical distance between lamps and the receiver surface is h, the theoretical relationship between the normalized received power P_r^i/P_0^i and the distance d can be represented as:

$$P_r^i/P_0^i = (\frac{h}{d_i})^4, \tag{4.3}$$

as depicted in Fig. 4.3 (a). Because the received power is fluctuated up and down slightly, P_0^i should be carefully selected with fine tuning for each lamp in order to match the modeling relationship. However, the theoretical power versus distance relationship could not match well with the experiment results, especially when the distance between the transmitter and receiver becomes larger, as Fig. 4.3 (a) indicated.

In [86], the light intensity received by the PD is measured at various positions with the only variable is the different distances to the transmitter. With the help of the Matlab tool for nonlinear fitting named "nlintool" to fit the measured results by curves, [86] proposed the following mathematical model for the light power received by the light sensor:

$$P_r^i = \frac{C}{d_i^2}\cos(\phi)\cos(\psi)^n P_t^i, i = 1, 2, 3, 4, \tag{4.4}$$

where $n = 1.4738$, rather than $n = 1$ in Eq. 4.1. This mathematical model also fits well with our experiment results, as shown in Fig. 4.3 (b). This is because for the Centronic OSD-15E, the effective area is under the glass surface for a certain of depth. So part or all of the effective area will be in shadow of the opaque walls if the incidence angle of light is large enough, which will bring an additional drop of received light power. The theoretical relationship between the normalized received power and the ranges can be expressed as

$$P_r^i / P_0^i = (\frac{h}{d})^{4.473}. \tag{4.5}$$

Thus, if the received power P_r^i from each LED is known at the receiver side, the distance between the lamp transmitter and the receiver can be calculated.

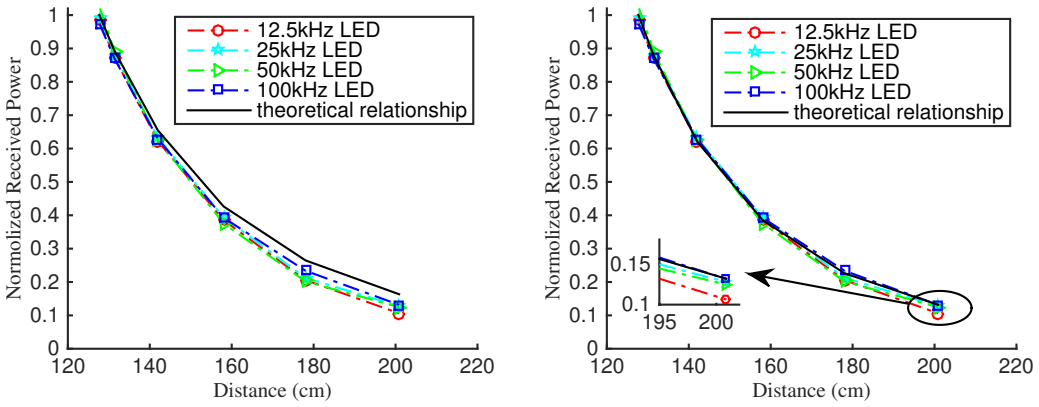

(a) (b)

Figure 4.3: The relationship between the normalized received power and distance: (a) n=1, (b) n=1.4738.

4.3 Indoor Positioning Algorithm

The target of the VLC positioning system is to estimate the location of the receiver. The Cartesian coordinate system is set up to determine the detail position of the receiver. As Fig. 4.1 (b) shows the LEDA's coordinate is (0, 118.5, 130), the LEDB's coordinate is (0, 0, 130), the LEDC's coordinate is (100, 118.5, 130) and the LEDD's coordinate is (100, 0, 130). The length of the test-bed is 100 cm while the width is 118.5 cm.

4.3.1 Two dimensional Positioning

When moving the receiver on the receiver plane 1.3 cm above the test-bed because of the receiver's structure (Fig. 4.1 (a)), the 2D positioning technique is applied. Because the height component is given in 2D positioning, the receiver's position can be expressed as (x^e, y^e). According to the basic trilateration method, the positioning process can be carried out as follows:

- The receiver obtains signals from four LED lamps, and uses the received

signal power to compute the distances between the transmitters and the receiver. Denote this distance from the LEDA, LEDB, LEDC, LEDD to the receiver projected on the receiver plane as $r_i, i = 1, 2, 3, 4$. The following distance equation can be established:

$$\begin{cases} \sqrt{(x^e)^2 + (width - y^e)^2} = r_1 \\ \sqrt{(x^e)^2 + (y^e)^2} = r_2 \\ \sqrt{(length - x^e)^2 + (width - y^e)^2} = r_3 \\ \sqrt{(length - x^e)^2 + (y^e)^2} = r_4 \end{cases} \tag{4.6}$$

- Among the four signals, the three signals with higher normalized power are selected and used to calculate the projected ranges between the lamps and the receiver according to the relationship as described in Eq. 4.4, because as can be seen in Fig. 4.3 (b), the larger distance will lead to larger misalignment between the modeling and realistic power-distance relationship. For example, when LEDA, LEDB, and LEDD are the three lights with relative stronger signal power when the receiver is at certain place. The equation system is as follows in this case:

$$\begin{cases} \sqrt{(x^e)^2 + (width - y^e)^2} = r_1 & (a) \\ \sqrt{(x^e)^2 + (y^e)^2} = r_2 & (b) \\ \sqrt{(length - x^e)^2 + (y^e)^2} = r_4 & (c) \end{cases} \tag{4.7}$$

From Eq. 4.7 (a) and (b), the y coordinate is determined as $\frac{r_2^2 - r_1^2 + width^2}{2 \times width}$ while from Eq. 4.7 (b) and (c), the x coordinate can be also expressed as $\frac{r_2^2 - r_4^2 + length^2}{2 \times length}$. Similar algorithm can be used to calculate the receiver's position on the whole receiver plane. The aforementioned process is also called linear least square estimation, which is widely used to provide the reliable localization service when there exist only small quantity of reference points [45, 87, 88].

4.3.2 Error Correction Algorithm in 2D positioning

Based on the above algorithm, the position detail of the receiver can be determined on the receiver plane with the knowledge of height component. However, because of the measurement error and fine tuning on P_0, sometimes, using the above mentioned algorithm, the positioning error is not as small as expected, especially at the corners of the test-bed where relatively larger misalignment happens. In [89], a new algorithm is proposed, which could lessen the gap between the practical measurements and the actual values by varying the radius of the three circles. We use a similar algorithm, so called ECA, to improve the accuracy.

In theoretical model, a suggested assumption is made: there is no error when estimating the distance between the receiver and the transmitter. Thus, three circles used for trilateration are intersect at one point. This is not the case in the practical settings. In reality, the distance estimated is not accurate, leading to the case that three circles have intersected but it's not at one point. The projected distance estimated can be written in the following form:

$$r_i^e = r_i \pm \varepsilon \quad \text{or} \quad r_i = r_i^e \mp \varepsilon, \tag{4.8}$$

where r_i is the exact projected distance between the LEDs and PD, ε is the measurement dependent error. When ε is small, $r_i^e \approx r_i$, we will use original 2D positioning algorithm to get the solution of (x^e, y^e). However, when ε is too large to ignore, an ECA solution is drawing to compensate the measurement error. Take the case that signals from LEDA, LEDB and LEDD are three relative stronger signals as an example again. The largest measurement error among different LEDs are the same in the example, the

new system of equations are:

$$\begin{cases} \sqrt{(x^e)^2 + (width - y^e)^2} = r_1 \pm \varepsilon & (a) \\ \sqrt{(x^e)^2 + (y^e)^2} = r_2 \pm \varepsilon & (b) \\ \sqrt{(length - x^e)^2 + (y^e)^2} = r_4 \pm \varepsilon & (c) \end{cases} . \tag{4.9}$$

Because the Eq. 4.9 can not be solved directly, the Newtown-Raphson (NR) method is utilized to do an approximation by considering ε as an error in the process of computing r_i^e. Eq. 4.9 can be expressed in an equivalent way as:

$$R_i \approx r_i \pm \varepsilon, \quad i = 1, 2, 4, \tag{4.10}$$

where

$$\begin{aligned} R_1 &= \sqrt{(x^e)^2 + (width - y^e)^2} \\ R_2 &= \sqrt{(x^e)^2 + (y^e)^2} \\ R_4 &= \sqrt{(length - x^e)^2 + (y^e)^2} \end{aligned} . \tag{4.11}$$

Some notations need to be introduced first. At the k-th iteration, let $(x^{e[k+1]}, y^{e[k+1]}, \varepsilon^{[k+1]})$ be the value of (x^e, y^e, ε). Define the residual function $f_i(x^e, y^e, \varepsilon)$ as:

$$\begin{aligned} f_1 &= (x^e)^2 + (width - y^e)^2 - (r_1 \mp \varepsilon)^2 \\ f_2 &= (x^e)^2 + (y^e)^2 - (r_2 \mp \varepsilon)^2 \\ f_4 &= (length - x^e)^2 + (y^e)^2 - (r_4 \mp \varepsilon)^2 \end{aligned} . \tag{4.12}$$

Then, the practical derivatives of f_i is defined as follows:

$$X_i^{'} = \frac{\partial f_i}{x^e} \tag{4.13}$$

$$Y_i^{'} = \frac{\partial f_i}{y^e} \tag{4.14}$$

$$E_i^{'} = \frac{\partial f_i}{\varepsilon} \tag{4.15}$$

Because the NR method is an iterative algorithm, the residual function at the k-th iteration need to be defined:

$$f_i^{[k]} = R_i^{[k]} - r_i \mp \varepsilon. \tag{4.16}$$

To get a close enough solution to the true position, $f_i^{[k]}$ is expected to be close to zero. In the next step, according to Calculus techniques [90], the following expression is derived:

$$\begin{aligned} & f_i^{[k+1]} - f_i^{[k]} \approx df_i \\ & = X_i^{'} dx^e + Y_i^{'} dy^e + E_i^{'} d\varepsilon \\ & = X_i^{'}(x^{e[k+1]} - x^{e[k]}) + Y_i^{'}(y^{e[k+1]} - y^{e[k]}) + E_i^{'}(\varepsilon^{[k+1]} - \varepsilon^{[k]}) \end{aligned} \tag{4.17}$$

As the residual function value is expected to be zero in the next iteration, let $f_i^{[k+1]} = 0$. Thus, the above equation could be established as:

$$\begin{aligned} & f_i^{[k]} + X_i^{'}(x^{e[k]}, y^{e[k]}, \varepsilon^{[k]})(x^{e[k+1]} - x^{e[k]}) + Y_i^{'}(x^{e[k]}, y^{e[k]}, \varepsilon^{[k]})(y^{e[k+1]} - y^{e[k]}) \\ & + E_i^{'}(x^{e[k]}, y^{e[k]}, \varepsilon^{[k]})(\varepsilon^{e[k+1]} - \varepsilon^{e[k]}) = 0. \end{aligned} \tag{4.18}$$

We can see that the value of $f_i^{[k]}, X_i^{'}, Y_i^{'}$ and $E_i^{'}$, $i = 1, 2, ..., m$ are determined at the end of the k-th iteration. According to the above analyst, the outlined algorithm of the NR method is presented:

step 1 Find the initial point for iteration, e.g.,

$$(x^{e[0]}, y^{e[0]}, z^{e[0]}, \varepsilon^{[0]}) = (0, 0, 0, 0). \tag{4.19}$$

step 2 Compute the residual function value of $f_i^{[k]}$ for $i = 1, 2, 3, 4$, as Eq. 4.12 shows.

step 3 Solve Eq. 4.17 for $(x^{e[k+1]}, y^{e[k+1]}, z^{e[k+1]}, \varepsilon^{[k+1]})$.

step 4 Continue until $f_i^{[k+1]}$ is small enough.

step 5 Let $k = k + 1$ and go to Step 2.

4.3.3 Three dimensional Positioning

When mobile phones are used for navigation in reality, the height of the receiver will vary because users can not only be adults with different heights, but also children, and even the disable and the aged sitting in the wheelchair. Thus, a 3D localization algorithm is developed and discussed in 3D space.

We choose the received power when the receiver is placed under the i-th LED lamp with the height $h_0 = 91.2$ cm as the reference received power P^i_{ref}. Because the radiation and incidence angles are kept at 0°, according to Eq. 4.4,

$$P^i_{ref} = \frac{C}{(h-h_0)^2} P^i_t. \tag{4.20}$$

In a similar way, when placing the receiver under the transmitters with h_{Rx} height, the received power P^{i*}_0 can be derived as

$$P^{i*}_0 = \frac{C}{(h-h_{Rx})^2} P^i_t. \tag{4.21}$$

Thus,

$$\frac{P^{i*}_0}{P^i_{ref}} = (\frac{h-h_0}{h-h_{Rx}})^2. \tag{4.22}$$

As Fig. 4.4 shows, changing the vertical distance between the transmitter and the receiver by putting the receiver under each lamp with different heights, the relationship between the normalized received power and the vertical distance from the experiment results fit well with the theoretical one, which is indicated in Eq. 4.22.

When the receiver is placed with h_{Rx} height, by replacing $\cos(\phi)$ and $\cos(\psi)$ as $\frac{h-h_{Rx}}{d_i}$ in Eq. 4.4, the received power can be represented as

$$P^i_R = \frac{C \times (h-h_{Rx})^{n+1}}{d_i^{n+3}} P^i_t. \tag{4.23}$$

From Eq. 4.20 and Eq. 4.23, the relationship between the normalized power

and distance is as follows:

$$P_R^i = \frac{(h-h_0)^2(h-h_{Rx})^{n+1}}{d_i^{n+3}} P_{ref}^i. \tag{4.24}$$

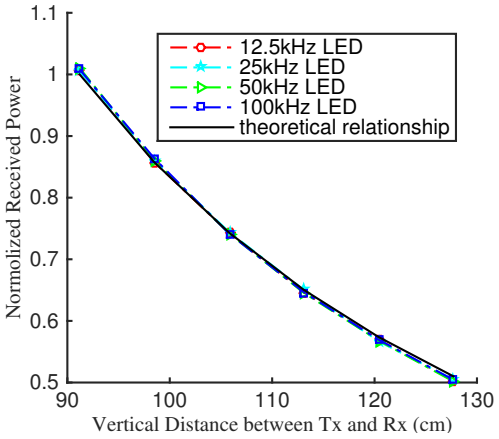

Figure 4.4: Normalized received power versus vertical distance when placing the receiver under the transmitter.

The main steps of 3D positioning process are performed as follows:

- The receiver obtains signals from four LED lamps (LEDA, LEDB, LEDC and LEDD), and uses the received signal power and h_{Rx} to express the ranges between the transmitter and the receiver as

$$d_i = \sqrt[n+3]{\frac{(h-h_0)^2(h-h_{Rx})^{n+1}P_{ref}}{P_R^i}} \tag{4.25}$$

  according to Eq. 4.24. Let the estimated distance be d_i, four LEDs' coordinates be (x_i, y_i, z_i) as shown in Fig. 4.1 (b), and the receiver's location (to be estimated) be (x^e, y^e, z^e). Then, the following distance equations can be written as:

$$\sqrt{(x_i-x^e)^2+(y_i-y^e)^2+(z_i-z^e)^2} = d_i. \tag{4.26}$$

- Among the four signals, the three signals with higher normalized power are selected and used to calculate d_i, according to the relationship as described in Eq. 4.25. For example, when LEDA, LEDC and LEDD are LED lights with relative stronger signal power when the receiver is at certain place. The equation system is as follows in this case:

$$\begin{cases} \sqrt{(x_1 - x^e)^2 + (y_1 - y^e)^2 + (z_1 - z^e)^2} = d_1 \\ \sqrt{(x_3 - x^e)^2 + (y_3 - y^e)^2 + (z_3 - z^e)^2} = d_3 \\ \sqrt{(x_4 - x^e)^2 + (y_4 - y^e)^2 + (z_4 - z^e)^2} = d_4 \end{cases} \tag{4.27}$$

The above equation system is derived from three spheres with the radius of the measured distance d_i and center of the reference points (x_i, y_i, z_i). Intersection between these three spheres is calculated as target position. The above equality holds if there is no error occurring when estimating the distances between the LED lamps and the PD. However, this assumption may not work in practical settings. The above system of equations should change to the following optimization problem.

$$\begin{aligned} \text{minimize} \quad & f_1 = (x_1 - x^e)^2 + (y_1 - y^e)^2 + (z_1 - z^e)^2 - d_1^2 \\ & f_2 = (x_3 - x^e)^2 + (y_3 - y^e)^2 + (z_3 - z^e)^2 - d_3^2 \\ & f_4 = (x_4 - x^e)^2 + (y_4 - y^e)^2 + (z_4 - z^e)^2 - d_4^2 \end{aligned} \tag{4.28}$$

In order to solve Eq. 4.28 using trust region method, the evaluation criterion σ is introduced:

$$\sigma = \underset{(x^e, y^e, z^e)}{\text{argmin}} \quad f_1^2 + f_2^2 + f_4^2 \tag{4.29}$$

The detail process for the realization of trust region method is described as follows:

step 1 Assume $h_{Rx}, 0 \leq h_{Rx} \leq h$ as the vertical height and substitute it into Eq. 4.25. Thus, $z^e = h - h_{Rx}$.

step 2 Estimate the coordinates (x^e, y^e, z^e) from solving Eq. 4.6.

step 3 Substitute the coordinates (x^e, y^e, z^e) into Eq. 4.29 to obtain the value of σ, and then update the trust region radius to minimize σ.

step 4 Iterate steps 1 to 2 in order to find the optimal estimated coordinates.

step 5 The value of h_{Rx} in step 1 is updated by the z^e optimized in step 3.

4.4 Experiment Results and Discussion

4.4.1 Two-dimensional Positioning

As shown in Fig. 4.2, an experimental platform is built in order to evaluate the system performance. After applying 2D positioning technique, the positioning error of x-axis and y-axis is indicated in Fig. 4.5 (a) and (b), respectively. Comparing with the dotted lines, which are the accurate position values, the maximum x-axis and y-axis positioning errors are 6.17 cm and 2.50 cm, respectively. The average positioning errors of x-axis and y-axis are 1.18 cm and 1.25 cm, respectively. In Fig. 4.5 (c), the disagreement between the estimated positioning points and real locations is demonstrated. The positioning error is quite small at most places of the receiver plane, which is acceptable. At four corners of the test-bed, relatively large disagreement happens. It is because when selecting the reference power, slight tuning is made in order to utmost match the experiment result to the theoretical model. However, this fine tuning leads to the misfit between the theoretical power versus distance relationship model and the real case for the points placed at the corner of the plane. Furthermore, the other LED lamps used to estimate the distance are a little far when the receiver is placed at the

corner of the test-bed. As can be seen in Fig. 4.3 (b), too far away distance between the transmitted and receiver is not a good news for the accurate positioning. What is more, the reflection of the wall is relatively larger at the corner of the test-bed, which will decrease the performance as well.

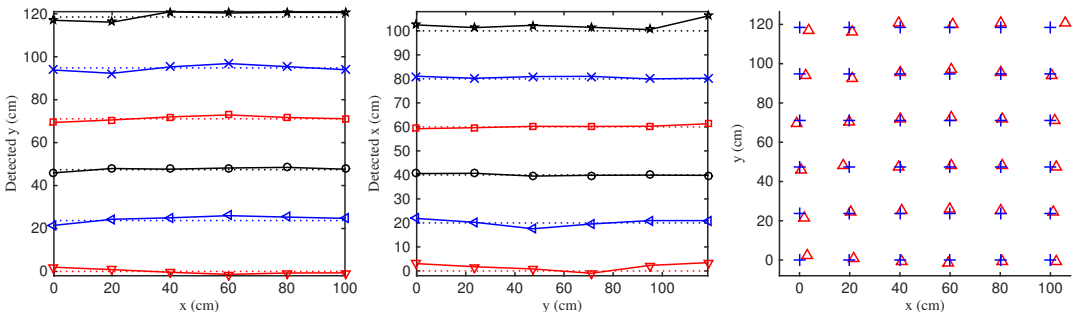

(a) (b) (c)

Figure 4.5: Experimental results of 2D positioning: (a) distance error at y-axis (dotted line is the accurate axis while full line is the estimated axis), (b) distance error at x-axis, (c) difference between the estimated position and real position (+ is the actual position while △ is the estimated position).

4.4.2 Error Correction Algorithm in 2D positioning

In Fig. 4.5 (c), it reveals that at most of the receiver plane, the positioning error is within 3 cm, where we assume small enough positioning error is achieved. However, at the corner of the receiver plane, the positioning error as large as 6.17 cm occurs, thus, the ECA is applied at these positions (corners of the receiver plane). An example is given in Fig. 4.6. When the receiver is placed at the point with coordinates (10, 11.85), the three LED lights used for localization are LEDA, LEDB and LEDD because they are nearer to the receiver and thus higher normalized power can be achieved. Then,

the projected distances r_1, r_2 and r_4 are measured: $r_1 = 104.45$, $r_2 = 15.39$ and $r_4 = 87.19$. Based on this, using the original 2D positioning algorithm, the estimated position coordinates are (13.55, 14.30) while after applying ECA to compensate the measurement error, the estimated position becomes (10.77, 11.80). Thus, the positioning error decreases from 4.31 cm to 0.77 cm. A more detail version is revealed in Fig. 4.6 (b).

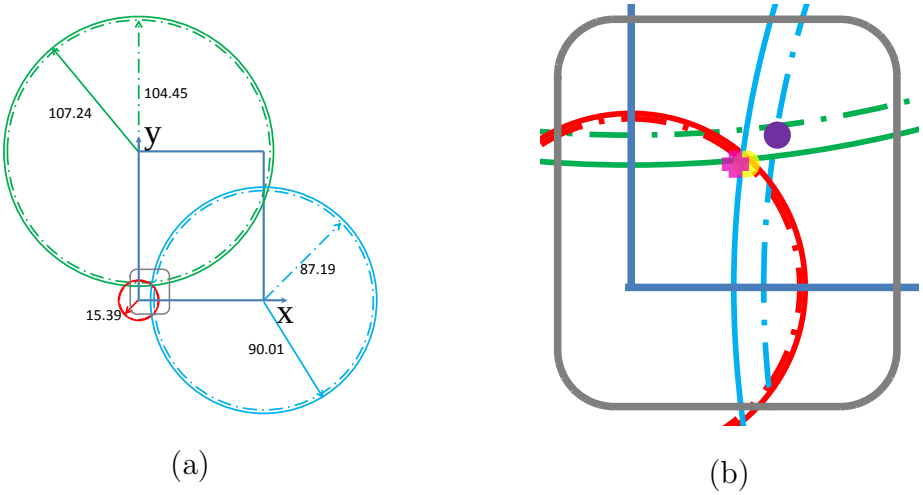

(a) (b)

Figure 4.6: The target position (10, 11.85): (a) ECA estimation, (b) comparison between the estimated position with ECA and without ECA (fuchsia cross is the actual position of the receiver, the yellow dot is the position estimated with ECA and the purple dot is the position estimated without ECA).

After ECA is applied, the positioning error at the corners becomes smaller observably. As shown in Fig. 4.7, the positioning performance is compared at four corners. With the help of ECA, the estimated positions become closer to the actual positions compared with the estimated results without ECA. At the lower left corner, the average positioning error is as large as 4.06 cm without ECA while it decreases to 0.90 cm with ECA. At the upper left corner, after applying ECA, the average positioning error decreases from 3.64

cm to 2.03 cm. For the upper right corner, the original algorithm leads to 4.87 cm average positioning error while the ECA algorithm leads to only 1.87 cm. For the lower right corner, the positioning accuracy is also improved. The estimated positioning error is 2.09 cm without ECA while 1.40 cm with ECA.

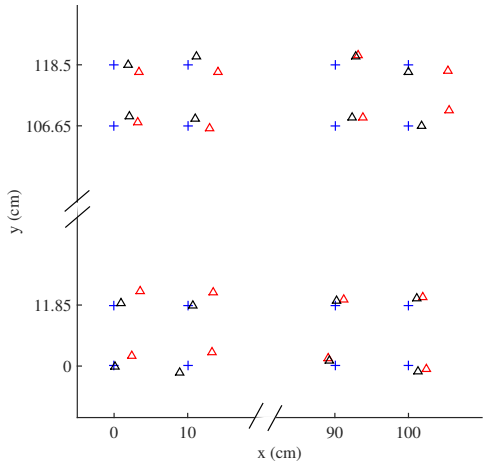

Figure 4.7: Difference between the estimated position and real position with ECA and without ECA at four corners (blue + is the actual position, red △ is the estimated position without ECA and black △ is the estimated position with ECA).

In Fig. 4.8, the performance details at four example positions for the cases of with and without ECA are shown. At the position with coordinates (0, 0), the mean positioning error of five-time measurements is 3.71 cm using the original 2D positioning algorithm while it decreases to 1.10 cm after applying ECA. Around the position (0, 0), such as the point at (10, 11.85), the mean positioning error is decreased from 3.69 cm to 1.27 cm with the help of ECA. The other two examples we have shown are at (100, 118.5) and (100, 106.65). For the test point with coordinate (100, 118.5), the average position error is

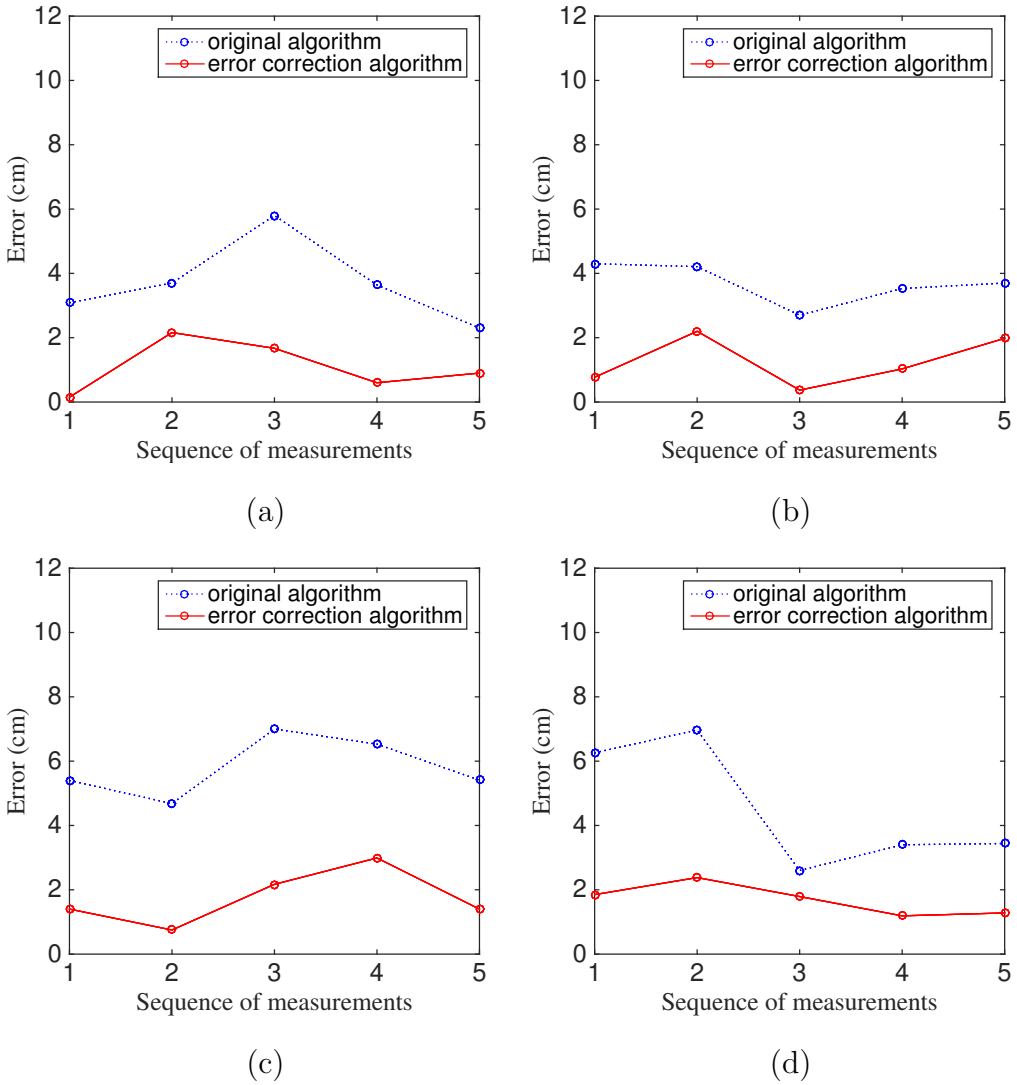

Figure 4.8: Comparison between experiment results with ECA and without ECA : (a) target (0, 0), (b) target (10, 11.85), (c) target (100, 118.5), (d) target (100, 106.65).

reduced from 5.80 cm to 1.74 cm while at (100, 106.65) the positioning error is decreased from 4.53 cm to 1.70 cm.

4.4.3 Three dimensional Positioning

After applying 3D positioning technique, the positioning error on the receiver plane with 1.3 cm height is demonstrated in Fig. 4.9. Comparing with the accurate position values, which is indicated using the dotted lines, the maximum positioning errors of x-axis and y-axis are 2.58 cm and 5.00 cm, respectively, as shown in Fig. 4.9 (a) and (b). The mean positioning errors of x-axis and y-axis are 0.90 cm and 1.54 cm, respectively. In Fig. 4.9 (c), the disagreements between the estimated positions and the actual locations are shown in 3D space. The maximum vertical positioning error is 2.20 cm while the mean vertical error is 0.66 cm.

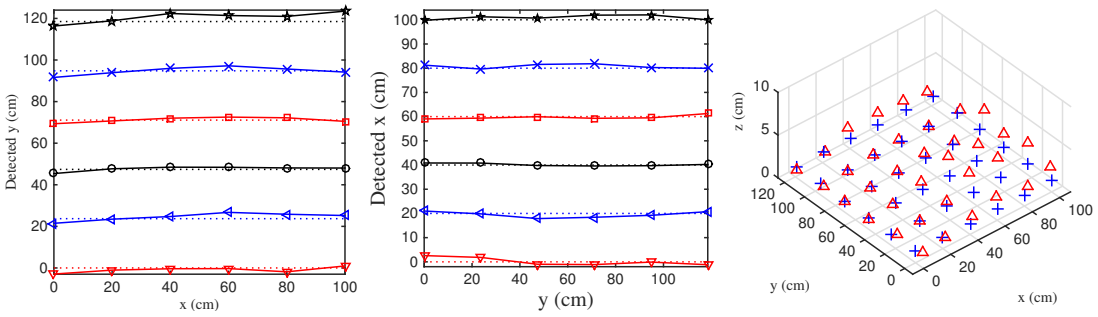

(a) (b) (c)

Figure 4.9: Experimental results of 3D positioning: (a) distance error at y-axis (dotted line is the actual axis while full line is the estimated axis), (b) distance error at x-axis, (c) difference between the estimated position and real position (+ is the actual position while △ is the estimated position).

After picking up several points with different vertical distance, Fig. 4.10

is drawn. The accurate x and y coordinates of the four points selected are (30, 94.8), (30, 35.55), (70, 94.8), and (70, 35.55). The four altitude levels chosen are 1.3 cm, 9.4 cm, 15.4 cm and 23.1 cm. On the 1.3 cm height receiver plane, the mean error of x-axis of these four points is 2.44 cm while the mean error of y-axis is 2.00 cm. The average distance error is 2.97 cm in 3D space. For the case when the altitude level is 9.4 cm, the mean error of x-axis is 1.58 cm while the mean error of y-axis is 0.87 cm. The average positioning error in 3D is 2.90 cm on the 9.4 cm height plane. On the receiver plane with 15.4 cm height, the average error of x-coordinate is 1.49 cm while for y-coordinate is 1.46 cm. The 3D distance error in space is 3.00 cm. When the altitude height increases to 23.1 cm, the mean error of x-axis is 1.52 cm while the y-axis mean error is 0.15 cm. The average distance error is 2.68 cm in 3D, which is still within 3 cm.

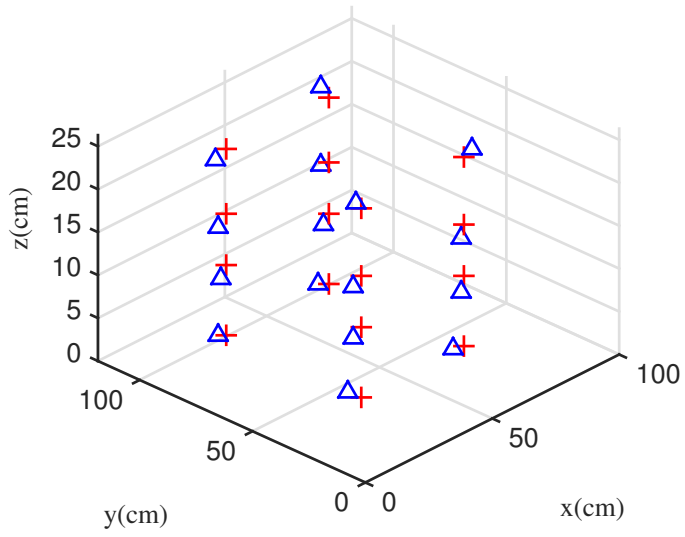

Figure 4.10: Experimental results of difference between the estimated position and real position on four levels (+ is the actual position while △ is the estimated position).

A random moving path is generated in the test-bed with 13 points. The experiment results reflecting the difference between the real reference points and the estimated points are shown in Fig. 4.11.

The actual path is indicated using the red line while the estimated one is indicated by the blue line. The maximum positioning error is 2.98 cm and the average difference between the calibration points and estimated ones is 2.09 cm.

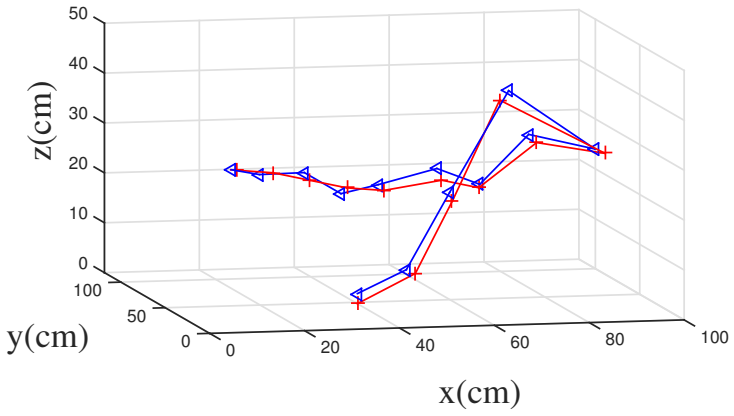

Figure 4.11: Experimental results of random tracking points in 3D space (+ is the actual position while △ is the estimated position).

In order to show the results clearer, Fig. 4.11 is separated into the horizontal and vertical views. As can be seen in Fig. 4.12 (a), the estimated points are slightly deviated from the true tracking path from the view of horizontal. The maximum deviation is 2.25 cm while the mean difference is 1.23 cm. As reflected in Fig. 4.12 (b), the estimated points are close to the calibration points from the vertical view. The maximum deviation of the vertical side is 2.97 cm and the mean deviation is only 1.48 cm. These results match well with the conclusion that the average distance error is within 3 cm in 3D space.

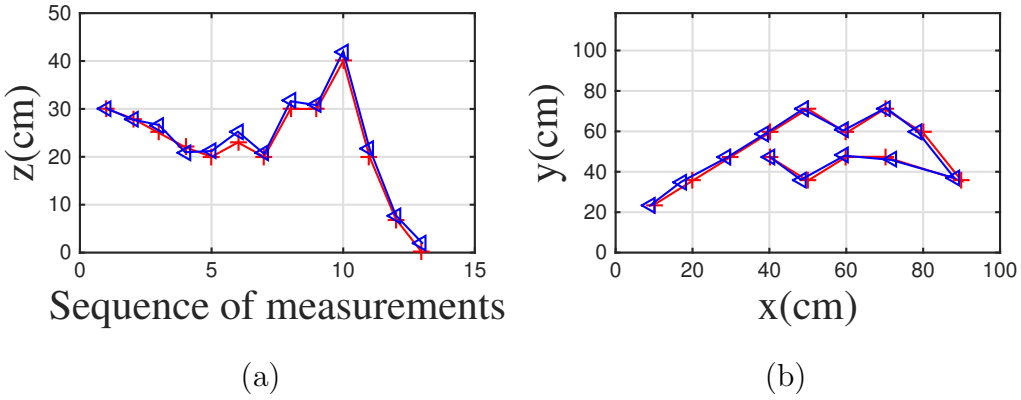

(a) (b)

Figure 4.12: Vertical and horizontal experimental results in 3D space: (a) vertical result, (b) horizontal result.

4.5 Conclusion

In this chapter, an asynchronous visible light positioning system was experimentally demonstrated. Frequency division multiple access was used to distinguish lights from different light sources. A pre-determined normalized received power-distance relationship was wielded to calculate the distances based on the received power. Then a trilateration method was used to determine the position of the receiver. An error correcting algorithm was used to improve the corners' positioning accuracy, where relatively large positioning errors happen. We found that the average positioning error at the four corners decreases from 3.67 cm to 1.55 cm after applying error correcting algorithm. Both 2D and 3D algorithms were investigated. The experimental results with high accuracy were presented.

Chapter 5

Asynchronous VLP system with CDMA

5.1 Overview

Usually, when extending localization to large areas, accurate positioning could be achieved by two steps. First step is that based on received signals, we decode IDs of related transmitters. When compared with pre-downloaded map, in which every lamp's ID is recorded, the lamps that are nearby can be determined. Thus a rough position of a receiver could be ascertained. In the second step, using division multiple access techniques to distinguish signals from different lamps. Apart from using the different frequencies to distinguish the signals from the different transmitters as introduced in Chapter 4, CDMA is also a multiple access technology which could be applied in VLP systems. Then, by combining with the ranging techniques, such as RSS, PDOA, and TDOA, an accurate position could be achieved.

For indoor localization systems such as ZigBee or WLAN [91], ID information of the nearest LEDs is transmitted to center office for localization

using a radio system. The disadvantage of applying this scheme is the low positioning resolution of the system and poor positioning performance within the shined area of the LED lamp. ID signals can also be modulated on different carrier frequencies [92], in which the interference between signal with different IDs could be reduced. However, with the increase of LED number, it becomes more and more difficult to choose different carrier frequencies. Because in order to distinguish the lamps assigned with different carrier frequencies, filters with higher orders are required, which are difficult to realize.

For a VLC positioning system, by using a suitable multiple access technology, information from multiple LEDs could be received simultaneously. Various multiple access technologies have been proposed for an IPS. Both TDMA [93] and dual tone multi-frequency (DTMF) [94] could achieve good positioning results in practical measurements. However, both systems require strict synchronization between LEDs, which requires a backbone network installation. If the LEDs can send their information asynchronously to the mobile devices, a VLC positioning system could be adapted more easily in current lighting installations. An asynchronous system based on FDMA could be built where every LED gets a different carrier frequency [95]. This multiple access technology uses analog signals which are added on a DC driving current for illumination. LEDs are controlled naturally by switched power supplies which can only use OOK for communication. However, with the increase of LED lamps, the bandwidth requirement for the FDMA is increased at the same time.

CDMA is a multiple access technology which could adapt OOK easily. In this solution, a unique code is assigned to each lamp to encrypt the data. Different LEDs transmit different data as their IDs. The receiver can use the

correlation properties of the codes to distinguish the data and retrieve the RSS of every LED. CDMA could be issued as multiple access technology in a VLP system. Synchronization is also necessary among LEDs when code division multiplexing technique is applied. Although the CDMA-based VLP system does not require synchronization between the transmitter and receiver as shown in [96], the transmitters share a common clock to synchronize the transmitted signals. However, in a commercial system, LED lamps may be turned on independently and randomly. Synchronization is very difficult to realize among LED lamps, since they are usually only be used as transmitters thus cannot receive synchronization signals. So, a CDMA with no synchronization requirement is promising. In [97], different types of pseudonoise codes are used to encode and decode data in order to realize asynchronous operation. Because the codes chosen have a low crosscorrelation for all possible timing offsets, the main disadvantage of this solution is that it needs to deal with multiple access interference (MAI). That means the contributions from other light sources cannot be not fully suppressed, which is undesirable.

In this chapter, we propose a delay compensation code division multiplexing technique for the first time in the literature. At the receiver side, we could decode the IDs of the relative LED transmitters and signal strengths from different lamps. Based on this, a trilateration is used to accurately determine the position of the receiver.

This chapter is organized as follows. The system model, including the asynchronous CDMA mechanism, the code type we used in this technique and an example to applying the mechanism are described in section 5.2. The positioning algorithm for indoor VLP system is proposed in section 5.3. The noise modeling are given in section 5.4 and the simulation results are listed

in section 5.5, followed the conclusion drawn in section 5.6.

5.2 System Design

In this section, a framework is demonstrated to achieve asynchronous CDMA-based VLC network. OOK is used in our system to modulate the visual signals. The lighting devices transmit the encoded messages following our proposed frame format while the receiver decodes the signal.

5.2.1 Asynchronous CDMA Mechanism

Fig. 5.1 represents the workflow. The i-th transmitter has a CDMA code $\overline{c_i}$, $i = 1, 2, \cdots, k$. These codes are mutually orthogonal, which will be discussed later. The vector $\overline{c_i}$ with length n can be expressed as:

$$\overline{c_i} = [c_{i1}, c_{i2}, \cdots, c_{in}], i = 1, 2, \cdots, k. \tag{5.1}$$

The transmitted data $\overline{d_i}$, $i = 1, 2, \cdots, k$ is assigned to i-th transmitter. $\overline{d_i}$ is assumed to be the data transmitted by the i-th transmitter and the vector contains m elements:

$$\overline{d_i} = [d_{i1}, d_{i2}, \cdots, d_{im}], i = 1, 2, \cdots, k. \tag{5.2}$$

Delay of the transmitted signal to the reference point: $\tau_1, \tau_2, \cdots, \tau_k$. Encoding process: $\overline{D_1} = \overline{d_1} \otimes \overline{c_1}$ $\overline{D_2} = \overline{d_2} \otimes \overline{c_2}$ $\cdots$ $\overline{D_i} = \overline{d_i} \otimes \overline{c_i}$ $\cdots$ $\overline{D_k} = \overline{d_k} \otimes \overline{c_k}$. The operation $\otimes$ is called encoding operation. In $\overline{d_i} \otimes \overline{c_i}$, from the $((j-1)n+1)$-th element to jn-th element in the encoded data can be expressed as $d_{ij} \times \overline{c_i}, j = 1, \cdots, m$. Thus, the length of the encoded data is mn.

As shown in Fig. 5.2, different from the RF signal, optical signal cannot be negative for the unipolar property of VLC. Thus, to transmit $\overline{D_i}$, the i-th

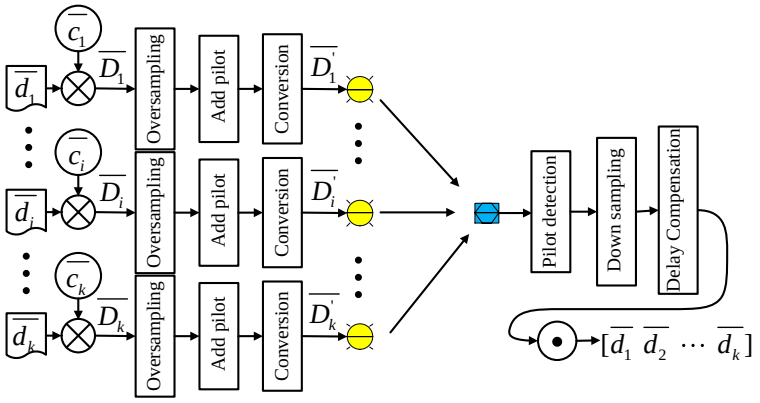

Figure 5.1: Flow diagram of the asynchronous CDMA mechanism.

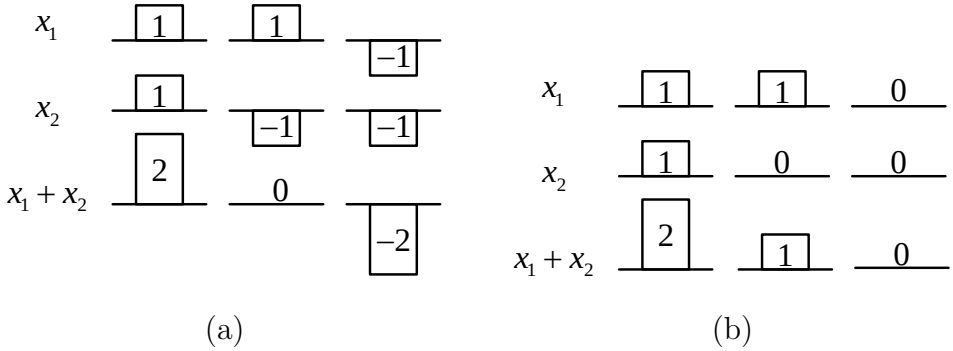

(a) (b)

Figure 5.2: Comparison of: (a) RF signal addition, (b) optical signal addition.

sender first converts the encoded data to unipolar data $\overline{D_i'}$ by changing all '-1' in $\overline{D_i}$ to '0' while each '1' unchanged. For example, an encoded (-1,1) will become (1,0), while an encoded (1,1) will keep unchanged [98].

When there is no delay, the transmitted signal could be:

$$signal = \overline{D_1} + \overline{D_2} + \cdots + \overline{D_k}. \tag{5.3}$$

In order to decode the data from i-th transmitter, $signal \odot \overline{c_i}$ is carried out. Because the codes used are orthogonal codes, the following equation holds:

$$\widetilde{d}_i = signal \odot \overline{c_i} = |\overline{c_i}|^2 \overline{d_i}, \tag{5.4}$$

where $\widetilde{d}_i$ is the estimated data from the i-th transmitter, $\odot$ is the decode operation and $|\ \ |$ is the norm of the vector.

When the delay exists, a left shift matrix is introduced to present the signal after delay. If the i-th encoded data without delay can be expressed as the vector $\overline{D_i}$, the encoded data with τ_i delay can be expressed as: $\overline{D_i} \times T(\tau_i)$, where operation $\times$ is the matrix production and $T(\tau_i)$ is the left shift matrix corresponding to the τ_i delay. The detail definition of $T(\tau_i)$ is as follows. First, we define a $p \times p$ identity matrix. When the length of vector $\overline{D_i}$ is mn, we define $p = mn$. If the identity matrix is as follows:

$$I = \begin{bmatrix} 1 & 0 & \cdots & 0 \\ 0 & 1 & \cdots & 0 \\ \vdots & \vdots & \ddots & \vdots \\ 0 & 0 & \cdots & 1 \end{bmatrix}_{p \times p}, \tag{5.5}$$

when τ_i delay exists, $T(\tau_i)$ can be generated by placing the last τ_i columns in matrix I forward. In a similar way, $T(-\tau_i)$ means placing the first τ_i columns backward. The left shift matrix with τ_i delay can be expressed as:

$$T(\tau_i) = \begin{bmatrix} \overbrace{0 & 0 & \cdots & 0}^{\tau_i} & 1 & 0 & \cdots & 0 \\ 0 & 0 & \cdots & 0 & 0 & 1 & \cdots & 0 \\ \vdots & \vdots & \ddots & \vdots & \vdots & \vdots & \ddots & \vdots \\ 0 & 0 & \cdots & 0 & 0 & 0 & \cdots & 1 \\ 1 & 0 & \cdots & 0 & 0 & 0 & \cdots & 0 \\ 0 & 1 & \cdots & 0 & 0 & 0 & \cdots & 0 \\ \vdots & \vdots & \ddots & \vdots & \vdots & \vdots & \ddots & \vdots \\ 0 & 0 & \cdots & 1 & 0 & 0 & \cdots & 0 \end{bmatrix}. \tag{5.6}$$

For example, when T is a 3×3 identity matrix, $T(1)$ and $T(-1)$ are:

$$T(1) = \begin{bmatrix} 0 & 1 & 0 \\ 0 & 0 & 1 \\ 1 & 0 & 0 \end{bmatrix}, \tag{5.7}$$

while

$$T(-1) = \begin{bmatrix} 0 & 0 & 1 \\ 1 & 0 & 0 \\ 0 & 1 & 0 \end{bmatrix}. \tag{5.8}$$

The signal transmitted is derived as:

$$signal = \overline{D_1} \times T(\tau_1) + \overline{D_2} \times T(\tau_2) + \cdots + \overline{D_k} \times T(\tau_k). \tag{5.9}$$

where the operation $\times$ is the matrix production.

The data can be estimated by the following decode process:

Step1: Compensate the delay and multiply the code for each transmitter, we can get the vector Y as Eq. 5.10 indicates. The operation $\cdot$ is the inner product.

$$Y = \left[signal \times T(-\tau_1) \odot \overline{c_1} \quad signal \times T(-\tau_2) \odot \overline{c_2} \quad \cdots \quad signal \times T(-\tau_k) \odot \overline{c_k} \right]. \tag{5.10}$$

Step 2: Substitute Eq. 5.9 into Eq. 5.10. Each element of Y can be expressed as Eq. 5.11.

$$\begin{aligned} signal \times T(-\tau_1) \odot \overline{c_1} &= |\overline{c_1}|^2 \overline{d_1} + \overline{D_2} \times T(\tau_2) \times T(-\tau_1) \odot \overline{c_1} + \cdots + \overline{D_k} \times T(\tau_k) \times T(-\tau_1) \odot \overline{c_1} \\ signal \times T(-\tau_2) \odot \overline{c_2} &= \overline{D_1} \times T(\tau_1) \times T(-\tau_2) \odot \overline{c_2} + |\overline{c_2}|^2 \overline{d_2} + \cdots + \overline{D_k} \times T(\tau_k) \times T(-\tau_2) \odot \overline{c_2} \\ &\vdots \\ signal \times T(-\tau_k) \odot \overline{c_k} &= \overline{D_1} \times T(\tau_1) \times T(-\tau_k) \odot \overline{c_k} + \overline{D_2} \times T(\tau_2) \times T(-\tau_k) \odot \overline{c_k} + \cdots + |\overline{c_k}|^2 \overline{d_k} \end{aligned} \tag{5.11}$$

The system of equations in Eq. 5.11 can be written

$$Y = \widetilde{D} \times M. \tag{5.12}$$

In the above expression, $\widetilde{D} = [\widetilde{d_1}, \widetilde{d_2}, \cdots, \widetilde{d_k}]$ and $\widetilde{d_i}$ is the estimated data for the i-th transmitter. M is a $k \times k$ matrix as follows:

$$M = \begin{bmatrix} |\overline{c_1}|^2 I & M_{12} & \cdots & M_{1k} \\ M_{21} & |\overline{c_2}|^2 I & \cdots & M_{2k} \\ \vdots & \vdots & \ddots & \vdots \\ M_{k1} & M_{k2} & \cdots & |\overline{c_k}|^2 I \end{bmatrix} \tag{5.13}$$

Step 3: determine M_{ij} accordingly. Because the expanded j-th element in the Eq. 5.10 can also be written as the j-th element of $\widetilde{D} \times M$:

$$signal \times T(-\tau_j) \odot \overline{c_j} = [\widetilde{d_1}\widetilde{d_2} \cdots \widetilde{d_k}] \times [M_{1j} M_{2j} \cdots M_{kj}]^T. \tag{5.14}$$

Substitute Eq. 5.9 into Eq. 5.14, we can get the following expression:

$$\overline{D_i} \times T(\tau_i) \times T(\tau_j) \odot \overline{c_j} = \widetilde{d_i} \times M_{ij} \tag{5.15}$$

The above equation is equivalent to:

$$\overline{d_i} \otimes \overline{c_i} \times T(\tau_i - \tau_j) \odot \overline{c_j} = \widetilde{d_i} \times M_{ij} \tag{5.16}$$

We assume code length as cl, delay between LED_i and LED_j as $\tau_i - \tau_j = \tau_{ij}$, data movement as dm and code movement as cm. Then, when $\tau_{ij} \geq 0$, $dm = \lfloor \tau_{ij}/cl \rfloor$ and when $\tau_{ij} < 0$, $dm = \lceil \tau_{ij}/cl \rceil$. Here, $\lfloor\rfloor$ is the downward integral function while $\lceil\rceil$ is the upward integral function. $cm = \tau_{ij}\%cl$, where operation % is to get reminder. When $i > j$, M_{ij} could be written as:

$$M_{ij} = \begin{bmatrix} a & b & 0 & \cdots & 0 \\ 0 & a & b & \cdots & 0 \\ \vdots & 0 & \ddots & \ddots & \vdots \\ 0 & \vdots & \cdots & a & b \\ b & 0 & \cdots & \cdots & a \end{bmatrix} \times T(dm) \tag{5.17}$$

while when $i < j$, M_{ij} could be expressed as:

$$M_{ij} = \begin{bmatrix} a & 0 & \cdots & 0 & b \\ b & a & 0 & \vdots & 0 \\ 0 & b & \ddots & 0 & \vdots \\ \vdots & \vdots & \ddots & a & 0 \\ 0 & 0 & \cdots & b & a \end{bmatrix} \times T(dm) \tag{5.18}$$

where $a = \overline{c_i}(1 : cl - cm) \cdot \overline{c_j}(cm + 1 : cl)$ and $b = \overline{c_i}(cl - cm + 1 : cl) \cdot \overline{c_j}(1 : cm)$.

5.2.2 Cyclic Orthogonal Walsh-Hadamard Codes

In CDMA communications, Walsh-Hadamard codes are widely used to define individual communication channels. In the zero phase, the codes generated from the Walsh-Hadamard Matrix are mathematically orthogonal inherently [99]. A Hadamard matrix H_{2^k}, $k > 1$ can be produced after setting $H_1 = [1]$:

$$H_{2^k} = \begin{bmatrix} H_{2^{k-1}} & H_{2^{k-1}} \\ H_{2^{k-1}} & -H_{2^{k-1}} \end{bmatrix} \tag{5.19}$$

The rows of the Hadamard matrices constitute the Walsh-Hadamard codes, which are mutually orthogonal to each other. However, if the codes are phase shifted, the orthogonality property lose. If Hadamard codes are used to spread the data in an asynchronous positioning system, MAI will be introduced by the codes' non-orthogonality at the receiver side.

To combat this asynchrony problem in CDMA-based VLC positioning system, here a special set of Hadamard codes is extracted from the H_{2^k} matrix, which are verified to be orthogonal to each other at any phase shift. This set of cyclically orthogonal codes is so called COWHC [99]. The following method is a process to randomly select a set of COWHC from the Hadamard matrix. Given the Hadamard matrix H_{2^k} with dimension $D = 2^k$,

and as defined in [100], $\mathcal{H}_i$ is the i-th row of H_{2^k}. H_{2^k} can be divided into several subsets:

$$\{\mathcal{H}_i\}_{i\in\mathcal{C}}, where\ \mathcal{C} = \{\bigcup_{l=1}^{k}\mathcal{C}_l\}\bigcup\{1\} \tag{5.20}$$

where $\mathcal{C}_l = \{2^{k-l}+1, \cdots, 2^{k-l+1}\}$. Given the subsets in Eq. 5.20, one can define a COWHC by chosing a single code from each subset. Take H_{2^4} as an example, as Eq. 5.20 indicates, the following subsets are generated:

$$\{1\}, \mathcal{C}_1 = \{2\}, \mathcal{C}_2 = \{3,4\}, \mathcal{C}_3 = \{5, \cdots, 8\}, \mathcal{C}_4 = \{9 \cdots 16\}$$

and hence, a COWHC set can be generated by selecting one code (row) from each of the above subsets (i.e., 1st, 2nd, 4th, 7th and 11th row of H_{2^k}).

5.2.3 Frame Structure for the Transmitted Signal

Below, a frame structure is proposed to support the signal transmission from LED sources. In order to estimate the relative delay between different transmitters, the pilot symbols are added in the front part of the transmitted signals. Different pilot symbols are assigned to different transistors. The encoded data needs to repeat several times after the pilot symbols. The more transmitters are, more times the encoded data need to repeat, because at least one period of encoded data is not polluted by the pilot symbols of other signals needs to be guaranteed. Then, as Fig. 5.3 shows, the pilot symbols with several repeated encoded data is one period of signal. The first step is selecting one arbitrary point as the beginning of the signal. Then, we search the pilot symbols along the received signal. For example, when the pilot symbol assigned to $signal_i$ is '0100', if the same pilot symbol appears at the p-th position for the first time, $\tau_i = p$. Using this method, the relative delay between the signals and the reference point could be determined. They

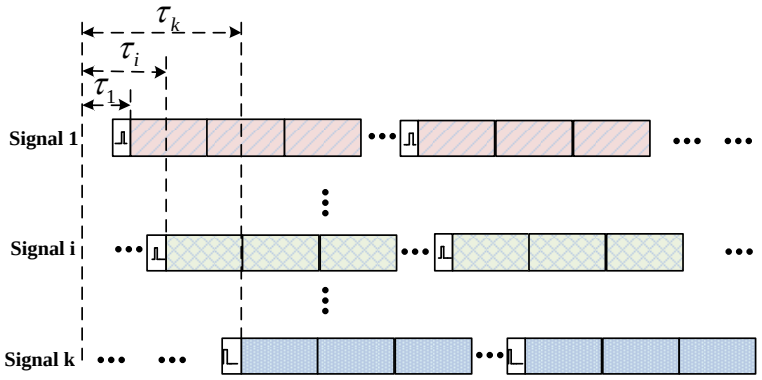

Figure 5.3: The structure of transmitted signals.

can be recorded as $\tau_1, \tau_2, \cdots, \tau_i, \cdots, \tau_k$. Thus, the delays between any two signals can be gotten.

5.2.4 An Example Applying the Asynchronous CDMA Mechanism

Here, an example is given when there are three transmitters (Tx_1, Tx_2, Tx_3). Different transmitters transmit different data sequences: $\overline{d_1} = [-1, 1, -1, 1]$, $\overline{d_2} = [1, 1, -1, -1]$ and $\overline{d_3} = [1, -1, -1, 1]$. Codes assigned to different transmitters are as follows: $\overline{c_1} = [-1, -1, -1, -1, 1, 1, 1, 1]$, $\overline{c_2} = [1, 1, -1, -1, 1, 1, -1, -1]$, and $\overline{c_3} = [1, -1, 1, -1, 1, -1, 1, -1]$. As can be verified, the three codes we have selected are COWHCs. As shown in Fig. 5.4, after the encode process, the encoded data for Tx_1 is:

$$\begin{aligned}\overline{D_1} = \overline{d_1} \otimes \overline{c_1} = [&1, 1, 1, 1, -1, -1, -1, -1,\\ &-1, -1, -1, -1, 1, 1, 1, 1,\\ &1, 1, 1, 1, -1, -1, -1, -1,\\ &-1, -1, -1, -1, 1, 1, 1, 1].\end{aligned} \tag{5.21}$$

The encoded data for Tx_2 and Tx_3 can be determined as:

$$\begin{aligned}\overline{D_2} = \overline{d_2} \otimes \overline{c_2} = [&1,1,-1,-1,1,1,-1,-1,\\ &1,1,-1,-1,1,1,-1,-1,\\ &-1,-1,1,1,-1,-1,1,1,\\ &-1,-1,1,1,-1,-1,1,1],\end{aligned} \tag{5.22}$$

and

$$\begin{aligned}\overline{D_3} = \overline{d_3} \otimes \overline{c_3} = [&1,-1,1,-1,1,-1,1,-1,\\ &-1,1,-1,1,-1,1,-1,1,\\ &-1,1,-1,1,-1,1,-1,1,\\ &1,-1,1,-1,1,-1,1,-1].\end{aligned} \tag{5.23}$$

In order to guarantee the optical signals are positive, we replace all '-1' to '0' in the encoded data and get $\overline{D_1'}, \overline{D_2'}, \overline{D_3'}$. Pilot symbol for Tx_1 is '0010', for Tx_2 is '0100' while for Tx_3 is '0110'. The delay of three signals assumed as $\tau_1 = -52, \tau_2 = -46, \tau_3 = -28$ are added. At the receiver side, after detecting the delays using pilot symbols, we can find one period of signal which is not effected by the pilot symbols. Then, after downsampling, the received signal could be written as:

$$\begin{aligned}Signal &= \overline{D_1'} \times T(\tau_1) + \overline{D_2'} \times T(\tau_2) + \overline{D_3'} \times T(\tau_3)\\ &= [1,0,1,0,2,1,1,0,3,2,2,1,2,3,1,2,\\ &\quad 1,2,1,2,0,1,1,2,1,2,2,3,2,1,3,2].\end{aligned} \tag{5.24}$$

The first step to estimate the data is compensating the signal with the delay and do the decode process as follows:

$$\begin{aligned}Y_1 = Signal \times T(-\tau_1) \odot \overline{c_1} = [&2,3,1,2,1,2,1,2,\\ &0,1,1,2,1,2,2,3,2,1,3,2,1,0,1,0,\\ &2,1,1,0,3,2,2,1] \odot [-1,-1,-1,-1,1,1,1,1]\\ &= [-2,4,-6,4].\end{aligned} \tag{5.25}$$

$$\begin{aligned} Y_2 = Signal \times T(-\tau_2) \odot \overline{c_2} = [1,2,0,1,1,2,1,2, \\ 2,3,2,1,3,2,1,0,1,0,2,1,1,0,3,2, \\ 2,1,2,3,1,2,1,2] \odot [1,1,-1,-1,1,1,-1,-1] \\ = [2,6,-6,-2]. \end{aligned} \tag{5.26}$$

$$\begin{aligned} Y_3 = Signal \times T(-\tau_3) \odot \overline{c_3} = [2,1,1,0,3,2,2,1, \\ 2,3,1,2,1,2,1,2,0,1,1,2,1,2,2,3, \\ 2,1,3,2,1,0,1,0] \odot [1,-1,1,-1,1,-1,1,-1] \\ = [4,-4,-4,4]. \end{aligned} \tag{5.27}$$

The second step is to calculate the M matrix. In this example, when we calculate M_{21}, $\tau_{21} = |\tau_1 - \tau_2| = 6$ should be determined at first step. Because code length $cl = 8$, we can calculate the code movement $cm = 6$ while data movement $dm = 0$. Thus, we calculate the parameters:

$$\begin{aligned} a &= \overline{c_2}(1 : cl - cm) \cdot \overline{c_1}(cm + 1 : cl) \\ &= \overline{c_2}(1 : 2) \cdot \overline{c_1}(7 : 8) \\ &= 2, \end{aligned} \tag{5.28}$$

$$\begin{aligned} b &= \overline{c_2}(cl - cm + 1 : cl) \cdot \overline{c_1}(1 : cm) \\ &= \overline{c_2}(3 : 8) \cdot \overline{c_1}(1 : 6) \\ &= -2, \end{aligned} \tag{5.29}$$

where operation $\cdot$ is the inner product. $dm = 0$,

$$T(0) = \begin{bmatrix} 1 & 0 & 0 & 0 \\ 0 & 1 & 0 & 0 \\ 0 & 0 & 1 & 0 \\ 0 & 0 & 0 & 1 \end{bmatrix} \tag{5.30}$$

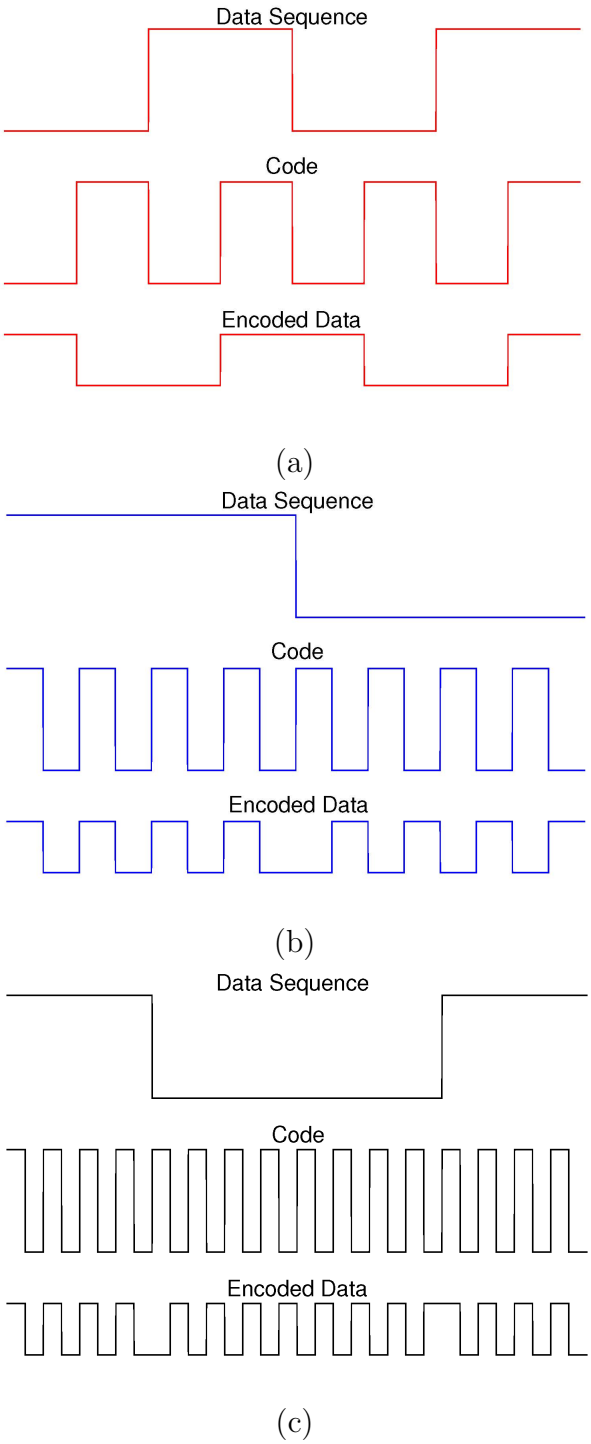

Figure 5.4: Generation of three encoded datas: (a) $\overline{d_1} = [-1, 1, -1, 1]$**,** $\overline{c_1} = [-1, -1, -1, -1, 1, 1, 1, 1]$ **(b)** $\overline{d_2} = [1, 1, -1, -1]$**,** $\overline{c_2} = [1, 1, -1, -1, 1, 1, -1, -1]$ **(c)** $\overline{d_3} = [1, -1, -1, 1]$**,** $\overline{c_3} = [1, -1, 1, -1, 1, -1, 1, -1]$**.**

Thus,

$$M_{21} = \begin{bmatrix} 2 & -2 & 0 & 0 \\ 0 & 2 & -2 & 0 \\ 0 & 0 & 2 & -2 \\ -2 & 0 & 0 & 2 \end{bmatrix} \times T(0) = \begin{bmatrix} 2 & -2 & 0 & 0 \\ 0 & 2 & -2 & 0 \\ 0 & 0 & 2 & -2 \\ -2 & 0 & 0 & 2 \end{bmatrix}. \tag{5.31}$$

In a similar way, we can calculate the M_{ij}, $i = 1, 2, 3$ and $j = 1, 2, 3$. At last, the M matrix can be written as:

$$M = \begin{bmatrix} 8I_{4\times4} & M_{12} & M_{13} \\ M_{21} & 8I_{4\times4} & M_{23} \\ M_{31} & M_{32} & 8I_{4\times4} \end{bmatrix} \tag{5.32}$$

where

$$M_{12} = M_{21}^T = \begin{bmatrix} 2 & 0 & 0 & -2 \\ -2 & 2 & 0 & 0 \\ 0 & -2 & 2 & 0 \\ 0 & 0 & -2 & 2 \end{bmatrix} \tag{5.33}$$

$$M_{13} = M_{31} = M_{23} = M_{32} = \begin{bmatrix} 0 & 0 & 0 & 0 \\ 0 & 0 & 0 & 0 \\ 0 & 0 & 0 & 0 \\ 0 & 0 & 0 & 0 \end{bmatrix} \tag{5.34}$$

Then, the estimated data could be written as:

$$[\widetilde{d}_1, \widetilde{d}_2, \widetilde{d}_3] = [Y_1, Y_2, Y_3] \times M^{-1} \tag{5.35}$$

where M^{-1} is the inverse of matrix M. When there is no noise in the transmission process, we can get the result that: $\widetilde{d}_1 = [-0.5, 0.5, -0.5, 0.5]$,

$\widetilde{d_2} = [0.5, 0.5, -0.5, -0.5]$ and $\widetilde{d_3} = [0.5, -0.5, -0.5, 0.5]$. After multiplying by 2, we can get the estimated ID for each transmitter. Random delays are chosen as shown in Fig. 5.5. After applying this asynchronous CDMA mechanism, the data could be estimated successfully.

5.3 Indoor Positioning Algorithm

LEDs can be modeled as Lambertian sources in a self-propagating beam divergence angle [101]. For each transmission, P_t is the power difference between the logical 0 and 1 transmissions. The power difference at the receiving end indicates P_r^i $(i = 1, 2, 3, 4)$. Without loss of generality, a simpler power relationship between the transmitter and receiver is [102]:

$$P_r^i = \frac{C}{d^2}\cos(\phi)\cos(\psi)P_t, i = 1, 2, 3, 4, \phi \leq \Psi, \psi \leq \Phi, \tag{5.36}$$

where ψ is the angle of incidence, ϕ is the angle of irradiance, d is the distance between the LED transmitter and the PD receiver and C is a constant value. Φ is the HPA and Ψ is the FOV of the receiver. Substituting the geometrical relationship $\cos(\phi) = \frac{h}{d}$ and $\cos(\psi) = \frac{h}{d}$ into Eq. 5.36, we can get $P_r^i = \frac{Ch^2}{d^4}P_t$. The theoretical relationship between the normalized received optical power and the distance can be represented as

$$P_r^i/P_0 = (\frac{h}{d})^4, \tag{5.37}$$

as depicted in Fig. 5.6. Here, P_0 is the reference power received at the location below the LED lamp with vertical distance h. Therefore, the distance from the lamp transmitter to the receiver can be calculated if each P_r^i can be measured at the receiving end.

The target of the VLC positioning system is to estimate the location of the receiver. The Cartesian coordinate system is set up to determine the

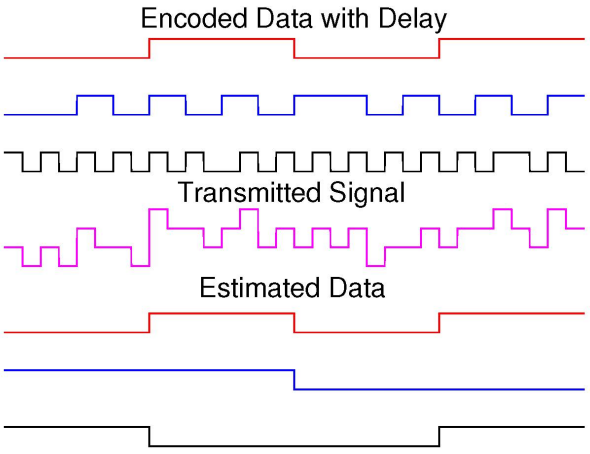

(a)

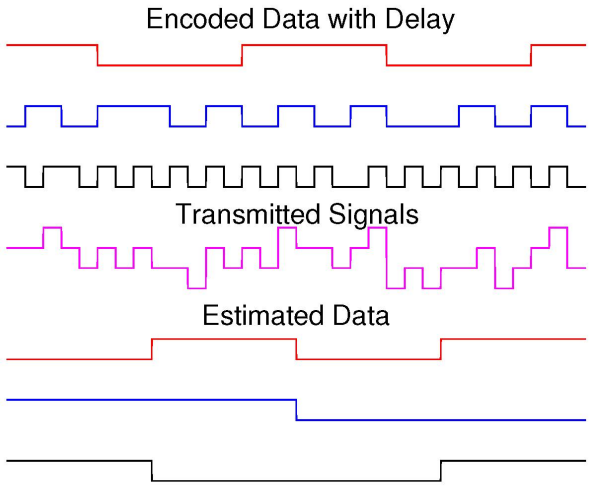

(b)

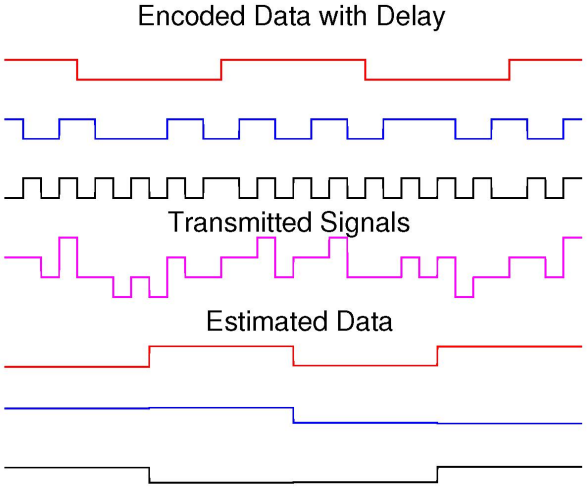

(c)

Figure 5.5: Examples of using delay compensation CDMA technique to estimated data with different delays: (a) $\tau_1 = -52$, $\tau_2 = -46$, $\tau_3 = -28$, **(b)** $\tau_1 = 1$, $\tau_2 = 7$, $\tau_3 = 11$, **(c)** $\tau_1 = -32$, $\tau_2 = 23$, $\tau_3 = -108$.

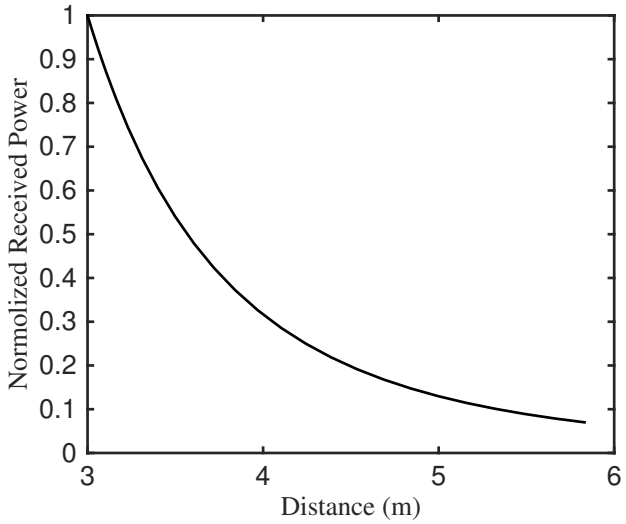

Figure 5.6: Theoretical relationship: the normalized power versus the distance.

detail position of the receiver. As Fig. 5.7 shows, three lights are used for trilateration calculation. The $LEDi$'s coordinates are (x_i, y_i, h), the $LEDj$'s coordinates are (x_j, y_j, h), the $LEDk$'s coordinates are (x_k, y_k, h). Because the height component is given, the receiver's position can be expressed as (x^e, y^e). According to the basic trilateration method, the positioning process can be carried out.

The receiver obtains the signals from the four LED lamps with noise added and uses the received signal power to compute the distance between the transmitters and the receiver. The noise model in this VLP system is the same as the one described in Eq. 2.13. Denote the distances from the $LEDi$, $LEDj$, $LEDk$ to the receiver projected on the receiver plane as r_i, r_j,andr_k. The following distance equations can be established:

$$\begin{cases} \sqrt{(x^e - x_i)^2 + (y^e - y_i)^2} = r_i \\ \sqrt{(x^e - x_j)^2 + (y^e - y_j)^2} = r_j. \\ \sqrt{(x^e - x_k)^2 + (y^e - y_k)^2} = r_k \end{cases} \tag{5.38}$$

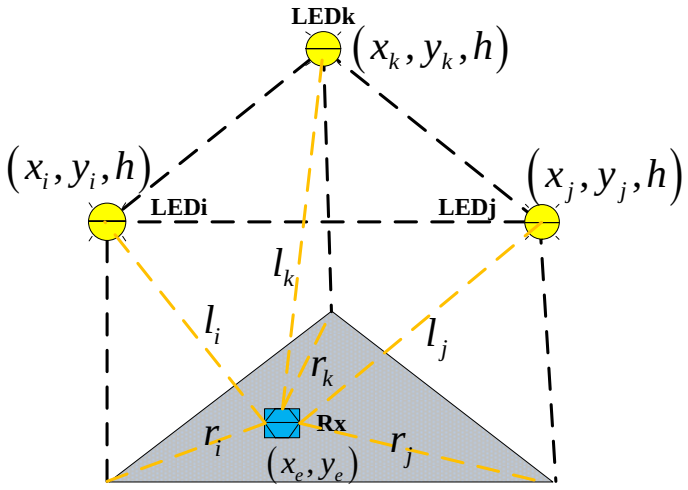

Figure 5.7: Schematic diagram of the trilateration method.

If the received power from these three transmitters are known, the projected ranges between the lamps and the receiver could be calculated according to the relationship as described in Eq. 5.37. Then, Eq. 5.38 could be used to calculate the estimate position of the receiver. The above equation system is derived from three circles with the radius of the measured distance r_i, r_j, r_k and center of the reference points (x_i, y_i), (x_j, y_j), (x_k, y_k). Intersection between these three circles is calculated as target position. The above equality holds if there is no error occurring when estimating the distances between the LED lamps and the PD. However, this assumption may not work in practical settings. The above system of equations should change to the following optimization problem, which can be solved by trust region method [103] efficiently as Eq. 5.39 shows.

$$\begin{aligned} \text{minimize} f_1 &= (x^e)^2 + (y^e)^2 - r_1^2 \\ f_2 &= (x^e - l)^2 + (y^e)^2 - r_2^2 \\ f_3 &= (x^e - \frac{l}{2})^2 + (y^e - \frac{\sqrt{3}l}{2})^2 - r_3^2 \end{aligned} \tag{5.39}$$

Table 5.1: Simulation parameters

Parameters	Value
Room dimensions	$4 \times 4 \times 3$ (m^3)
Φ	45°
Ψ	80°
γ	0.53 (A/W)
Power of each LED bulb	1.2 (W)
Positions of LED bulbs	LED1 (2, 2, 3) LED2 (1, 0.268, 3) LED3 (3, 3.732,3)
Modulation bandwidth (B)	20 (MHz)

5.4 Results and Discussion

Fig. 5.8 depicts a proposed system configuration for a typical indoor environment. Three LED lamps are mounted on the ceiling. The receiver is a PD with 80° FOV. When the receiver is moving on the receiver plane, signals from three LED lamps are collected and then distinguished by the asynchronous CDMA technique. RSS measurements can be translated into estimated distances between the LED transmitters and the PD receiver and then trilateration algorithm is used to determine the position details of the receiver. Parameters of the simulation are listed in Table 5.1.

As Fig 5.9 shows, when there are only three lights in the room, the positioning technique cannot be applied in the whole room. Because when the distance between the transmitter and receiver is far, the signal could not be received and then be used for trilateration. For the positions where signals from three lights are all received, after applying trilateration, the receiver's position could be estimated. For the estimated position inside the

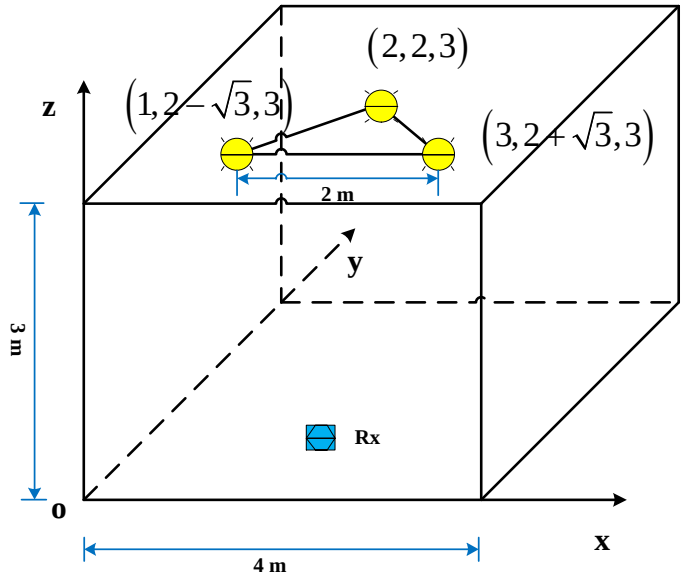

Figure 5.8: System diagram with three lights installed on the ceiling.

triangle which is enclosed by the projected points of three lamps, the mean positioning error is 1.84 cm while outside the triangle, the mean positioning error is 2.63 cm.

In order to get positioning estimate in the whole room, we increase the lamp numbers as Fig 5.10 shows. $LED1$ to $LED7$ are installed as Fig 5.11 indicated. These seven lamps compose a large hexagon with length of side equal to 2 m. $LED1$ is still at the middle of the room with coordinates (2, 2, 3). Thus, other six lamps' coordinates can be determined accordingly.

With the increase of COWHC number, the code length will become much longer to keep the characteristic of COWHC. In order to add one COWHC, the code length needs to be doubled, which means the computing of M matrix will become much complicated. What we want is consuming the least amount of the code resources and achieving the best effect. Thus, we begin with the case that reuse only three codes.

When there are only three codes that are applied to these seven lamps,

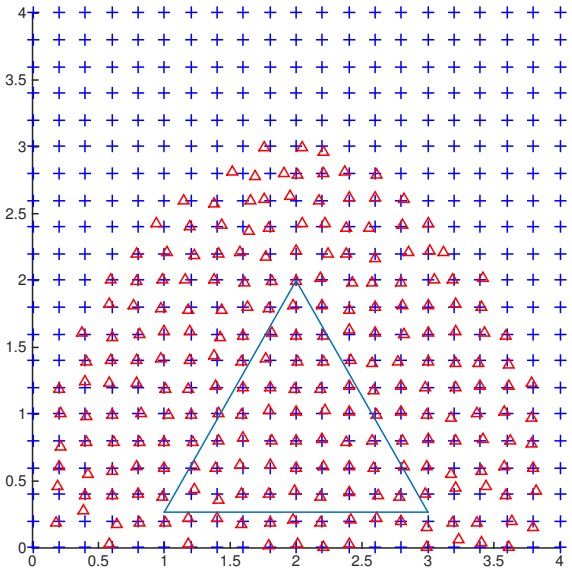

Figure 5.9: Results of positioning accuracy (+ is the actual position while △ is the estimated position) when only three lights in the room.

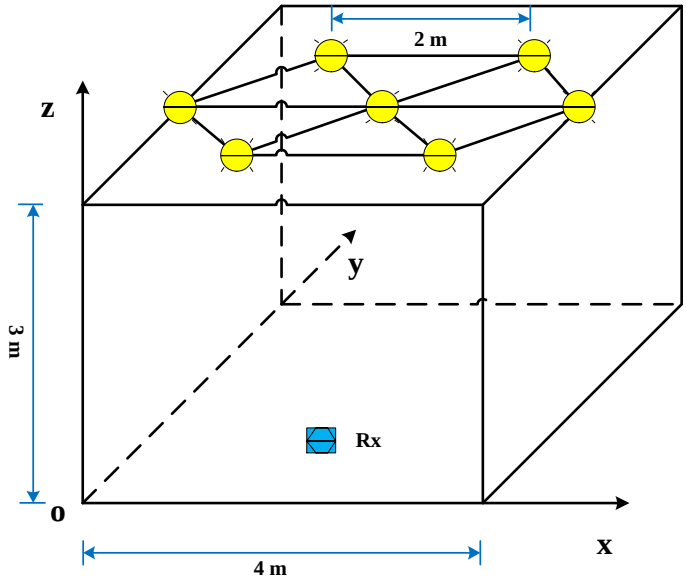

Figure 5.10: System diagram with six lights installed on the ceiling.

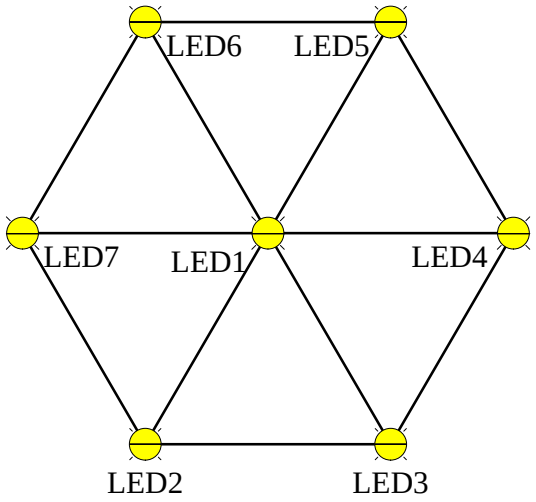

Figure 5.11: Six LED arrangement on the ceiling.

as Fig 5.12 (a) shows, the lamps with the same color in the figure share the same code. All positions in the room can finish position estimation. At any position on the receiver plane, find the nearest three lamps at first. Then, detect the delays between the lamps and the next step is using the proposed asynchronous CDMA technique to decode the signals. After getting the three signals' amplitudes, power-distance relationship is applied to get the distance estimations between the LED lamps and the receiver. At last, trilateration is applied to get the estimated position. However, we found that the accuracy is quit low. The average positioning error is 32.78 cm. Inside the hexagon, which is enclosed area projected by the seven lamps on the receiver plane, the mean positioning error is 34.61 cm while outside the hexagon, the average positioning error is 30.28 cm. The positioning error is so large mainly caused by the same code interference. For example, when the nearest three lamps detected is $LED1, LED3$ and $LED4$, not only the signals from these three lamps are received, but also the signals from $LED2, LED5$, and even $LED6, LED7$. As we know, because $LED2$ and $LED6$ share the same code with $LED4$ while $LED5, LED7$ share the same code with $LED3$, they will

have large interference to the signal we want to decode and this interference cannot be eliminated by our asynchronous CDMA method.

When four codes are applied to estimate the position, as shown in 5.12 (c), the distance between two lamps sharing the same code increases from previous $2\sqrt{3}$ to 4. In this case, we first find the four lamps with relatively larger received amplitudes. Then, our delay compensation CDMA method is used to decode the received signal and based on the decoded signals, three signals with relatively large amplitudes are selected. The third step is to use the power-distance relationship to calculate the distances between the LEDs and the receiver based on the received power. At last, trilateration is applied. The average positioning error using four codes is 22.18 cm. The mean positioning error inside the hexagon is 21.14 cm while outside is 23.60 cm. Although the positioning error is still large, compared with the previous case, we can see that the interference between the same code is decreased.

If we increase the number of codes to seven, that means no the same code is used in the whole room. Each transmitter is assigned an independent COWHC. We apply our method to get all the seven lamps' IDs and signal amplitudes. Then, similar as the previous case, we choose the three signals with relative larger amplitudes for trilateration. Because there is no interference from the signals with the same code, the estimated error is quit small. As Fig. 5.13 shows, the mean positioning error is 0.96 cm on the whole plane. The mean positioning error inside the hexagon is 0.89 cm while the mean error outside is 1.06 cm.

When the rooms are very large, such as in supermarkets or large shopping malls or when the rooms are with irregular shapes, how to apply our method to those cases? Next, we will discuss how to extend our method to a larger plane.

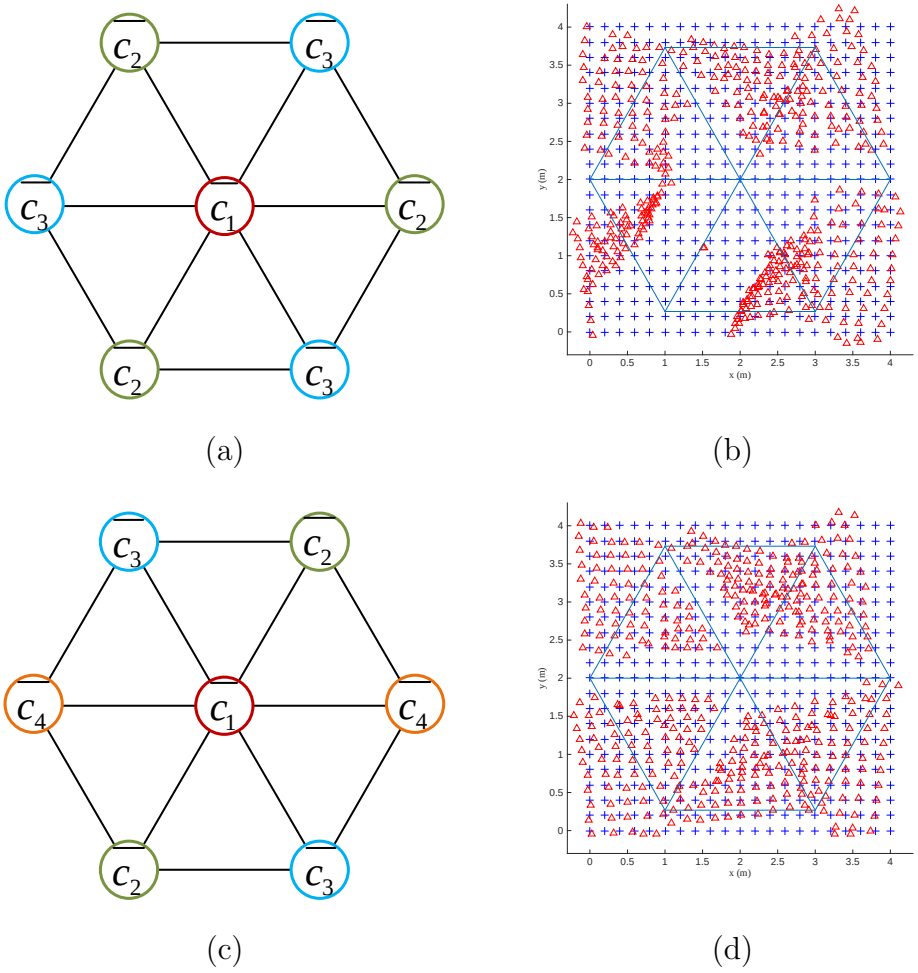

Figure 5.12: (a) Three-codes assignment for seven lamps (b) Results of positioning accuracy (+ is the actual position while △ is the estimated position) when three codes are applied. (c) Four-codes assignment for seven lamps (d) Results of positioning accuracy when four codes are applied.

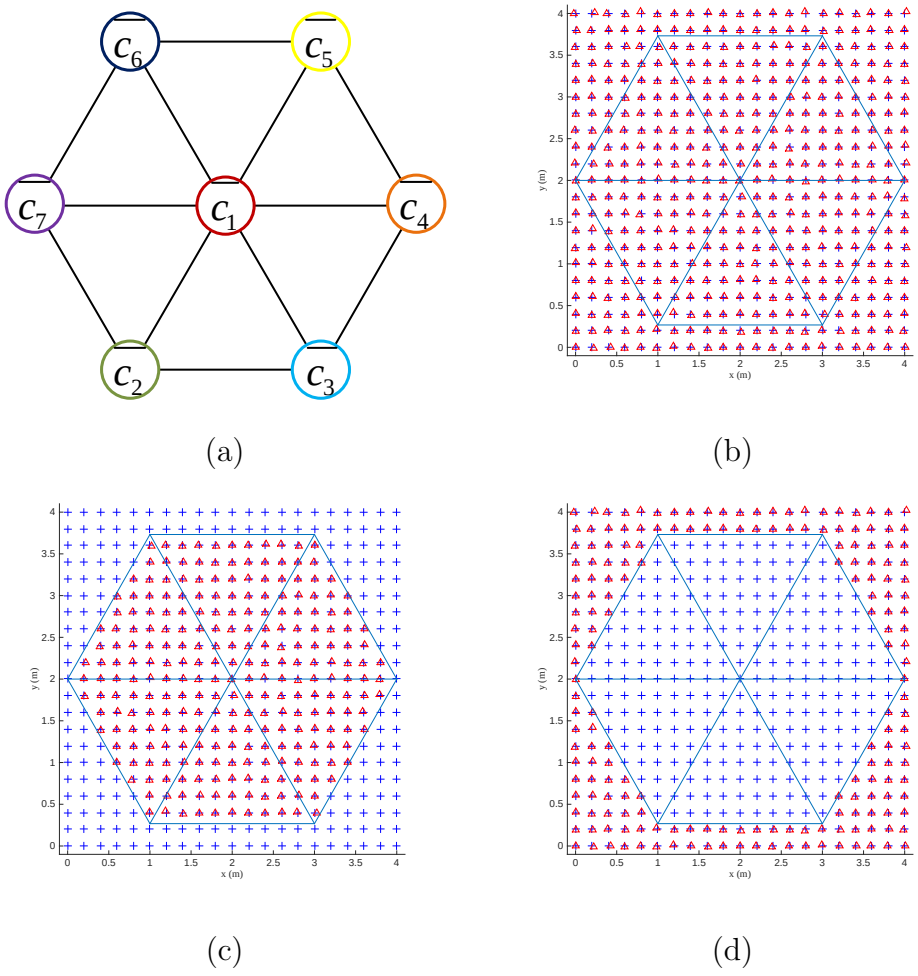

(a) (b)

(c) (d)

Figure 5.13: (a) Seven-codes assignment for seven lamps (b) Results of positioning accuracy (+ is the actual position while △ is the estimated position) when seven codes are applied in the room. (c) Difference between the estimated position inside the hexagon and real position (d) Difference between the estimated position outside the hexagon and real position.

As Fig 5.14 shows, our lamps used for trilateration are extended to a larger plane. We assume the nearest distance between two lamps is 3 m, which means the length of side for the smallest triangle cell is 3 m. For any point on the receiver plane, it could be included in one small triangle cell. It could at maximum receive the signals from the nearest 12 lamps, as drawn in Fig. 5.14. Because for the further lamps, the minimum irradiance angle is 60°, which is larger than the HAP we have assumed. Thus, we couldn't receive the signals from the further lamps. So, for any point on the receiver plane, only the nearest 12 lamps interference need to be considered. The positioning is only carried out in the gray triangle cell in the later discussion, which is the center triangle cell of the 12 lamps. The accurate positioning process is carried out in two steps. For the driver circuit modulates the ID information on the LED light, after the receiver receives the signal and decodes the IDs, the nearest 12 lamps is determined. Thus, the receiver can know its rough position based on the information from the light fixtures and a pre-downloaded map, which is the first step. The second step is according to the decoded signal amplitudes to apply trilateration, which is detail discussed as follows.

When we use three codes for the extension case, as Fig. 5.15 (a) shows. The lamps using the same color means they share the same code. We found the three signals with largest amplitudes and apply the delay compensation CDMA technique to decode the signals. Then, changing the signal amplitudes to the distances between the LED transmitters and the receiver according to the power-distance relationship. At last, the trilateration is applied. In Fig. 5.15 (b), the difference between the estimated position and the actual position is drawn. The mean positioning error is 14.54 cm.

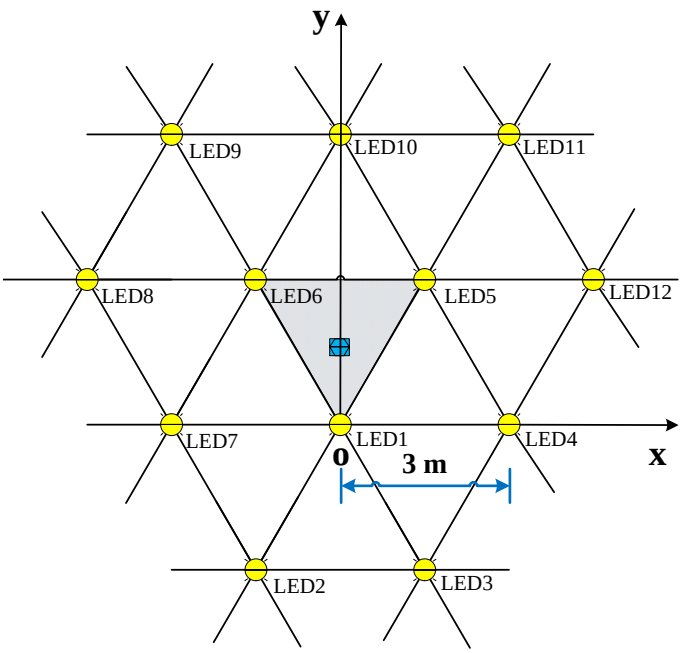

Figure 5.14: The extended LED arrangement.

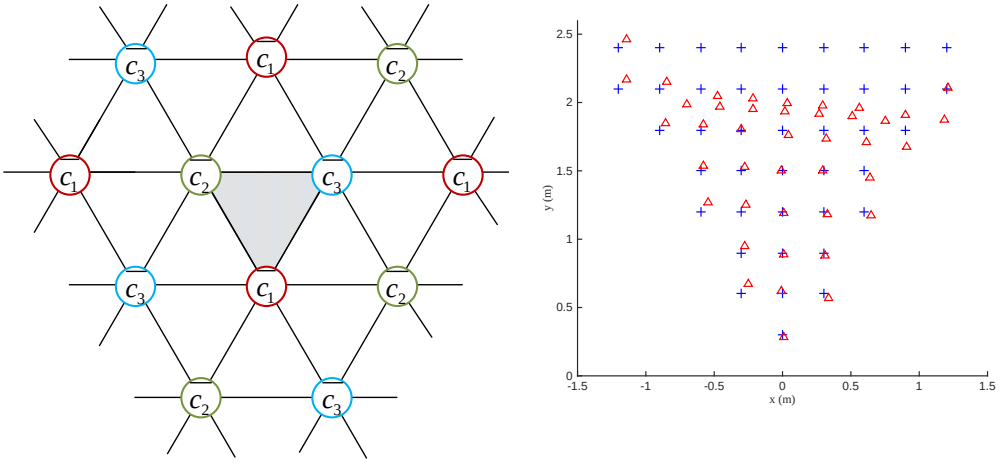

(a) (b)

Figure 5.15: (a) Three-codes assignment for the LEDs in an extended plane (b) Results of positioning accuracy (+ is the actual position while △ is the estimated position) on the receiver plane.

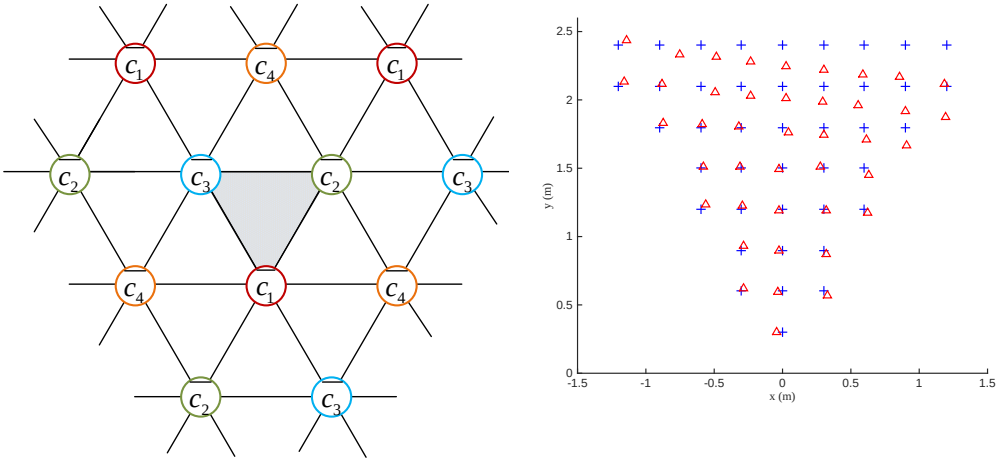

(a) (b)

Figure 5.16: (a) Four-codes assignment for the LEDs in an extended plane (b) Results of positioning accuracy (+ is the actual position while △ is the estimated position) on the receiver plane.

When four codes are reused, as Fig. 5.16 shows. Four signals with largest amplitudes are detected at the first step. Then, applying the asynchronous CDMA to decode these four signals. The third step is to choose three strongest signals from the four signals to finish trilateration. The average positioning error is 8.56 cm in this case, as shown in Fig. 5.16 (b).

For the case when nine codes are used to extend, as Fig. 5.17 shows, the first step is to found the pilot with largest amplitude and then determine which seven codes are used for decoding. For example, if $LED5$ is the lamp with largest signal amplitude, then $LED1, LED4, LED5, LED6, LED10, LED11$ and $LED12$ are used to apply the delay compensation CDMA technique. Then, after decoding the transmitted data and amplitudes, we choose three received signals with largest amplitudes to estimate the position. The mean positioning error is 1.23 cm, which is quite small, as shown in Fig. 5.17 (b). Then how about

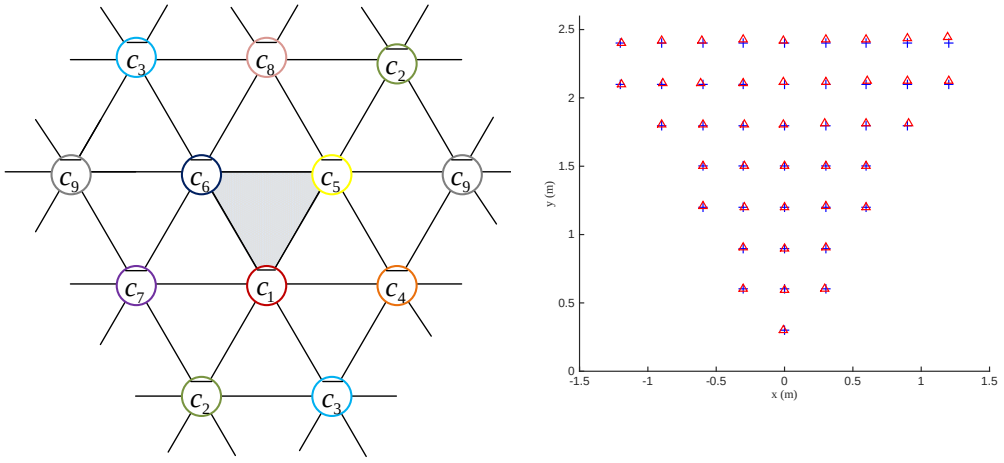

(a) (b)

Figure 5.17: (a) Nine-codes assignment for the LEDs in an extended plane (b) Results of positioning accuracy (+ is the actual position while △ is the estimated position) on the receiver plane.

using more codes, such as 12, 27 or more? On one hand, with the increase of different codes, the code length will increase fastly. As mentioned in Eq. 5.20, the code length with K different codes is 2^{K-1}. That means adding one code will lead to double the code length, which add the complexity of calculating M matrix. On the other hand, the positioning accuracy cannot be improved obviously. Because in the nine-codes case, the interference from lamps sharing the same code is very little since the distance between two lamps sharing the same code is large enough. Thus, even though apply more codes, the performance of positioning will not be improved.

5.5 Conclusion

In this chapter, a delay compensation code division multiple access technique has been proposed and derived. This technique can be used in indoor

positioning system and there is no synchronization requirement between the transmitters. The simulation was carried out in a typical room with dimensions 4m $\times$ 4m $\times$ 3m. The cases of reusing codes were discussed and compared. The best performance were achieved when seven Cyclic Orthogonal Walsh-Hadamard codes were used and the mean positioning error is as small as 0.96 cm. The code arrangements for the larger rooms or rooms with irregular shapes were also studied. When nine different cyclic orthogonal codes were applied, the average positioning error could be as small as 1.23 cm.

Chapter 6

Conclusions and Future Work

6.1 Conclusions

This thesis focused on designing and analyzing the visible light based communication and positioning systems, which are becoming promising candidates for the future indoor wireless communication and positioning systems under light emitting diodes (LEDs) lighting environments. LEDs are occupying a growing market. When compared with the conventional bulbs, LEDs have many advantages, such as long life time, high tolerance to humidity, energy efficiency and ecologically friendly. Modulating signal on the visible light emitted from the LEDs, not only can be used for illumination, but also be the light sources for data communication and positioning.

In Chapter 3, we have inversely designed the optimal LED arrangement for indoor visible light communication (VLC) systems, which can provide both sufficient illumination and uniform signal-to-noise ratio (SNR) over the receiving plane. The root mean square (RMS) delay spread of the system was also investigated to show the tolerance for the inter-symbol interference (ISI) in the proposed design. Under the optimal design, the SNR fluctuation

is only 0.7 dB and the horizontal brightness varies from 450 lx to 648 lx. Furthermore, a suboptimal design has been proposed to accommodate the cabling issue of practical implementation. Numerical results showed that a SNR fluctuation of 2.8 dB and sufficient illumination can be achieved by the suboptimal design. Besides, both the optimal and suboptimal systems can realize the ISI-free transmission for the non return-to-zero (NRZ) on-off keying (OOK) signals.

In Chapter 4, we have demonstrated an indoor positioning system (IPS) using LED lamps. We used Hamming filters to distinguish the signals from the different light sources. A pre-determined relationship between the normalized received power and distance is used to calculate the distances from the transmitters to the receiver. A two dimensional (2D) positioning algorithm was developed to determine the receiver's coordinates. In the experimental space of 100 cm $\times$ 118.5 cm $\times$ 128.7 cm, the mean distance errors of x-axis and y-axis are 1.18 cm and 1.25 cm, respectively. An error correcting algorithm was used to decrease the positioning errors at the corners of the receiver plane, where relatively large positioning errors happened. A three dimensional (3D) positioning algorithm was also demonstrated. On the plane with 1.3 cm height, the mean positioning error of x-axis, y-axis and vertical are 0.90 cm, 1.54 cm and 0.66 cm, respectively. The experimental results of error distribution on four altitude levels were presented and the average distance errors on each test plane are all within 3 cm. A random track in the 3D space was also measured and the positioning errors are within 3 cm.

Different from the visible light positioning (VLP) system based on frequency division multiple access (FDMA) as discussed in Chapter 4, Chapter 5 proposed a VLP system based on another multiple access

technology, which is named delay compensation code division multiple access (CDMA). Synchronization is necessary among LEDs when putting CDMA into use. However, in a commercial system, the synchronization is difficult to realize as LED lamps are usually used only as transmitters thus cannot receive synchronization signals. The delay compensation CDMA technique that we have proposed is an asynchronous mechanism. It not only decoded the IDs of the relative LED transmitters but also got the signal strengths from the different lamps. Simulation was carried out in a typical room with dimensions of 4 m $\times$ 4 m $\times$ 3 m. The best performance was achieved when seven cyclic orthogonal walsh-hadamard codes (COWHC) were used. The mean positioning error is only 0.96 cm. The code arrangements for the larger rooms or rooms with irregular shapes were also discussed. When nine codes were applied, the average positioning error could be as small as 1.23 cm.

6.2 Future Work

In this thesis, work has been done on the visible light communication and positioning systems. Besides, the following topics are worth to be studied in the future work.

Some possible future directions on VLC are the following.

Firstly, precoding technology can be applied to VLC systems. The study of multi-user multiple input and multiple output (MIMO) VLC systems has emerged recently as an important research topic. [51] introduced an optical code-division multiple access (OCDMA) system for multi-user VLC, which utilized random optical codes (ROCs) as coding sequences. Nevertheless, these complicated systems have high requirement for terminal's signal processing ability. The main difficulty for transmission is the separation

of received data for different user terminals. Precoding algorithm can be adopted in the proposed system to eliminate multi-user interference (MUI). Block diagonalization (BD) precoding algorithm has been studied in [104]. This problem can also be addressed through a precoding technique called Tomlinson-Harashima precoding, which has not been studied. Different precoding algorithms can be analyzed and applied in the VLC systems.

Secondly, further study can be carried out in OFDM-based VLC systems. On one hand, in order to further improve communication capacity and quality, orthogonal frequency division multiplexing (OFDM), which proves to be a promising technology in optical fiber systems, has been usually applied to increase the relatively narrow band of white LEDs and counteract severe multi-path effect caused by indoor light reflection. On the other hand, the brightness of LEDs should be adjusted for the convenience of daily life and work. Thus dimming control support in VLC systems should receive adequate attention for different needs and for the consideration of saving energy. There are many schemes for dimming control, among which pulse width modulation (PWM) is widely adopted by adjusting the duty cycle instead of varying the LED current. A method to combine OFDM and PWM can be studied to realize a new dimming mechanism for a dimming control system.

Thirdly, designing an angle diversity receiver for VLC systems could be a meaningful and interesting topic, which can help to achieve a better performance. Basically, the angle diversity detection can be obtained by using conventional receiver with multiple photodetectors [105]. Different photodetectors are oriented in various directions. An imaging diversity receiver is composed of an optical concentrator that focuses on a segmented photodetector array, and a sectored receiver which is a hemisphere [106–108].

For the hemisphere, a set of parallels and meridians defines the photodetector boundaries. In [109], it is found that the design of the conventional receiver structure using angle diversity that yields improved performance with respect to the main indoor infrared (IR) channel parameters. Thus, applying angle diversity receiver in VLC systems could be a interesting topic, and we can predict that angle diversity receiver could also improve the system performance.

Some possible future directions on VLP systems are described below.

Firstly, widely used techniques in positioning systems primarily assume a line of sight (LOS) channel where transmitters and receivers have aligned their field of view (FOV) to maximize channel response. However, in more practical scenarios, receiver movements and orientation changes are common. For example, in VLC-based indoor access network, user's smartphone equipped with a light sensor can move and rotate based on user's actions. This means that receiver's FOV cannot always be aligned with transmitters. Thus, the drop of received optical power can be significant due to such misalignment. It is necessary to design techniques that can ensure high data rates even in the presence of FOV misalignment cases. This requires design and development of methods that can provide graceful degradation in data rate using optical power of reflected lights. Designing such techniques is challenging and interesting.

Secondly, apart from FOV alignment problem, another critical limitation is imposed by shadowing events. When an object or human blocks LOS component, observed optical power degrades substantially, resulting in severe data rate reduction. Limited research has been done to model the effect of shadowing event on VLP systems. When an LOS is blocked by a shadowing event, it is not only necessary to exploit reflected optical power of diffuse

channels but it is also necessary to do so in a timely manner as typical blockage events can be of very short duration, such as human passing by. Thus, it is imperative to design techniques that can quickly react to changes in received power due to shadowing.

Thirdly, applying machine learning algorithms to VLP system is promising. As we know, machine learning is a field of artificial intelligence dealing with algorithms that improve performance over time with experience. Supervised learning algorithms for regression can be trained on data with the correct value given along with each variable. This allows the learner to build a model based on the attributes that best fit the correct value. By giving more data to the algorithm the model is able to be improved. With an increasing number of sensors being made available in the majority of mobile devices, large amounts of data can be collected and used to aid in a localization process. Machine learning algorithms may also provide a fast, efficient method for indoor tracking, which will often be more useful to applications than static localization. Machine learning algorithm are widely used in Wi-Fi or infra red based localization [110–112]. However, seldom research has been done to combine visible light and machine learning algorithms. Developing new algorithms is also an interesting topic for future study on VLP systems.

Bibliography

[1] S. Arnon, J. Barry, and G. Karagiannidis, *Advanced optical wireless communication systems*. Cambridge university press, 2012.

[2] Z. Ghassemlooy, W. Popoola, and S. Rajbhandari, *Optical wireless communications: system and channel modelling with Matlab®*. CRC Press, 2012.

[3] C. Medina, M. Zambrano, and K. Navarro, "Led based visible light communication: Technology, applications and challenges-a survey," *International Journal of Advances in Engineering & Technology*, vol. 8, no. 4, p. 482, 2015.

[4] A. G. Bell, W. Adams, W. Preece *et al.*, "Discussion on 'the photophone and the conversion of radiant energy into sound," *Telegraph Engineers, Journal of the Society of*, vol. 9, no. 34, pp. 375–383, 1880.

[5] M. Groth, "Photophones revisited," *Amateur Radio Magazine*, pp. 13–17, 1987.

[6] D. K. Jackson, T. K. Buffaloe, and S. B. Leeb, "Fiat lux: A fluorescent lamp digital transceiver," *IEEE Transactions on industry applications*, vol. 34, no. 3, pp. 625–630, 1998.

[7] O. Bouchet, M. El Tabach, M. Wolf, D. C. O'Brien, G. E. Faulkner, J. W. Walewski, S. Randel, M. Franke, S. Nerreter, K.-D. Langer *et al.*, "Hybrid wireless optics (hwo): Building the next-generation home network," in *Communication Systems, Networks and Digital Signal Processing, 2008. CNSDSP 2008. 6th International Symposium on.* IEEE, 2008, pp. 283–287.

[8] M. C. Al Naboulsi, H. Sizun, and F. de Fornel, "Wavelength selection for the free space optical telecommunication technology," in *Photonics Europe.* International Society for Optics and Photonics, 2004, pp. 168–179.

[9] J. K. Kim and E. F. Schubert, "Transcending the replacement paradigm of solid-state lighting," *Optics Express*, vol. 16, no. 26, pp. 21 835–21 842, 2008.

[10] G. Pang, T. Kwan, C.-H. Chan, and H. Liu, "Led traffic light as a communications device," in *Intelligent Transportation Systems, 1999. Proceedings. 1999 IEEE/IEEJ/JSAI International Conference on.* IEEE, 1999, pp. 788–793.

[11] K. Kulhavy, "Home: ronja," 2012.

[12] Y. Tanaka, T. Komine, S. Haruyama, and M. Nakagawa, "Indoor visible light data transmission system utilizing white led lights," *IEICE transactions on communications*, vol. 86, no. 8, pp. 2440–2454, 2003.

[13] Y. Tanaka, S. Haruyama, and M. Nakagawa, "Wireless optical transmissions with white colored led for wireless home links," in *Personal, Indoor and Mobile Radio Communications, 2000. PIMRC*

2000. The 11th IEEE International Symposium on, vol. 2. IEEE, 2000, pp. 1325–1329.

[14] J. Vučić, C. Kottke, S. Nerreter, K.-D. Langer, and J. W. Walewski, "513 mbit/s visible light communications link based on dmt-modulation of a white led," *Journal of lightwave technology*, vol. 28, no. 24, pp. 3512–3518, 2010.

[15] A. Khalid, G. Cossu, R. Corsini, P. Choudhury, and E. Ciaramella, "1-gb/s transmission over a phosphorescent white led by using rate-adaptive discrete multitone modulation," *IEEE Photonics Journal*, vol. 4, no. 5, pp. 1465–1473, 2012.

[16] G. Cossu, A. Khalid, P. Choudhury, R. Corsini, and E. Ciaramella, "3.4 gbit/s visible optical wireless transmission based on rgb led," *Optics express*, vol. 20, no. 26, pp. B501–B506, 2012.

[17] D. Tsonev, H. Chun, S. Rajbhandari, J. J. McKendry, S. Videv, E. Gu, M. Haji, S. Watson, A. E. Kelly, G. Faulkner *et al.*, "A 3-gb/s single-led ofdm-based wireless vlc link using a gallium nitride μ led," *IEEE Photonics Technology Letters*, vol. 26, no. 7, pp. 637–640, 2014.

[18] M. Kavehrad and P. Amirshahi, "Hybrid mv-lv power lines and white light emitting diodes for triple-play broadband access communications," *IEC Comprehensive Report on Achieving the Triple Play: Technologies and Business Models for Success*, pp. 167–178, 2006.

[19] C. Zhu, Y. Huo, J. Jiang, H. Sun, C. Dong, R. Zhang, and L. Hanzo, "Hierarchical colour-shift-keying aided layered video streaming for the visible light downlink," *IEEE Access*, 2016.

[20] A. P. S. Louvros and D. Fuschelberger, "Vlc technology for indoor lte planning," in *System-Level Design Methodologies for Telecommunication*. Springer, 2014, pp. 21–41.

[21] H. Haas, *Harald Haas: Wireless data from every light bulb*. TED, 2011.

[22] M. Yoshino, S. Haruyama, and M. Nakagawa, "High-accuracy positioning system using visible led lights and image sensor," in *2008 IEEE Radio and Wireless Symposium*. IEEE, 2008, pp. 439–442.

[23] W. Zhang and M. Kavehrad, "A 2-d indoor localization system based on visible light led," in *2012 IEEE Photonics Society Summer Topical Meeting Series*, 2012.

[24] Y. U. Lee and M. Kavehrad, "Long-range indoor hybrid localization system design with visible light communications and wireless network," in *2012 IEEE Photonics Society Summer Topical Meeting Series*, 2012.

[25] M. Axrtek, "Axrtek inc."

[26] M. Saadi, L. Wattisuttikulkij, Y. Zhao, and P. Sangwongngam, "Visible light communication: opportunities, challenges and channel models," *International Journal of Electronics & Informatics*, vol. 2, no. 1, pp. 1–11, 2013.

[27] T. Komine and M. Nakagawa, "Fundamental analysis for visible-light communication system using led lights," *IEEE transactions on Consumer Electronics*, vol. 50, no. 1, pp. 100–107, 2004.

[28] M. Bhalerao, S. Sonavane, and V. Kumar, "A survey of wireless communication using visible light," *International Journal of Advances in Engineering & Technology*, vol. 5, no. 2, pp. 188–197, 2013.

[29] J. J. George, M. H. Mustafa, N. M. Osman, N. H. Ahmed, and D. M. Hamed, "A survey on visible light communication," *Int. J. Eng. Comput. Sci*, vol. 3, no. 2, pp. 3805–3808, 2014.

[30] Y. He, L. Ding, Y. Gong, and Y. Wang, "Real-time audio & video transmission system based on visible light communication," *Optics and Photonics Journal*, vol. 3, no. 02, p. 153, 2013.

[31] T. Yamazato, I. Takai, H. Okada, T. Fujii, T. Yendo, S. Arai, M. Andoh, T. Harada, K. Yasutomi, K. Kagawa *et al.*, "Image-sensor-based visible light communication for automotive applications," *IEEE Communications Magazine*, vol. 52, no. 7, pp. 88–97, 2014.

[32] R. Perez-Jimenez, J. Rufo, C. Quintana, J. Rabadan, and F. Lopez-Hernandez, "Visible light communication systems for passenger in-flight data networking," in *2011 IEEE International Conference on Consumer Electronics (ICCE)*, 2011.

[33] D. Iturralde, C. Azurdia-Meza, N. Krommenacker, I. Soto, Z. Ghassemlooy, and N. Becerra, "A new location system for an underground mining environment using visible light communications," in *Communication Systems, Networks & Digital Signal Processing (CSNDSP), 2014 9th International Symposium on.* IEEE, 2014, pp. 1165–1169.

[34] I. C. Rust and H. H. Asada, "A dual-use visible light approach to integrated communication and localization of underwater robots with application to non-destructive nuclear reactor inspection," in *Robotics and Automation (ICRA), 2012 IEEE International Conference on*. IEEE, 2012, pp. 2445–2450.

[35] Y. Zhai and S. Zhang, "Visible light communication channel models and simulation of coal workface energy coupling," *Mathematical Problems in Engineering*, vol. 2015, 2015.

[36] S. Arnon, "Underwater optical wireless communication network," *Optical Engineering*, vol. 49, no. 1, pp. 015 001–015 001, 2010.

[37] H. Uema, T. Matsumura, S. Saito, and Y. Murata, "Research and development on underwater visible light communication systems," *Electronics and Communications in Japan*, vol. 98, no. 3, pp. 9–13, 2015.

[38] S.-K. Lim, K. G. Ruling, I. Kim, and I. S. Jang, "Entertainment lighting control network standardization to support vlc services," *IEEE Communications Magazine*, vol. 51, no. 12, pp. 42–48, 2013.

[39] D. O'Brien, H. Le Minh, L. Zeng, G. Faulkner, K. Lee, D. Jung, Y. Oh, and E. T. Won, "Indoor visible light communications: challenges and prospects," in *Optical Engineering Applications*. International Society for Optics and Photonics, 2008, pp. 709 106–709 106.

[40] D. Karunatilaka, F. Zafar, V. Kalavally, and R. Parthiban, "Led based indoor visible light communications: State of the art," *IEEE Communications Surveys & Tutorials*, vol. 17, no. 3, pp. 1649–1678, 2015.

[41] P. H. Pathak, X. Feng, P. Hu, and P. Mohapatra, "Visible light communication, networking, and sensing: A survey, potential and challenges," *IEEE Communications Surveys & Tutorials*, vol. 17, no. 4, pp. 2047–2077, 2015.

[42] J. Grubor, O. Jamett, J. Walewski, S. Randel, and K.-D. Langer, "High-speed wireless indoor communication via visible light," *ITG-Fachbericht-Breitbandversorgung in Deutschland-Vielfalt für alle?*, 2007.

[43] J. Grubor, S. Randel, K.-D. Langer, and J. W. Walewski, "Broadband information broadcasting using led-based interior lighting," *Journal of Lightwave technology*, vol. 26, no. 24, pp. 3883–3892, 2008.

[44] T. Komine and M. Nakagawa, "Fundamental analysis for visible-light communication system using led lights," *IEEE transactions on Consumer Electronics*, vol. 50, no. 1, pp. 100–107, 2004.

[45] W. Zhang, M. S. Chowdhury, and M. Kavehrad, "Asynchronous indoor positioning system based on visible light communications," *Optical Engineering*, vol. 53, no. 4, pp. 045 105–045 105, 2014.

[46] A. Goldsmith, *Wireless communications*. Cambridge university press, 2005.

[47] W. Zhang and M. Kavehrad, "Comparison of vlc-based indoor positioning techniques," in *SPIE OPTO*. International Society for Optics and Photonics, 2013, pp. 86 450M–86 450M.

[48] H.-S. Kim, D.-R. Kim, S.-H. Yang, Y.-H. Son, and S.-K. Han, "An indoor visible light communication positioning system using a rf carrier

allocation technique," *Journal of Lightwave Technology*, vol. 31, no. 1, pp. 134–144, 2013.

[49] L. Li, P. Hu, C. Peng, G. Shen, and F. Zhao, "Epsilon: A visible light based positioning system," in *11th USENIX Symposium on Networked Systems Design and Implementation (NSDI 14)*, 2014, pp. 331–343.

[50] S. De Lausnay, L. De Strycker, J.-P. Goemaere, N. Stevens, and B. Nauwelaers, "A visible light positioning system using frequency division multiple access with square waves," in *Signal Processing and Communication Systems (ICSPCS), 2015 9th International Conference on.* IEEE, 2015, pp. 1–7.

[51] M. Guerra-Medina, O. Gonzalez, B. Rojas-Guillama, J. Martin-Gonzalez, F. Delgado, and J. Rabadan, "Ethernet-ocdma system for multi-user visible light communications," *Electronics letters*, vol. 48, no. 4, pp. 227–228, 2012.

[52] J. A. Salehi, "Code division multiple-access techniques in optical fiber networks. i. fundamental principles," *IEEE Transactions on communications*, vol. 37, no. 8, pp. 824–833, 1989.

[53] J. A. Salehi and C. A. Brackett, "Code division multiple-access techniques in optical fiber networks. ii. systems performance analysis," *IEEE Transactions on Communications*, vol. 37, no. 8, pp. 834–842, 1989.

[54] J. A. Martin-Gonzalez, E. Poves, and F. J. Lopez-Hernandez, "Random optical codes used in optical networks," *IET communications*, vol. 3, no. 8, pp. 1392–1401, 2009.

[55] P. V. Kumar, R. Omrani, J. Touch, A. E. Willner, and P. Saghari, "Cth01-5: A novel optical cdma modulation scheme: Code cycle modulation," in *IEEE Globecom 2006*. IEEE, 2006, pp. 1–5.

[56] M. F. Guerra-Medina, B. Rojas-Guillama, O. González, J. A. Martín-González, E. Poves, and F. J. López-Hernández, "Experimental optical code-division multiple access system for visible light communications," in *Wireless Telecommunications Symposium (WTS), 2011*. IEEE, 2011, pp. 1–6.

[57] J. Lian, M. Noshad, and M. Brandt-Pearce, "Multiuser miso indoor visible light communications," in *2014 48th Asilomar Conference on Signals, Systems and Computers*. IEEE, 2014, pp. 1729–1733.

[58] Z. Zhou, M. Kavehrad, and P. Deng, "Indoor positioning algorithm using light-emitting diode visible light communications," *Optical Engineering*, vol. 51, no. 8, pp. 085 009–1, 2012.

[59] Y. Kim, J. Hwang, J. Lee, and M. Yoo, "Position estimation algorithm based on tracking of received light intensity for indoor visible light communication systems," in *2011 Third International Conference on Ubiquitous and Future Networks (ICUFN)*. IEEE, 2011, pp. 131–134.

[60] A. Küpper, *Location-based services: fundamentals and operation*. John Wiley & Sons, 2005.

[61] A. Kushki, K. N. Plataniotis, and A. N. Venetsanopoulos, *WLAN positioning systems: principles and applications in location-based services*. Cambridge University Press, 2012.

[62] S. De Lausnay, L. De Strycker, J.-P. Goemaere, B. Nauwelaers, and N. Stevens, "A survey on multiple access visible light positioning,"

in *Emerging Technologies and Innovative Business Practices for the Transformation of Societies (EmergiTech), IEEE International Conference on*. IEEE, 2016, pp. 38–42.

[63] H. Liu, H. Darabi, P. Banerjee, and J. Liu, "Survey of wireless indoor positioning techniques and systems," *IEEE Transactions on Systems, Man, and Cybernetics, Part C (Applications and Reviews)*, vol. 37, no. 6, pp. 1067–1080, 2007.

[64] M. A. Al-Ammar, S. Alhadhrami, A. Al-Salman, A. Alarifi, H. S. Al-Khalifa, A. Alnafessah, and M. Alsaleh, "Comparative survey of indoor positioning technologies, techniques, and algorithms," in *Cyberworlds (CW), 2014 International Conference on*. IEEE, 2014, pp. 245–252.

[65] K. Al Nuaimi and H. Kamel, "A survey of indoor positioning systems and algorithms," in *Innovations in information technology (IIT), 2011 international conference on*. IEEE, 2011, pp. 185–190.

[66] A. Burton, H. Le Minh, Z. Ghasemlooy, and S. Rajbhandari, "A study of led lumination uniformity with mobility for visible light communications," in *Optical Wireless Communications (IWOW), 2012 International Workshop on, Publication Year*, 2012, pp. 1–3.

[67] Z. Wang, C. Yu, W.-D. Zhong, J. Chen, and W. Chen, "Performance of a novel led lamp arrangement to reduce snr fluctuation for multi-user visible light communication systems," *Optics express*, vol. 20, no. 4, pp. 4564–4573, 2012.

[68] H. Chun, C.-J. Chiang, A. Monkman, and D. OBrien, "A study of illumination and communication using organic light emitting diodes," *Journal of Lightwave Technology*, vol. 31, no. 22, pp. 3511–3517, 2013.

[69] L. A.-H. Azizan, M. S. Ab-Rahman, and K. Jumiran, "Analytical approach on snr performance of visible light communication for modern lighting layout," in *Innovation Management and Technology Research (ICIMTR), 2012 International Conference on.* IEEE, 2012, pp. 332–336.

[70] C. Chow, Y. Liu, C. Yeh, J. Sung, and Y. Liu, "A practical in-home illumination consideration to reduce data rate fluctuation in visible light communication," *IEEE Wireless Communications*, vol. 22, no. 2, pp. 17–23, 2015.

[71] J. Ding, Z. Huang, and Y. Ji, "Evolutionary algorithm based uniform received power and illumination rendering for indoor visible light communication," *JOSA A*, vol. 29, no. 6, pp. 971–979, 2012.

[72] Y. Liu, Y. Peng, Y. Liu, and K. Long, "Optimization of receiving power distribution using genetic algorithm for visible light communication," in *Applied Optics and Photonics China (AOPC2015).* International Society for Optics and Photonics, 2015, pp. 96 790I–96 790I.

[73] T. Komine, J. H. Lee, S. Haruyama, and M. Nakagawa, "Adaptive equalization system for visible light wireless communication utilizing multiple white led lighting equipment," *IEEE Transactions on Wireless Communications*, vol. 8, no. 6, pp. 2892–2900, 2009.

[74] T. Y. Elganimi, "Performance comparison between ook, ppm and pam modulation schemes for free space optical (fso) communication systems:

analytical study," *International Journal of Computer Applications*, vol. 79, no. 11, 2013.

[75] [Online]. Available: http://www.osram.de(DOT-it)

[76] Z. Wu, J. Chau, and T. Little, "Modeling and designing of a new indoor free space visible light communication system," in *Networks and Optical Communications (NOC), 2011 16th European Conference on.* IEEE, 2011, pp. 72–75.

[77] J. Grubor, S. C. J. Lee, K.-D. Langer, T. Koonen, and J. W. Walewski, "Wireless high-speed data transmission with phosphorescent white-light leds," *ECOC 2007*, 2007.

[78] H. Zheng, C. Yu, J. Chen, X. You, and Z. Ghassemlooy, "Led arrangement optimization for visible light communication systems," in *Opto-Electronics and Communications Conference (OECC), 2015.* IEEE, 2015, pp. 1–3.

[79] S.-Y. Jung, S. Hann, and C.-S. Park, "Tdoa-based optical wireless indoor localization using led ceiling lamps," *IEEE Transactions on Consumer Electronics*, vol. 57, no. 4, pp. 1592–1597, 2011.

[80] K. Panta and J. Armstrong, "Indoor localisation using white leds," *Electronics letters*, vol. 48, no. 4, pp. 228–230, 2012.

[81] M. Yasir, S.-W. Ho, and B. N. Vellambi, "Indoor positioning system using visible light and accelerometer," *Journal of Lightwave Technology*, vol. 32, no. 19, pp. 3306–3316, 2014.

[82] S.-H. Yang, H.-S. Kim, Y.-H. Son, and S.-K. Han, "Three-dimensional visible light indoor localization using aoa and rss with multiple optical

receivers," *Journal of Lightwave Technology*, vol. 32, no. 14, pp. 2480–2485, 2014.

[83] H. Zheng, Z. Xu, C. Yu, and M. Gurusamy, "Indoor three-dimensional positioning based on visible light communication using hamming filter," in *Signal Processing in Photonic Communications*. Optical Society of America, 2016, pp. SpM4E–3.

[84] F. R. Gfeller and U. Bapst, "Wireless in-house data communication via diffuse infrared radiation," *Proceedings of the IEEE*, vol. 67, no. 11, pp. 1474–1486, 1979.

[85] M. Yasir, S.-W. Ho, and B. N. Vellambi, "Indoor localization using visible light and accelerometer," in *2013 IEEE Global Communications Conference (GLOBECOM)*. IEEE, 2013, pp. 3341–3346.

[86] S.-W. Ho, J. Duan, and C. S. Chen, "Location-based information transmission systems using visible light communications," *Transactions on Emerging Telecommunications Technologies*, 2015.

[87] W. Gu, M. Aminikashani, P. Deng, and M. Kavehrad, "Impact of multipath reflections on the performance of indoor visible light positioning systems," *Journal of Lightwave Technology*, vol. 34, no. 10, pp. 2578–2587, 2016.

[88] A. Noroozi and M. A. Sebt, "Weighted least squares target location estimation in multi-transmitter multi-receiver passive radar using bistatic range measurements," *IET Radar, Sonar & Navigation*, 2016.

[89] M. M. Zaniani, A. M. Shahar, and I. A. Azid, "Trilateration target estimation improvement using new error correction algorithm," in *2010 18th Iranian Conference on Electrical Engineering*, 2010.

[90] G. B. Thomas and R. L. Finney, *Calculus and analytic geometry*. Addison Wesley Publishing Company, 1984.

[91] Y. Lee, S. Baang, J. Park, Z. Zhou, and M. Kavehrad, "Hybrid positioning with lighting leds and zigbee multihop wireless network," in *SPIE OPTO*. International Society for Optics and Photonics, 2012, pp. 82 820L–82 820L.

[92] C.-W. Hsu, J.-T. Wu, H.-Y. Wang, C.-W. Chow, C.-H. Lee, M.-T. Chu, and C.-H. Yeh, "Visible light positioning and lighting based on identity positioning and rf carrier allocation technique using a solar cell receiver," *IEEE Photonics Journal*, vol. 8, no. 4, pp. 1–7, 2016.

[93] T.-H. Do, J. Hwang, and M. Yoo, "Tdoa based indoor visible light positioning systems," in *2013 Fifth International Conference on Ubiquitous and Future Networks (ICUFN)*. IEEE, 2013, pp. 456–458.

[94] P. Luo, Z. Ghassemlooy, H. Le Minh, A. Khalighi, X. Zhang, M. Zhang, and C. Yu, "Experimental demonstration of an indoor visible light communication positioning system using dual-tone multi-frequency technique," in *Optical Wireless Communications (IWOW), 2014 3rd International Workshop in*. IEEE, 2014, pp. 55–59.

[95] H.-S. Kim, D.-R. Kim, S.-H. Yang, Y.-H. Son, and S.-K. Han, "An indoor visible light communication positioning system using a rf carrier allocation technique," *Journal of Lightwave Technology*, vol. 31, no. 1, pp. 134–144, 2013.

[96] W. Guan, Y. Wu, S. Wen, H. Chen, C. Yang, Y. Chen, and Z. Zhang, "A novel three-dimensional indoor positioning algorithm design based

on visible light communication," *Optics Communications*, vol. 392, pp. 282–293, 2017.

[97] T. C. Schenk, L. Feri, H. Yang, and J.-P. M. Linnartz, "Optical wireless cdma employing solid state lighting leds," in *Summer Topical Meeting, 2009. LEOSST'09. IEEE/LEOS.* IEEE, 2009, pp. 23–24.

[98] Y.-A. Chen, Y.-T. Chang, Y.-C. Tseng, and W.-T. Chen, "A framework for simultaneous message broadcasting using cdma-based visible light communications," *IEEE Sensors Journal*, vol. 15, no. 12, pp. 6819–6827, 2015.

[99] A. Tawfiq, J. Abouei, and K. N. Plataniotis, "Cyclic orthogonal codes in cdma-based asynchronous wireless body area networks," in *2012 IEEE International Conference on Acoustics, Speech and Signal Processing (ICASSP).* IEEE, 2012, pp. 1593–1596.

[100] Y. Xia, P. Li, X. Shan, and Y. Ren, "Cyclically orthogonal subsets of walsh functions," in *Communication Systems, 2002. ICCS 2002. The 8th International Conference on*, vol. 1. IEEE, 2002, pp. 107–111.

[101] F. R. Gfeller and U. Bapst, "Wireless in-house data communication via diffuse infrared radiation," *Proceedings of the IEEE*, vol. 67, no. 11, pp. 1474–1486, 1979.

[102] H. Zheng, Z. Xu, C. Yu, and M. Gurusamy, "Indoor three-dimensional positioning based on visible light communication using hamming filter," in *Signal Processing in Photonic Communications.* Optical Society of America, 2016, pp. SpM4E–3.

[103] E. Bertolazzi, "Trust region method," 2005.

[104] Y. Hong, J. Chen, Z. Wang, and C. Yu, "Performance of a precoding mimo system for decentralized multiuser indoor visible light communications," *IEEE Photonics Journal*, vol. 5, no. 4, pp. 7 800 211–7 800 211, 2013.

[105] A. G. Al-Ghamdi and J. M. Elmirghani, "Analysis of diffuse optical wireless channels employing spot-diffusing techniques, diversity receivers, and combining schemes," *IEEE Transactions on Communications*, vol. 52, no. 10, pp. 1622–1631, 2004.

[106] S. Jivkova, B. Hristov, and M. Kavehrad, "Power-efficient multispot-diffuse multiple-input-multiple-output approach to broad-band optical wireless communications," *IEEE Transactions on Vehicular Technology*, vol. 53, no. 3, pp. 882–889, 2004.

[107] P. Djahani and J. M. Kahn, "Analysis of infrared wireless links employing multibeam transmitters and imaging diversity receivers," *IEEE Transactions on Communications*, vol. 48, no. 12, pp. 2077–2088, 2000.

[108] S. Rodríguez, B. Mendoza, O. González, A. Ayala, and R. P. Jiménez, "Considerations on the design of conventional receivers for wireless optical channels using a monte carlo based ray-tracing algorithm," in *SPIE Europe Microtechnologies for the New Millennium*. International Society for Optics and Photonics, 2009, pp. 736 316–736 316.

[109] S. R. Pérez, B. R. Mendoza, R. P. Jiménez, O. G. Hernández, and A. G.-V. Fernández, "Design considerations of conventional angle diversity receivers for indoor optical wireless communications,"

EURASIP Journal on Wireless Communications and Networking, vol. 2013, no. 1, pp. 1–15, 2013.

[110] D. Mascharka and E. Manley, "Machine learning for indoor localization using mobile phone-based sensors," *arXiv preprint arXiv:1505.06125*, 2015.

[111] A. H. Salamah, M. Tamazin, M. A. Sharkas, and M. Khedr, "An enhanced wifi indoor localization system based on machine learning," in *Indoor Positioning and Indoor Navigation (IPIN), 2016 International Conference on*. IEEE, 2016, pp. 1–8.

[112] C. ASPLUND, "Object classification and localization using machine learning techniques."

List of Publications

Journal Papers

1. H. Zheng, J. Chen, C. Yu, and M. Gurusamy, "Inverse design of LED arrangement for visible light communication systems," *Optics Communications*, vol. 382, pp. 615–623, 1 Jan. 2017.

2. H. Zheng, Z. Xu, C. Yu, and M. Gurusamy, "A 3-D high accuracy positioning system based on visible light communication with novel positioning algorithm," *Optics Communications*, vol. 396, pp. 160-168, 1 Aug. 2017.

3. H. Zheng, Z. Xu, C. Yu, and M. Gurusamy, " Asynchronous indoor positioning system based on delay compensation code devision multiple access technique," *Journal of Lightwave Technology*, under review.

4. X. You, J. Chen, H. Zheng, C. Yu, "Efficient Data Transmission Using MPPM Dimming Control in Indoor Visible Light Communication," *IEEE Photonics Journal,* Volume 7, Number 4, Aug. 2015.

5. X. You, J. Chen, C. Yu and H. Zheng,"Time domain reshuffling for OFDM based indoor visible light communication systems," *Optics Express*, accepted.

Conference Papers

1. H. Zheng, C. Yu, and H. Kim, "The performance of inter-satellite BFSK and 4FSK optical communication system with pointing error," *2014 OptoElectronics and Communication Conference and Australian Conference on Optical Fibre Technology*, pp. 210–212, 6-10 July 2014.

2. H. Zheng, C. Yu, J. Chen, X. You, and Z. Ghassemlooy, "LED Arrangement Optimization for Visible Light Communication Systems," *2015 Opto-Electronics and Communications Conference (OECC),* pp. 1–3, June 28-July 2 2015.

3. H. Zheng, A. Burton, J. Chen, C. Yu, and Z. Ghassemlooy, "Power coverage optimization for visible light communications based on convex optimization," *IEEE Photonics Global Conference (PGC) 2015,* Paper H2-4, pp. 1, Singapore, June 28-July 3, 2015.

4. H. Zheng, Z. Xu, C. Yu, and M. Gurusamy, "Indoor three-dimensional positioning based on visible light communication using Hamming filter," *Signal Processing in Photonic Communications 2016,* SpM4E, Canada, 18-20 July, 2016.

5. H. Zheng, Z. Xu, C. Yu, and M. Gurusamy, "Asynchronous visible light positioning system using FDMA and ID techniques," *2017 Opto-Electronics and Communications Conference (OECC)*, accepted.

6. Z. Xu, H. Zheng, C. Yu, and Y. Kam, "Performance of pilot-assisted maximum-likelihood sequence detection in a rotated-8QAM coherent optical system," *2014 OptoElectronics and Communication Conference and Australian Conference on Optical Fibre Technology*, pp. 896–898, 6-10 July 2014.

7. J. Chen, Y. Hong, X. You, H. Zheng, and C. Yu, "Conceptual design of multi-user visible light communication systems over indoor lighting infrastructure, Communication Systems," *2014 9th International Symposium on Networks & Digital Signal Processing (CSNDSP)*, pp. 1154–1158, 23-25 July 2014.

8. J. Chen, X. You, H. Zheng, C. Yu, "Excess signal transmission with dimming control pattern in indoor visible light communication systems," *Optoelectronic Devices and Integration Proc.* SPIE 9270V, 927014 (October 24, 2014).

9. J. Chen, X. You, Y. Hong, H. Zheng, and C. Yu, "On practical considerations for designing indoor visible light communication systems," *IEEE Photonics Global Conference (PGC) 2015,* Paper H3-1, pp. 1, Singapore, June 28-July 3, 2015 (Invited).

10. X. You, J. Chen, H. Zheng, and C. Yu, "Time domain reshuffling for OFDM based indoor visible light communication systems," *IEEE Photonics Global Conference (PGC) 2015,* Paper H2-2, pp. 1, Singapore, June 28-July 3, 2015.